Characterization of Objects by Fitting the Polarization Tensor

Ahmad Khairuddin, Taufiq Khairi bin

2016

MIMS EPrint: **2016.55**

Manchester Institute for Mathematical Sciences
School of Mathematics

The University of Manchester

ISSN 1749-9097

CHARACTERIZATION OF OBJECTS BY FITTING THE POLARIZATION TENSOR

A thesis submitted to the University of Manchester
for the degree of Doctor of Philosophy
in the Faculty of Engineering and Physical Sciences

2016

Taufiq Khairi bin Ahmad Khairuddin
School of Mathematics

Contents

Word count 23015

List of Tables

List of Figures

The University of Manchester

Taufiq Khairi bin Ahmad Khairuddin
Doctor of Philosophy
Characterization of Objects by Fitting the Polarization Tensor
November 28, 2016

This thesis focuses on some mathematical aspects and a few recent applications of the polarization tensor (PT). Here, the main concern of the study is to characterize objects presented in electrical or electromagnetic fields by only using the PT. This is possible since the PT contains significant information about the object such as shape, orientation and material properties. Two main applications are considered in the study and they are electrosensing fish and metal detection. In each application, we present a mathematical formulation of the PT and briefly discuss its properties.

The PT in the electrosensing fish is actually based on the first order generalized polarization tensor (GPT) while the GPT itself generalizes the classical PT called as the Pólya-Szegő PT. In order to investigate the role of the PT in electrosensing fish, we propose two numerical methods to compute the first order PT. The first method is directly based on the quadrature method of numerical integration while the second method is an adaptation of some terminologies of the boundary element method (BEM). A code to use the first method is developed in *Matlab* while a script in *Python* is written as an interface for using the new developed code for BEM called as *BEM++*. When comparing the two methods, our numerical results show that the first order PT is more accurate with faster convergence when computed by *BEM++*. During this study, we also give a strategy to determine an ellipsoid from a given first order PT. This is because we would like to propose an experiment to test whether electrosensing fish can discriminate a pair of different objects but with the same first order PT such that the pair could be an ellipsoid and some other object. In addition, the first order PT (or the Pólya-Szegő PT) with complex conductivity (or complex permittivity) which is similar to the PT for Maxwell's equations is also investigated.

On the other hand, following recent mathematical foundation of the PT from the eddy current model, we use the new proposed explicit formula to compute the rank 2 PT for a few metallic targets relevance in metal detection. We show that the PT for the targets computed from the explicit formula agree to some degree of accuracy with the PT obtained from metal detectors during experimental works and simulations conducted by the engineers. This suggests to alternatively use the explicit formula which depends only on the geometry and material properties of the target as well as offering lower computational efforts than performing measurements with metal detectors to obtain the PT. By using the explicit formula of the rank 2 PT, we also numerically investigate some properties of the rank 2 PT where, the information obtained could be useful to improve metal detection and also in other potential applications of the eddy current. In this case, if the target is magnetic but non-conducting, the rank 2 PT of the target can also be computed by using the explicit formula of the first order PT.

Weakly electric fish *Gnathonemus petersii*

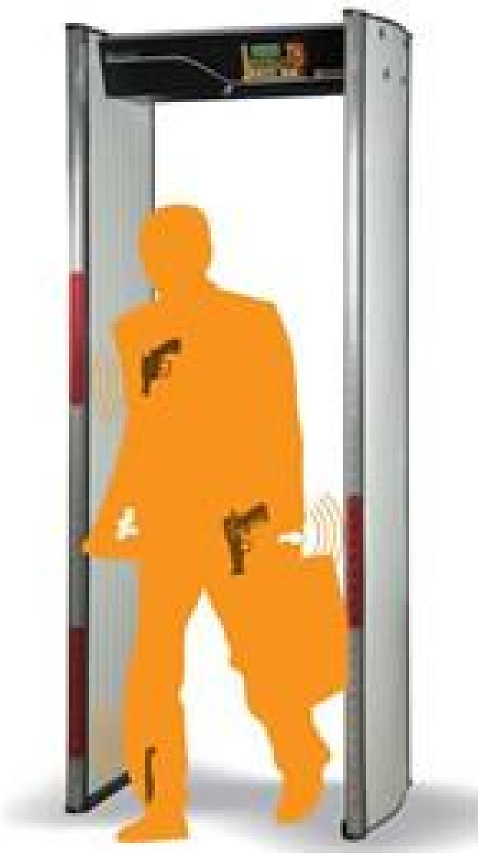

(a) (b)

Metal detectors : (a) Walk-through metal detector (b) Landmine detector

Declaration

No portion of the work referred to in the thesis has been submitted in support of an application for another degree or qualification of this or any other university or other institute of learning.

Copyright Statement

to my late brother

Allahyarham *Ahmad Khairul Nizam bin Ahmad Khairuddin* (1987-2000)

the first programmer I ever knew

Acknowledgements

In the name of Allah, the most Gracious, the most Merciful. Praise be to Him, due to His blessing, I am able to complete this thesis and finish my PhD. Praise of Allah to the beloved Prophet Muhammad, because of his efforts, I am able to practice Islam and achieve success in my life especially in my studies.

I would like to take this opportunity to thank a large number of people who have helped me a lot during my studies in Manchester for four years. First and foremost, I want to express my sincere appreciation to Professor Bill Lionheart, the supervisor of my PhD study, for his enthusiasm and guidance on the project. I am trully indebted to his determination, motivation and toleration while working with me.

Next, I would like to acknowledge Dr Manuchehr Soleimani and Professor Tony Peyton for their meaningful comments and suggestions in improving the thesis. I am also very grateful to Dr Paul Ledger for his assistance on polarization tensor for metal detection. I also enjoy the enlightening discussions about metal detectors that I had with Professor Peyton's group, especially with Dr Liam Marsh and Dr Bachir Dekdouk.

My deepest gratitude also to Dr Wojciech Śmigaj for spending his precious time to help me working with *BEM++*. Thanks also to Dr Timo Betcke for his promotion and explanation about *BEM++*. Also are not forgotten, Dr Jonathan Boyle and Dr Chris Paul, for their technical supports on IT, which makes me able to use *BEM++* and *hp*-FEM on my computer for computing polarization tensors at the school.

I also appreciate the constructive feedbacks about my works from the experts of the polarization tensor, Professor Habib Ammari and Professor Hyeonbae Kang. It was a very wonderful experience to meet both of you in Bandung, Indonesia last time. Besides, I want to thank Professor Gerhard von der Emde for meeting me in person in Bonn, Germany and listen to my explanation about my works on electrosensing fish before giving a few wonderful comments and hints to improve the studies.

I still remember how I knew about Bill Lionheart by searching through Google "industry mathematics uk" in 2011. At that time, my employer at the Department of Mathematics (now known as the Department of Mathematical Sciences), Universiti Teknologi Malaysia (UTM) wanted me to pursue my study on mathematics with industrial applications. For that reason, I must acknowledge my immense debt of gratitude to Professor Zainal Abd Aziz for his support on my application to continue my study at the University of Manchester. I never imagine in my life to be in Manchester, although I am a very big fan of Manchester United Football Club. I also have to thank the late Allahyarham Tuan Haji Ramli Ibrahim who managed my application for study leave from my employer so that I could come and live temporarily in Manchester. I am still sad for not being able to meet you one last time after I have came back to Malaysia. May Allah reward you with His heaven.

In completing my research works, I am also indebted to the Government of Malaysia and UTM for supporting me financially during the study which includes the support to attend the World Congress on Engineering 2015 in London. I also appreciate many technical contributions that I received from the staffs of the School of Mathematics, The University of Manchester during my study and the school also gave me some fundings for my participation in BAMC Cardiff 2014. I also want to acknowledge CIMPA Research School in France for supporting my accomodation during CIMPA-Indonesia Research School 2014.

A special thanks is also due to my friends in Manchester : (i) my fellow Malaysians especially Nurul Aimi, Wan Mohamad Husni, Iskandar, Norshah Afizi, Rashid Redza, Ezak, Shaheer, Zubir and Muhammad Izzat, (ii) my fellow postgraduates, Kyriakos, Mike, Russell, Naeem, Sophia and Francis and (iii) my international friends Zahid and Osmend, for your friendship and helping me to live happily in Manchester. My best pals Abdul Rahman and Sharidan, thanks for your prays from Malaysia. And to my former teachers and my colleagues at the Department of Mathematical Sciences, UTM, thank you for your kind supports.

Finally, I am very thankful to my family members : my parents, grandparents, brother, sister, aunts, uncle and cousins, for their love and supports, especially from my mother. I am only able to overcome many obstacles and achieve this success with you guys standing by my side. And to Asyiqin, I thank you for your understanding, patience and courage.

Taufiq Khairi bin Ahmad Khairuddin,
His Servant,
PhD student at The University of Manchester,
Lecturer at Universiti Teknologi Malaysia,
September 2016.

Chapter 1

Introduction

The terminology polarization tensor (PT) has some useful applications in electric and electromagnetic inverse problems. Some researchers study the PT to improve image reconstruction in electrical imaging for industrial or biomedical applications. Furthermore, the PT also provides additional information about the electrical images with lower computational cost than full image reconstruction. On the other hand, since metal detection is normally expensive, difficult and time consuming, the PT is adapted in metal detectors by the engineers during security screening and landmine clearance. In this study, we present and describe some mathematical aspects and applications of the first order PT. By using the PT from electrical imaging, we investigate the PT in electrosensing fish. Moreover, based on recent mathematical foundation of the PT for the eddy current, we numerically explore the PT for metal detection and compare it with the PT from engineering perspective for this problem.

1.1 Research Background

The PT is actually an old branch of mathematics and appears for examples, in the classical problems of potential theory. Many years ago, Pólya [1] invented a PT called the virtual mass in his investigation about motion of a solid through a fluid. The virtual mass was then extended and the new PT (we call it as the Pólya-Szegő PT) was introduced in the studies of hydrodynamics and theory of electricity by [2] and [3]. Furthermore, another different PT known as the polarizibility tensor was used by Kleinman and Senior [4] to formulate the induced electric and magnetic dipole moments in low frequency electromagnetic scattering. They also gave several examples about the polarizibility tensor for each electric and magnetic dipole moment of the homogeneous Maxwell's equations in [5].

After some periods, between year 2001 and 2010, a few nice books about the PT with a specific applications were written. The PT called as the polarizibility tensor and appeared in Milton [6] was used in the theoretical studies of composite. Another polarizibility tensor was also investigated by Raab and De Lange [7] during their studies on multipole moments in electromagnetism. In addition, Ammari and Kang [8] provided some extensive mathematical analysis for the PT and applied it to improve electrical imaging and also to determine effective properties for some mediums. This suggests that researches in this area are very wide, promising and also interesting.

In this research, our main reference to study and apply the PT is the book by Professors Habib Ammari and Hyeonbae Kang entitled *Polarization and Moment Tensors : with Applications to Inverse Problems and Effective Medium Theory.* According to Ammari and Kang [8], their PT actually generalizes the concept of Pólya-Szegő PT in [3]. In this case, the Pólya-Szegő PT is the first order of the generalized polarization tensor (GPT) of [8]. If an object has zero conductivity or it is insulated, the Pólya-Szegő PT for the object here reduces to the virtual mass in [3]. In order to achieve our purpose here, we first review some properties of the first order GPT (or simply called as the first order PT) for three dimensional domains. After that, the first order PT is adapted to investigate the PT for electrosensing fish. Finally, we extend the first order PT to study the PT in some applications of Maxwell's and eddy current equations.

1.1.1 Electrical impedance imaging and electrosensing fish

During recent development in imaging techniques, biomedical engineers measure voltages on the surface of a body to create an image inside of the body for medical purposes from a system called as Electrical Impedance Tomography (EIT) (see [9, 10]). The same analogy to the EIT known as Electrical Resistivity Tomography (ERT) is applied by geophysicists for examples to locate minerals and archeological relics. Furthermore, weakly electric fish also use a very similar approach to EIT to navigate and locate prey where, in this context, we say that the fish perform electrosensing.

From the mathematical model of the EIT, Ammari and Kang [8] have used the method of asymptotic expansions and layer potential techniques to derive an asymptotic formula representing the perturbation in the electrical field due to the presence of a conducting object. The leading order term of the asymptotic formula is actually described by the GPT which depends only on the geometry and conductivity of the presented object. In their study [8], the GPT is applied to improve image reconstruction of the object inclusion in the electrical fields. However, using the GPT itself could be sufficient to alternatively describe the inclusion especially when image reconstruction is not needed, such as in metal detection. In our study, we focus on using the PT to provide information about electrical and electromagnetic objects inclusion with lower computational effort than fully reconstructing the image of the object.

For the the purpose of characterizing objects with the PT without knowing their images, we first investigate the PT in electrosensing fish. Weakly electric fish are equipped with an electric discharge organ and hundreds of voltage sensing cells on their body to perform electrosensing for navigation as well as to characterize objects and locate prey [11, 12, 13, 14]. Species such as Peters' elephantnose fish *Gnathonemus petersii* generates a broad spectrum pulse like signal while the black ghost knifefish *Apteronotus albifrons* uses a signal like a sine wave [14, 15, 16]. They are able by electrosensing to recognize and discriminate between conducting and insulating objects with different type of shapes [12]. Besides, another previous studies have shown that fish also perform similar face recognition like human to distinguish objects in a variety of orientations and lightning conditions [13]. Amazingly, when a weakly eletric fish typically moves in the water approaching an object, its electric source looks to act in a similar way to switching between driven electrodes in an EIT system where the voltages are measured through the sensing cells on the surface of its body (see Nelson [14]). The main difference here is only a single electric source is used by the fish while multiple switched sources are used typically in medical and geophysical EIT.

Due to the similarity between electrosensing fish and EIT system, it could be useful to relate the terminology of EIT in electrosensing to further describe electrosensing by the fish. Ammari et. al [17] have recently modelled electrosensing fish in a two dimensional problems where the same model as the EIT has been used. After that, the GPT is also applied in their reconstruction algorithm when simulating images classification and objects identification by electrosensing fish in [18]. Furthermore, in reality, it will be a suprise if the fish are able to perform complete image reconstruction as it has only a small brain. It is possible that the fish only fit the objects with their PT to characterize and discriminate the objects since the PT contains significant information about the shape and material of the object. Therefore, in this thesis, we compute the first order PT for some objects in the real experiments conducted by von der Emde and Fetz [12] and use the results to investigate whether the fish can measure the first order PT when making decision about the objects. In this case, our approach is totally different with [18] since we consider electrosensing fish in the three dimensional space and specifically investigate the role of only the first order PT for characterizing objects without using the image of the objects.

1.1.2 Metal detection

A metal detector usually has a transmitting and a receiving coil. A magnetic field is produced when electrical currents flow inside the transmitting coil. Consequently, the magnetic field will interact with a nearby conducting metallic object and induce eddy currents in the object. The eddy current itselft will produce magnetic field and this magnetic field will perturb the background magnetic field where, the perturbation in the magnetic field is then detected by the receiving coil. Previous researches such as [19, 20, 21, 22] have focused on improving the performance of metal detectors based on this standard knowledge.

Nowadays, there is a rapid growth in using metal detector for many reasons. These include nondestructive testing to ensure quality products in manufacturing [19], increasing consumer safety in the food industry [22, 23], security screening [24, 25] at the airport, embassy and prison or landmine clearance [20, 21, 26]. Some people just use metal detectors for their hobbies such as treasure hunting to discriminate between cluttered objects with coins and jewelry. Due to variety purposes for metal detectors, several criteria are required and must be established when building it. For examples, security screening and landmine clearance often are slow processes so, metal detectors with a low-false alarm will be the most welcomed here. Moreover, agencies with limited budget requiring the use of metal detector will appreciate if it has a low maintenance. Besides, a hobbyist metal detector usually prefers a cheap metal detector.

During this study, we will further explore the PT (or the magnetic polarizibility tensor) used by [24, 25, 26] to describe several known metallic objects and hope to improve metal detection especially for security screening and landmine clearance. Previously, Marsh et al. [24, 25] in their engineering works have reconstructed the magnetic polarizability tensor of several detected objects by performing experiments and making measurements of the fields generated by the walk-through metal detector in order to describe the location, dimension, orientation and material property of the metallic targets for security screening. Similarly, Dekdouk et al. [26] have estimated the magnetic polarizability tensor for metal components of landmines by simulating the fields generated by metal detectors to improve the possibilities of detecting them in a contaminated field environment. However, for a specific known metallic object, they [24, 25, 26] do not have an explicit formula to compute its magnetic polarizability tensor. As our knowledge about what to detect improves upon previous experiences, a formula if it exists, will enable us to compute the magnetic polarizibilty tensor and match it with the one obtained from the experiments and simulations. This then will increase the possibility of correctly identifying the object from the magnetic polarizibility tensor. Furthermore, using the explicit formula to obtain magnetic the polarizibility tensor also offers lower computational efforts than performing fields measurement for locating and identifying the target.

In the eddy current approximation to Maxwell's equations, Ammari et al. [27] have derived an asymptotic formula that represents the perturbation of the magnetic fields due to the presence of an isolated conducting object. Two PT are introduced from the formula, namely the conductivity polarization tensor (CPT) and the magnetic polarization tensor (MPT). They have also designed a statistical algorithm to locate a spherical target based on induction data derived from the eddy currents by using the CPT in [27] and have extended it for an arbitrary target in [28]. On the other hand, based on the foundation given in [27], Ledger and Lionheart [29] further investigate the MPT and CPT to describe conducting and magnetic objects. The reduction in the number of independent coefficients for the CPT and MPT for objects with rotational and mirror symmetries are also highlighted. They also apply tensor operations to introduce a new PT by combining MPT and CPT. After that, a *hp*-FEM method to numerically compute the new introduced PT are proposed and several properties of the

PT are also investigated. In addition, it is recently shown in [29, 30] that the magnetic polarizibilty tensor in [24, 25, 26] is the same as the rank 2 PT of [29] that combines both CPT and MPT. Thus, the magnetic polarizibility tensor (or just the polarizibility tensor) for an object presented in a metal detector can now be computed for the first time based on the shape and material properties of the object by using the explicit formula of the rank 2 PT given in [29].

In this thesis, we will compute the rank 2 PT of [29] for a few objects in [24, 25, 26] with the given explicit formula and compare them with the polarizibility tensors obtained during experiments and simulations conducted by [24, 25, 26]. After that, some properties of the rank 2 PT of [29] will be numerically investigated, where, the information obtained could be useful in the future applications. Besides, by using the theoretical results in [29], for magnetic non-conducting objects, we give numerical examples to show that the polarizibility tensor can also be obtained from the explicit formula of the first order PT of [8]. Alternatively, a few studies conducted for examples by [31, 32] have suggested to use the ground penetrating radar (GPR) for landmine clearance. Therefore, we will investigate the possibility of improving the GPR by using the PT as well.

1.2 Mathematical Background of the GPT

The concept of PT which arise from a transmission problem discussed by many literatures (for examples in [8], [9] and [10]) is firstly presented here. Following [8], consider a Lipschitz bounded domain B in $\mathbb{R}^3$ such that the origin O is in B and let the conductivity of B be equal to k where $0 < k \neq 1 < +\infty$ (we can choose the conductivity of the background to be equal to 1 so that k is the ratio between conductivity of the object to the conductivity of the background). Suppose that H is a harmonic function in $\mathbb{R}^3$ and u be the solution to the following problem.

$$\begin{cases} \operatorname{div}(1 + (k-1)\chi(B)\operatorname{grad}(u)) = 0 \text{ in } \mathbb{R}^3 \\ u(x) - H(x) = O(1/|x|^2) \text{ as } |x| \to \infty \end{cases} \tag{1.1}$$

where χ denotes the characteristic function of B. The mathematical formulation (1.1) actually appears in many industrial applications such as medical imaging, landmine detector and material sciences [3, 8, 9, 10]. The PT is then defined (for example by [8]) through the following far-field expansion of u as

$$(u-H)(x) = \sum_{|i|,|j|=1}^{+\infty} \frac{(-1)^{|i|}}{i!j!} \partial_x^i \Gamma(x) M_{ij}(k,B) \partial^j H(0) \text{ as } |x| \to +\infty \tag{1.2}$$

for $i = (i_1, i_2, i_3)$, $j = (j_1, j_2, j_3)$ multi indices, Γ is a fundamental solution of the Laplacian and $M_{ij}(k, B)$ is the generalized polarization tensor (GPT).

Generally, the GPT is referred as the dipole in electromagnetic applications by physicists because it shows the distribution of the conductivity in $\mathbb{R}^3$ with the presence of B. Furthermore, the definition of GPT in (1.2) is extended by Ammari and Kang [8] through an integral equation over the boundary of B by

$$M_{ij} = \int_{\partial B} y^j \phi_i(y) d\sigma(y) \tag{1.3}$$

where $\phi_i(y)$ is given by

$$\phi_i(y) = (\lambda I - \mathcal{K}_B^*)^{-1}(v_x \cdot \nabla x^i)(y) \tag{1.4}$$

for $x, y \in \partial B$ with v_x is the outer unit normal vector to the boundary ∂B at x and λ is defined by $\lambda = (k+1)/2(k-1)$. $\mathcal{K}_B^*$ is a singular integral operator defined with Cauchy principal value $P.V.$ by

$$\mathcal{K}_B^* \phi(x) = \frac{1}{4\pi} P.V. \int_{\partial B} \frac{\langle x-y, v_x \rangle}{|x-y|^3} \phi(y) d\sigma(y) \tag{1.5}$$

for $\phi(x) \in L^2(\partial B)$ such that $L^2(\partial B)$ is the space of square integrable functions on ∂B.

Note that the GPT presented in this section is derived based on the asymptotic expansion of the solution u of (1.1). It can be applied to EIT and also in electro-sensing fish. Moreover, it is the fundamental to every other PT discussed in this study. The PT introduced from the time harmonic Maxwell's equations by Ammari, Vogelius and Volkov in [33] might be useful for the radar, GPR and microwave tomography while the PT for metal detection considered by Ledger and Lionheart [29] are based on the eddy current approximation to Maxwell's equations. However, we will see later on in this thesis that for some special cases, GPT somehow can be related to the other two PT.

1.3 Objectives of the Study

This thesis presents some mathematical aspects and a few applications of the PT. Generally, the studies in this thesis are conducted based on the following objectives :

a. to mathematically review the PT in the related applications.

b. to compute the first order GPT for three dimensional (3D) domains.

c. to describe objects presented in eletric or electromagnetic fields by the PT.

d. to discuss some potential applications of the PT.

e. to investigate a few properties of the PT.

Based on these objectives, a code is written each in *Matlab* and *Python* (specifically with *BEM++*) to compute the first order PT. Besides, some real applications of the PT specifically to identify and characterize objects are discussed. A few properties of the PT which are useful to further describe the objects are also investigated.

1.4 Contributions and Originality of the Research

The original contributions of the research are as follow. First of all, in order to review some properties of the first order PT, we develop a numerical method for computing it for 3D domains with *Matlab*. Alternatively, a method to compute the first order PT by using the terminologies of Boundary Element Method (BEM) with the code in *BEM++* is also presented. After that, we numerically fit an ellipsoid from a given first order PT where, some results about existence and uniqueness for the ellipsoid are highlighted and a strategy to numerically determine the ellipsoid is also given. Next, the first order PT with complex conductivity is investigated since this terminology could be useful in the applications of Maxwell's equations. We also further investigate the possible role of the first order PT with real and complex conductivity to the weakly electric fish in identifying and characterizing objects. Based on recent formulation of the PT for metal detection from the eddy current model, we also show numerical agreements between the PT computed by the new proposed formula with the PT obtained from metal detectors during experimental works and simulations conducted by the engineers. Finally, we numerically explore some invariants (rotation and translation) and material properties of the PT for the eddy current problems to hopefully improve metal detection and increase our understanding in using the PT in the future.

1.5 Thesis Outline

Following the previous objectives and contributions, this thesis is organized into 9 chapters. As usual, this chapter introduces the study for the thesis while the last chapter summarizes the study and recommends a few future works. The other eight chapters in the thesis are the contents of the study where, the contents can actually be divided into two parts according to the applications considered. Chapter 2 until Chapter 6 cover the PT for EIT (and also eletrosensing fish) whereas Chapter 7 and Chapter 8 cover for metal detection. Readers who are only interest with metal detection can start with Chapter 2 before jumping straight away to Chapter 7 and Chapter 8.

Chapter 2 basically reviews computational aspects and some properties of the first order PT for 3D domains. Following Chapter 2, Chapter 3 presents alternative method to numerically compute the 3D first order PT with *BEM++*. A strategy to fit ellipsoids with another objects based on the first order PT of the objects is given in Chapter 4. Next, a few numerical examples for the first order PT with complex conductivity and complex permittivity are given in Chapter 5 where, frequency response for the first order PT with complex permittivity are also investigated. We then demonstrate the first application of the PT considered in the study through our investigation on electrosensing fish in Chapter 6. The second application of the PT which is for metal detection is presented in Chapter 7. Finally, Chapter 8 explores a few properties of the PT, specifically for the eddy current problems.

Chapter 2

Some Properties of the 3D First Order GPT

An approach to determine the PT from solving integral equations (1.3), (1.4) and (1.5) has been recently introduced by Ammari and Kang [8]. Although the integrals can only be solved by numerical methods, finding the PT from these integrals also have other advantages such that the formulas depend only on the shape of the object B and the conductivity k whereas, solving (1.1) and using (1.2) to find the PT require more parameters of the problem. Previously, Capdeboscq et al. [34] has successfully developed an algorithm to numerically compute the GPT but only for two dimensional (2D) domains. Similarly, although Ammari and Kang [8] describe and apply GPT for many applications, most of the studies have focused on 2D problems. Therefore, this chapter presents a technique for computing specifically the first order GPT for 3D domains by numerical integration method according to (1.3), (1.4) and (1.5) to review a few of its properties before using it in the later applications of this study.

2.1 Preliminaries

We will recall some terminologies concerning the first order PT from [8] as they will be used to describe our results in this chapter.

2.1.1 The first order PT

At this stage, we will only focus on the first order PT and some of its properties. The first order PT can be evaluated by using (1.3) for $i, j = (1,0,0), (0,1,0)$ and $(0,0,1)$ so that $|i| = i_1 + i_2 + i_3 = 1 = |j|$. By combining all possible values of i and j, the first order PT denoted by M is a real 3×3 matrix in the form

$$M = \begin{bmatrix} M_{(1,0,0)(1,0,0)} & M_{(1,0,0)(0,1,0)} & M_{(1,0,0)(0,0,1)} \\ M_{(0,1,0)(1,0,0)} & M_{(0,1,0)(0,1,0)} & M_{(0,1,0)(0,0,1)} \\ M_{(0,0,1)(1,0,0)} & M_{(0,0,1)(0,1,0)} & M_{(0,0,1)(0,0,1)} \end{bmatrix}. \tag{2.1}$$

2.1.2 The explicit formula for the first order PT for ellipsoids

Suppose that B is an ellipsoid in the Cartesian coordinate system represented by $\frac{x^2}{a^2} + \frac{y^2}{b^2} + \frac{z^2}{c^2} = 1$ where a, b and c each is the length of semi principal axes of B such that $0 < c \leq b \leq a$. The first order PT of B at conductivity k is derived by [6] and is given in [8] in the form

$$M(k,B) = (k-1)|B| \begin{bmatrix} \frac{1}{(1-P)+kP} & 0 & 0 \\ 0 & \frac{1}{(1-Q)+kQ} & 0 \\ 0 & 0 & \frac{1}{(1-R)+kR} \end{bmatrix} \tag{2.2}$$

where $|B|$ is the volume of B while P, Q and R are constants defined by

$$\begin{aligned} P &= \frac{bc}{a^2} \int_1^{+\infty} \frac{1}{t^2 \sqrt{t^2 - 1 + (\frac{b}{a})^2} \sqrt{t^2 - 1 + (\frac{c}{a})^2}} dt, \\ Q &= \frac{bc}{a^2} \int_1^{+\infty} \frac{1}{(t^2 - 1 + (\frac{b}{a})^2)^{\frac{3}{2}} \sqrt{t^2 - 1 + (\frac{c}{a})^2}} dt, \\ R &= \frac{bc}{a^2} \int_1^{+\infty} \frac{1}{\sqrt{t^2 - 1 + (\frac{b}{a})^2} (t^2 - 1 + (\frac{c}{a})^2)^{\frac{3}{2}}} dt. \end{aligned} \tag{2.3}$$

By setting $a = b = c$ in (2.2), the first order PT for a sphere is also given in [8] as

$$M(k,B) = (k-1)|B| \begin{bmatrix} \frac{3}{2+k} & 0 & 0 \\ 0 & \frac{3}{2+k} & 0 \\ 0 & 0 & \frac{3}{2+k} \end{bmatrix}. \tag{2.4}$$

2.1.3 Symmetry, positivity and transformation of the first order PT

This section gives several properties of the first order PT. These properties have already been proven by Ammari and Kang [8]. They are restated here in the following theorems.

Theorem 1. *The first order PT is a symmetrical matrix.*

Theorem 2. *Let R be a unitary matrix transformation of a domain B and R^T is the transpose of R such that $B' = RB$. If $M(k, B)$ and $M(k, B')$ are the first order PT associated to domains B and B' respectively for a conductivity* $0 < k \neq 1 < +\infty$ *then* $M(k, B') = RM(k, B)R^T$.

Theorem 3. *The first order PT is positive definite when* $k > 1$ *while it is negative definite when* $0 < k < 1$.

2.2 Numerical Method and Matrices

In order to review the previous properties of the 3D first order PT, we first discuss the procedures to numerically compute the first order PT for a 3D domain according to (1.3), (1.4) and (1.5) in this section. As we need to perform integrations over the boundary of an object B, the discretization of the boundary of the object into triangular elements will be discussed first. Besides, some properties of elementary linear algebra which will be used to describe the first order PT are also stated in this section.

2.2.1 Triangularization of an object

The boundary of a 3D object is actually a surface. For the purpose of computation, the surface is discritized into a finite number of triangles by using *Netgen Mesh Generator* [35] (see Figure 2.1 for example). After the geometry of an object in a `.geo` file is created (some examples are given in the manual [36]) and loaded to *Netgen*, a mesh of triangular elements for the surface of the object can be automatically generated and the information about the triangular elements will then be used to calculate the first order PT for the object. In order to get a better approximation for the boundary, the mesh can be refined in *Netgen* however with some limitations, for example, user cannot

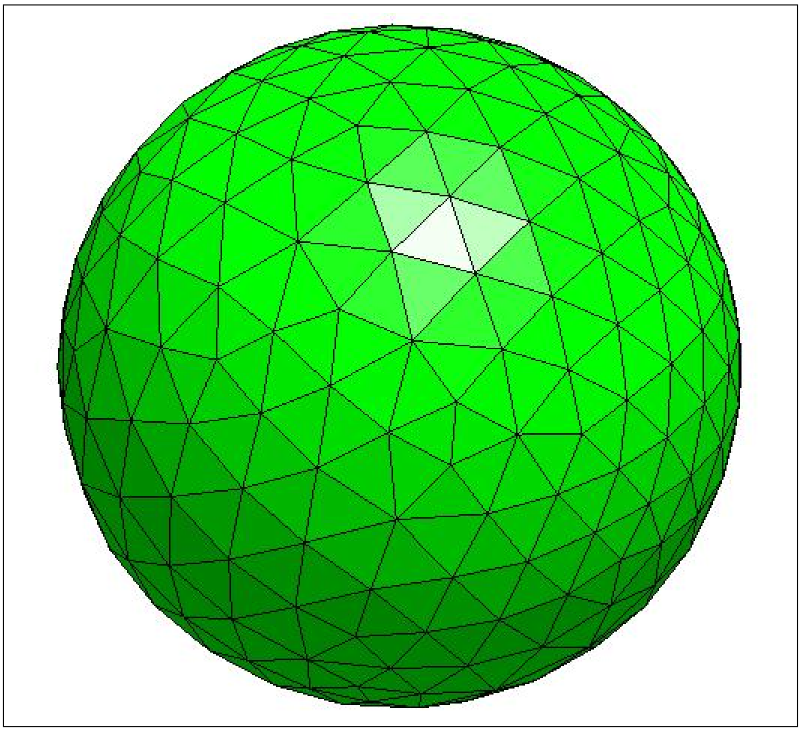

Figure 2.1: Triangularization of a sphere with 620 surface elements

exactly set the number of the elements for the mesh. Table 2.1 shows an improvement of the surface area of a triangularized sphere with radius 1 to the exact surface area, $4\pi = 12.5714$ as the number of the elements for the mesh increase. This suggests that uniformly increasing the number of elements for the mesh will give more accurate results.

Table 2.1: The approximated surface area for a triangularized sphere

Total Surface Elements	Approximated Surface Area
122	11.9546
242	12.2488
620	12.4405

2.2.2 Numerical approximation of the 3D first order PT

After the mesh with `N` elements (which are triangles) for the boundary of the chosen object B is created, by adapting collocation method in [37] to approximate Fredholm integral equation of the first kind and using quadrature method for surface integrals with piecewise constant basis function (see [38]), (1.5) is firstly expressed as

$$\mathcal{K}_B^*\phi(x_s) = \frac{1}{4\pi}\left(w_t\frac{\langle x_s - x_t, v_{x_s}\rangle}{|x_s - x_t|^3}\right) \tag{2.5}$$

for $s = 1, ..., \mathtt{N}$ and $t = 1, ..., \mathtt{N}$. Here, each x_s and x_t is the barycentre for the s-th and t-th element respectively, v_{x_s} is the outer unit normal vector to the s-th element and w_t is the area of t-th element. Moreover, $\langle x_s - x_t, v_{x_s}\rangle$ denotes the dot product between vectors $x_s - x_t$ and v_{x_s} while $|x_s - x_t|$ is the distance between x_s and x_t. Consequently, (2.5) is a $\mathtt{N} \times \mathtt{N}$ matrix in the form

$$\mathcal{K}_B^*\phi(x_s) = \frac{1}{4\pi}\begin{bmatrix} w_1K(x_1,x_1) & \dots & w_NK(x_1,x_N) \\ \vdots & \ddots & \vdots \\ w_1K(x_N,x_1) & \cdots & w_NK(x_N,x_N) \end{bmatrix} \tag{2.6}$$

where $K(x_s, x_t) = \frac{\langle x_s - x_t, v_{x_s}\rangle}{|x_s - x_t|^3}$ for $s = 1, ..., \mathtt{N}$, $t = 1, ..., \mathtt{N}$. However, due to the singularity, $K(x_s, x_t)$ for every $s = t$ cannot be calculated. Therefore, an analytic procedure is used to approximate $K(x_s, x_t)$ for $s = t$ by solving the original integral equation (1.5) over a plane triangle. This approach is briefly explained in the next lemma and will actually result all diagonals element of (2.6) to be equal to 0.

Lemma 1. *If T is a plane triangle and v_x is the outward unit normal vector to T at x, then for any $y \in T$*

$$P.V.\int_T \frac{\langle x - y, v_x\rangle}{|x - y|^3} dA_T(y) = 0. \tag{2.7}$$

Proof. In order to evaluate the Cauchy principal integral (2.7), consider a ball with radius ϵ and centered at $x \in T$ denoted by $B_\epsilon(x)$. Then for any $y \in T$,

$$P.V.\int_T \frac{\langle x-y,v_x\rangle}{|x-y|^3} dA_T(y) = \lim_{\epsilon\to 0^+}\int_{T\cap B_\epsilon(x)'} \frac{\langle x-y,v_x\rangle}{|x-y|^3} dA_T(y)$$

where $B_\epsilon(x)'$ is the complement of $B_\epsilon(x)$. However, $|x - y| \neq 0$ but $\langle x - y, v_x\rangle = (x - y)\cdot v_x = 0$ for any $x, y \in T \cap B_\epsilon(x)'$. Therefore,

$$\lim_{\epsilon\to 0^+}\int_{T\cap B_\epsilon(x)'} \frac{\langle x-y,v_x\rangle}{|x-y|^3} dA_T(y) = \lim_{\epsilon\to 0^+} 0 = 0.$$

□

Next, for a choosen k, (1.4) is solved for $\phi_i(y)$ by using $\mathcal{K}_B^*$ in (2.6) and since $\mathcal{K}_B^*\phi(x_s)$ is $\mathtt{N} \times \mathtt{N}$ matrix, I then must be the identity matrix of size $\mathtt{N}$. Note that $(v_x \cdot \nabla x^i)(y)$ is the derivative of every point $x \in \partial B$ to the power of index i in the direction v_x, the outer unit normal vector to ∂B at x. This expression can be easily computed for the first order PT such that when $i = (1,0,0), (0,1,0)$ and $(0,0,1)$ by using properties of indices. This will only yield $(v_x \cdot \nabla x^i)(y)$ to be the first, second and third component of v_x. Therefore, due to the triangularization of the surface, for $i = (1,0,0), (0,1,0)$ and $(0,0,1)$, the solution to the system of equations (1.4) can be expressed in the form of $\mathtt{N}\times 3$ matrix $\phi_i(y) = (\lambda I - \mathcal{K}_B^*)^{-1}(v_{x_t})$ or equivalently as follows

$$\phi_i(y) = \left[(\lambda I - \mathcal{K}_B^*)^{-1}(v_{x_t}^{\text{1st}}) \;\vdots\; (\lambda I - \mathcal{K}_B^*)^{-1}(v_{x_t}^{\text{2nd}}) \;\vdots\; (\lambda I - \mathcal{K}_B^*)^{-1}(v_{x_t}^{\text{3rd}})\right] \tag{2.8}$$

where the columns are $(\lambda I - \mathcal{K}_B^*)^{-1}$ multiply by the first, second and third component of v_{x_t} for every $t = 1, ...\mathtt{N}$.

Finally, by applying the same quadrature rule to (1.3), the first order PT of a 3D object B at conductivity k denoted by $M(k, B)$ can be approximated by

$$M(k,B) = \sum_{t=1}^{\mathtt{N}} w_t y_t^j \phi_i(y). \tag{2.9}$$

when $i, j = (1,0,0), (0,1,0)$ and $(0,0,1)$. However, (2.9) can be further simplified by considering all combinations between i and j. Notice that $y_t^{(1,0,0)}$, $y_t^{(0,1,0)}$ and $y_t^{(0,0,1)}$ each is actually the x-coordinate, y-coordinate and z-coordinate of the barycentre of the t-th element. So, by expanding (2.9) and using (2.8), (2.9) can be obtained through matrix multiplication

$$M(k,B) = [\phi_i(y)]^T D(w) B(y) \tag{2.10}$$

where the $3\times\mathtt{N}$ matrix $[\phi_i(y)]^T$ is the transpose of (2.8), $D(w)$ is the diagonal $\mathtt{N}\times\mathtt{N}$ matrix with the $t-th$ diagonal is the surface area w_t of the $t-th$ element and $B(y)$ is a $\mathtt{N}\times 3$ matrix containing x-coordinate, y-coordinate and z-coordinate of the barycentre of the t-th element in each of its column. This will imply (2.10) is exactly in the same form as (2.1).

2.2.3 Positive-definite and rotation matrix

Two properties of matrices from linear algbera given in [39, 40], which will be used later on in this chapter are recalled and stated in the next definitions.

Definition 1. *Rotation Matrix in 3D*

The following rotation matrices rotate vectors in 3D by an angle θ about the x,y and z-axis.

$$R_x(\theta) = \begin{bmatrix} 1 & 0 & 0 \\ 0 & \cos\theta & -\sin\theta \\ 0 & \sin\theta & \cos\theta \end{bmatrix}.$$

$$R_y(\theta) = \begin{bmatrix} \cos\theta & 0 & \sin\theta \\ 0 & 1 & 0 \\ -\sin\theta & 0 & \cos\theta \end{bmatrix}.$$

$$R_z(\theta) = \begin{bmatrix} \cos\theta & -\sin\theta & 0 \\ \sin\theta & \cos\theta & 0 \\ 0 & 0 & 1 \end{bmatrix}.$$

Definition 2. *Positive and Negative-definite Matrix*

A square real matrix A is positive definite if for all non-zero vector $\boldsymbol{v} \in \mathbb{R}^3$, $\boldsymbol{v}^T A\boldsymbol{v} > 0$. In contrast, A is negative definite if $\boldsymbol{v}^T A\boldsymbol{v} < 0$.

2.3 Results and Discussions

In order to investigate whether the approximated first order PT is influenced by the conductivity k, by following [34], the first order PT for a sphere is firstly approximated in *Matlab* based on the previous proposed method at various conductivities k and compared with the analytical formula (2.4). Then, the first order PT for a few ellipsoids are approximated and compared to the analytical solutions where the analaytical solutions are obtained by transforming the first order PT for elliposid in (2.2). The positivity and negativity of the first order PT in Theorem 3 are also tested for a few approximated first order PT.

2.3.1 The approximated first order PT for a sphere

The first order PT for the sphere $x^2 + y^2 + z^2 = 1$ is approximated in *Matlab* with different total elements, `N` for the mesh at conductivities $k = 0.000001$, 0.00005, 0.01, 0.08, 0.2, 1.00004, 1.5, 8, 15, 100, 500 and 10000. For these computations, the sphere is triangularized three different times in *Netgen* by `moderate`, `fine` and `very fine meshing option` to consist 122, 242 and 620 total elements. Figure 2.2 compares between values of the diagonals of the first order PT for the sphere approximated in *Matlab* (on a mesh with total elements `N` = 122, 242 and 620) and values of the diagonals obtained from (2.4) as the conductivity increased, while Figure 2.3 compares between the non-diagonals.

Based on Figure 2.2, we can see that performing the calculation by using larger `N` will give better approximation to the diagonals of the first order PT for the sphere at every conductivity k. Furthermore, all graphs in Figure 2.2 (a), Figure 2.2 (b) and Figure 2.2 (c) are similar and thus consistent with the analytical solution of the first order PT for the sphere in (2.4) that has the same diagonals. Moreover, by following (2.4), the figures also indicate that the approximated first order PT for the sphere approaches respectively to $-2\pi = -6.2857$ and to $4\pi = 12.5714$ as $k \to 0$ and as $k \to \infty$. On the other hand, using more `N` does not generally produce better approximation to the non-diagonals of the first order PT for the sphere at every conductivity k as given by Figure 2.3. However, the non-diagonals are small and closer to 0 as required by the analytical solution (2.4). In addition, the non-diagonals become more symmetrical when larger `N` is used as required by Theorem 1. Generally, all elements of the approximated first order PT for the sphere are much closer to the analytical solution whenever the conductivity is less than and around 1. In this case, this result is similar to the approximated first order PT for 2D cases by [34].

Figure 2.4 next shows the error, e between the analytic first order PT, M given by (2.4) and the approximated first order PT, $\bar{M}$ (on the mesh with `N`=122, 242 and 620) against conductivity k where $e = \left\|M - \bar{M}\right\|_2 / \left\|M\right\|_2$. Here, $\|A\|_2$ denotes the entry-wise norm $\sqrt{\sum_{i=1}^{3}\sum_{j=1}^{3}|A_{ij}|^2}$ for the 3×3 matrix A. Based on the figure, when `N` is increased, e is unbounded as $k \to 0$ but the values for e as $k \to 0$ are still small. On the other hand, at k near 1 and as $k \to \infty$, e for the approximated first order PT decreases when `N` is increased. But, e decreases faster at k near 1 than e as $k \to \infty$ when `N` increased. According to Ammari and Kang [8], the operator $\lambda I - \mathcal{K}_B^*$ is one to one and also invertible on $L^2(\partial B)$ when $-\infty < \lambda \leq -(1/2)$ and $(1/2) < \lambda < +\infty$ so, the solution to (1.4) exists and is unique for $\lambda > (1/2)$ (or $k > 1$) and $\lambda \leq -(1/2)$ (or

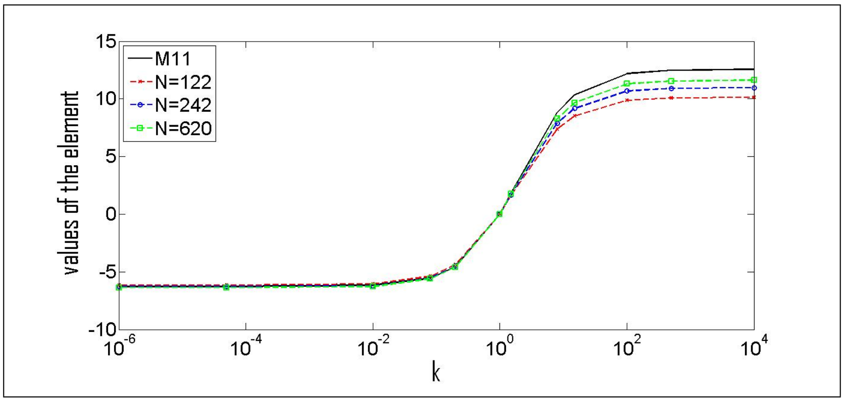

(a)

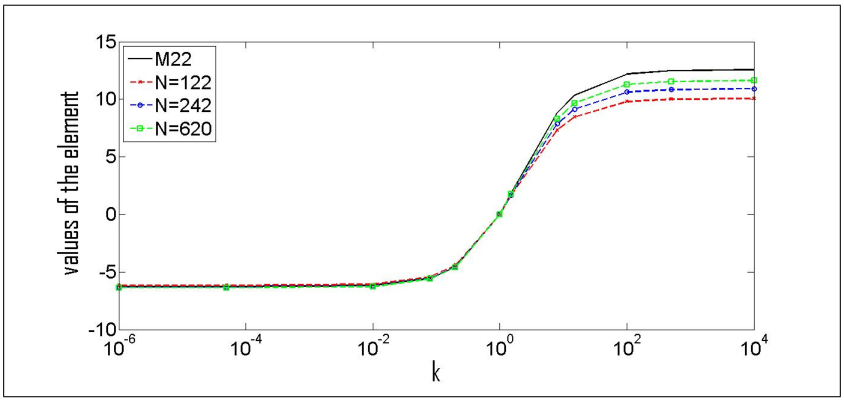

(b)

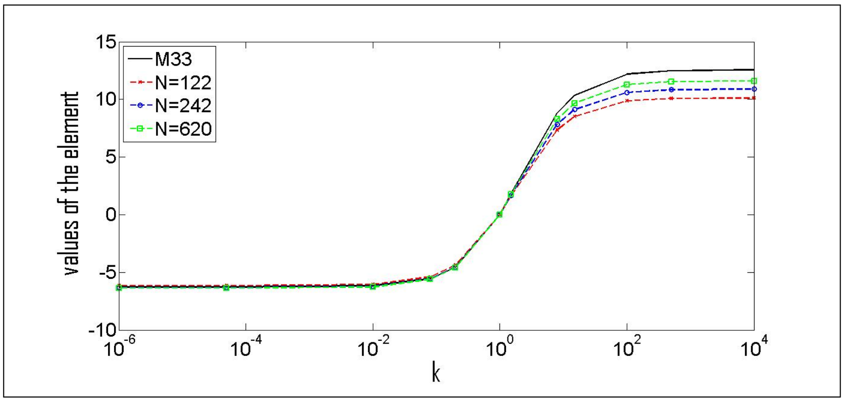

(c)

Figure 2.2: The diagonals of the approximated first order PT for a sphere triangularized by 122, 242 and 620 elements and the diagonals of the analytic first order PT (M11, M22 and M33) against conductivity, k (a) first diagonal (b) second diagonal (c) third diagonal

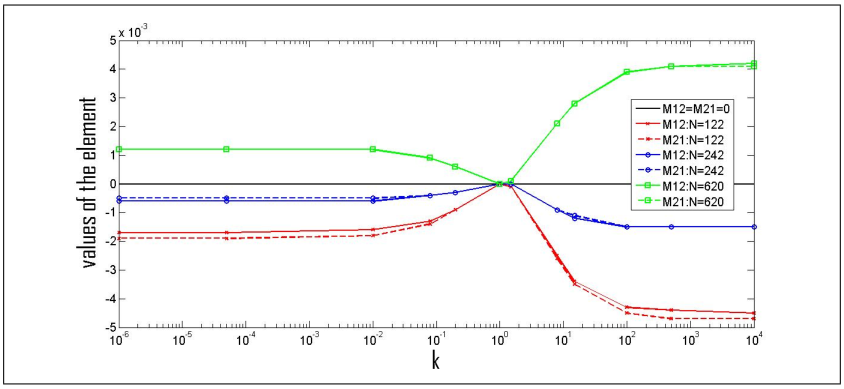

(a)

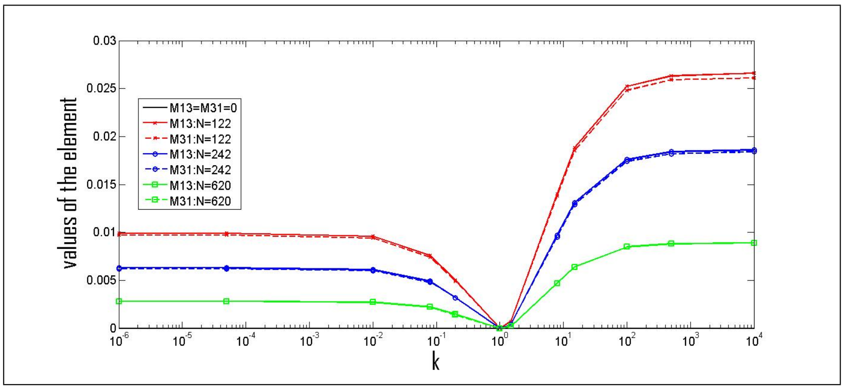

(b)

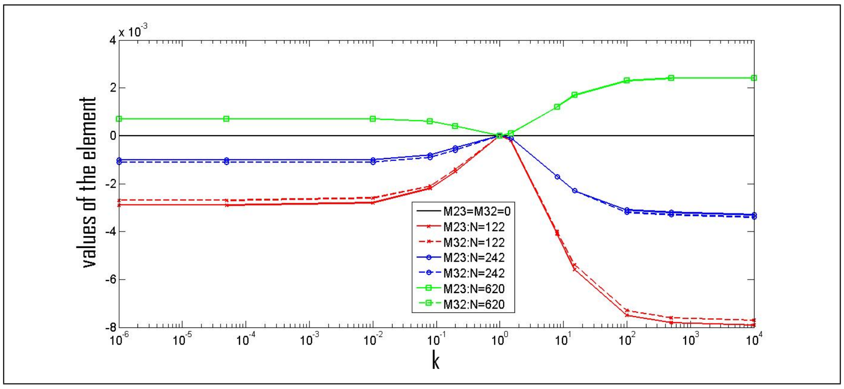

(c)

Figure 2.3: The non-diagonals of the approximated first order PT for a sphere triangularized by 122, 242 and 620 elements and the non-diagonals of the analytic first order PT (M12, M13, M21, M23, M31 and M32) against conductivity, k (a) element in the first row-second column, M12 and element in the second row-first column, M21 (b) element in the first row-third column, M13 and element in the third row-first column, M31 (c) element in the second row-third column, M23 and element in the third row-second column, M32

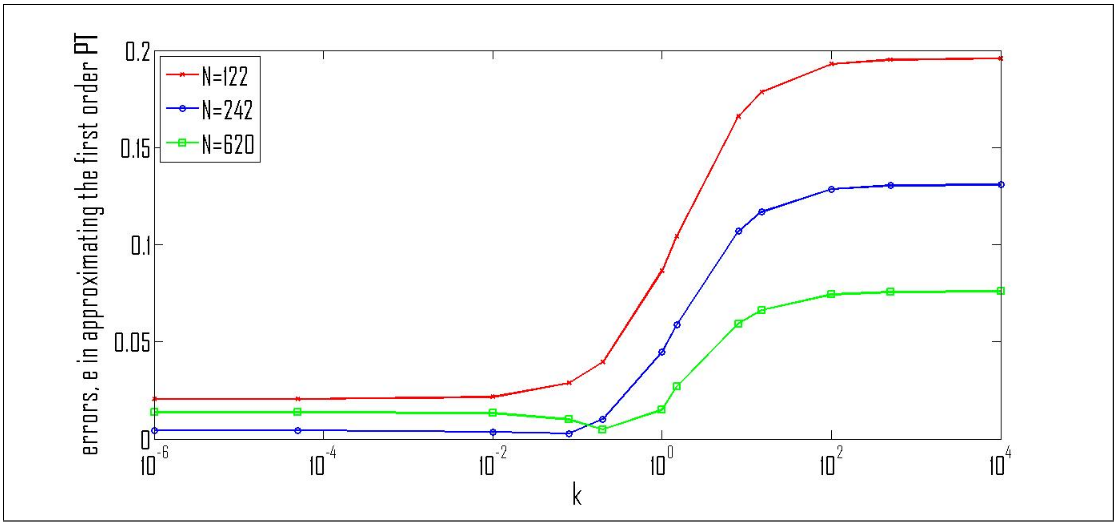

Figure 2.4: The error, e when the first order PT for the sphere of radius 1 is approximated on the mesh with 122, 242 and 620 triangles against conductivity, k

$0 \leq k < 1$) where in our case, $0 < k \neq 1 < +\infty$. However, it is less efficient to solve (1.4) as $\lambda \to (1/2)$ due to the singularity of the operator $\lambda I - \mathcal{K}_B^*$ as $\lambda \to (1/2)$. This is because the operator $\lambda I - \mathcal{K}_B^*$ is not invertible at $\lambda = (1/2)$ (as $k \to +\infty$).

Moreover, based on Lemma 1, the singular integrals in (2.6) are approximated by 0 on the mesh of a finite number of flat triangles with this method. However, the singular integral (1.5) is non-zero for an object that has curved boundary segments so, the results from this method will be less accurate for the mesh of objects that have curved boundary segments. Therefore, in the next chapter, we will present an alternative method to improve the approximation of the 3D first order PT, especially at high conductivity k.

2.3.2 Transformation of the first order PT for ellipsoids

Since the proposed method produces better approximation at conductivity k around 1, we create mesh of `N` elements by using `very fine meshing option` in *Netgen* for ellipsoids $(\frac{x}{2})^2 + (\frac{y}{3})^2 + z^2 = 1$, $x^2 + (\frac{y}{2})^2 + (\frac{z}{3})^2 = 1$ and $(\frac{x}{3})^2 + y^2 + (\frac{z}{2})^2 = 1$ and approximate their first order PT at conductivity 1.5 to further investigate the method. Since these ellipsoids do not satisfy condition $0 < c \leq b \leq a$, formula (2.2) cannot be used to determine their analytical first order PT. Therefore, we firstly use (2.2) to determine analytically the first order PT for ellipsoid $(\frac{x}{3})^2 + (\frac{y}{2})^2 + z^2 = 1$ at $k = 1.5$ and denote it as $M(E, 1.5)$. As $(\frac{x}{3})^2 + (\frac{y}{2})^2 + z^2 = 1$ can be rotated to produce all

Table 2.2: The analytic first order PT for rotated $(\frac{x}{3})^2 + (\frac{y}{2})^2 + z^2 = 1$

Ellipsoid, B'	Relation	$M(1.5, B')$
$(\frac{x}{2})^2 + (\frac{y}{3})^2 + z^2 = 1$	$R_z(90°)M(1.5, B)R_z^T(90°)$	$\begin{bmatrix} 11.0856 & 0 & 0 \\ 0 & 11.6555 & 0 \\ 0 & 0 & 9.7544 \end{bmatrix}$
$x^2 + (\frac{y}{2})^2 + (\frac{z}{3})^2 = 1$	$R_y(90°)M(1.5, B)R_y^T(90°)$	$\begin{bmatrix} 9.7544 & 0 & 0 \\ 0 & 11.0856 & 0 \\ 0 & 0 & 11.6555 \end{bmatrix}$
$(\frac{x}{3})^2 + y^2 + (\frac{z}{2})^2 = 1$	$R_x(90°)M(1.5, B)R_x^T(90°)$	$\begin{bmatrix} 11.6555 & 0 & 0 \\ 0 & 9.7544 & 0 \\ 0 & 0 & 11.0856 \end{bmatrix}$

$(\frac{x}{2})^2 + (\frac{y}{3})^2 + z^2 = 1$, $x^2 + (\frac{y}{2})^2 + (\frac{z}{3})^2 = 1$ and $(\frac{x}{3})^2 + y^2 + (\frac{z}{2})^2 = 1$, the first order PT for $(\frac{x}{3})^2 + (\frac{y}{2})^2 + z^2 = 1$, $M(E, 1.5)$ can be used to determine the analytical first order PT at conductivity 1.5 for the other three ellipsoids by using Theorem 2 and Definition 1 (see Table 2.2). Here, the rotation matrix from Definition 1 used in Theorem 2 to obtain the analytic first order PT for each ellipsoid is also shown in Table 2.2.

For each ellipsoid B' in Table 2.2, we then show the agreement between all elements of the approximated and analytic first order PT for B' in Figure 2.5 (a), Figure 2.5 (b) and Figure 2.5 (c) where in each graph, the elements for both approximated and analytic first order PT are denoted by mij for $i, j = 1, 2, 3$. Note that directly using formula (2.2) and neglecting the condition $0 < c \leq b \leq a$ to determine the analytic first order PT for ellipsoids B' will lead to the same results as in Table 2.2. Therefore, we will simply use formula (2.2) for any ellipsoids in this thesis later on.

2.3.3 Positivity and negativity of the first order PT

It can be seen from (2.2) and (2.4) that the first order PT for sphere and ellipsoid satisfy the positivity and negativity of the first order PT as stated in Theorem 3. In order to further explore positivity and negativity of the first order PT for other objects, we approximate the first order PT at the same value of conductivities as in Section

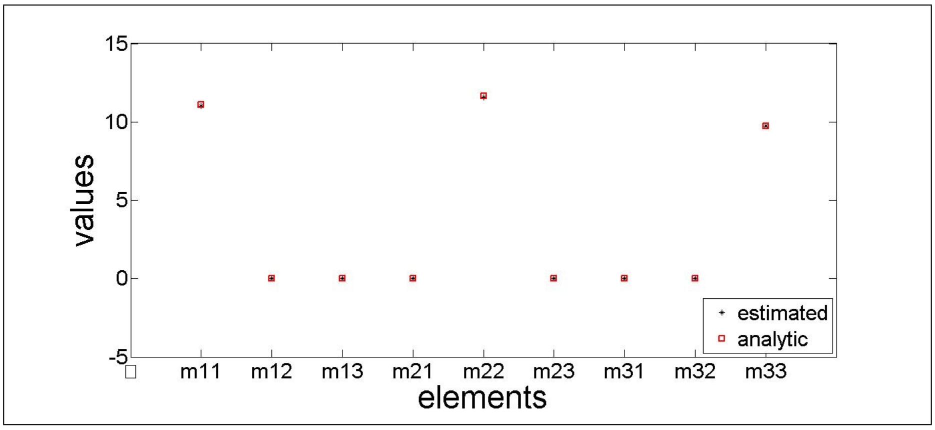

(a)

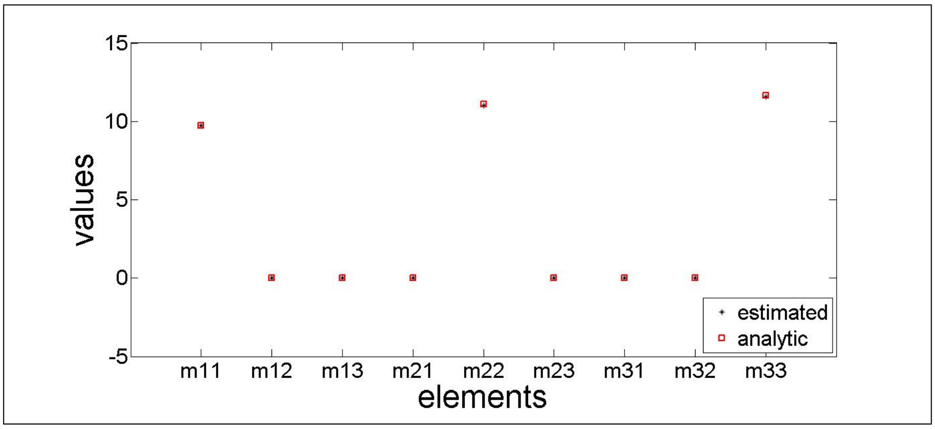

(b)

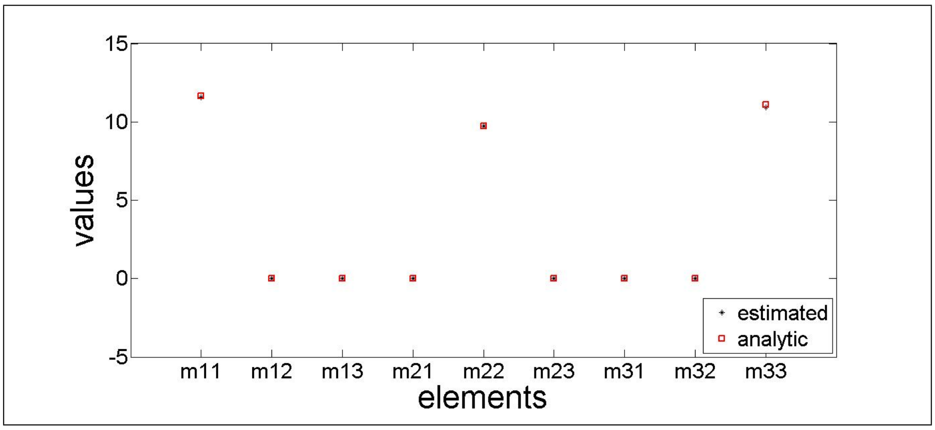

(c)

Figure 2.5: The approximated first order PT and the analytical first order PT both at conductivity 1.5 for (a) $(\frac{x}{2})^2 + (\frac{y}{3})^2 + z^2 = 1$ (triangularized by `N`=8342 elements) (b) $x^2 + (\frac{y}{2})^2 + (\frac{z}{3})^2 = 1$ (triangularized by `N`=8882 elements) (c) $(\frac{x}{3})^2 + y^2 + (\frac{z}{2})^2 = 1$ (triangularized by `N`=7870 elements)

2.3.1 for a few common objects in the engineering applications which are cube with dimension $2 \times 2 \times 2$, cylinder with both diameter and height equal to 2 and hemisphere with radius 1.5. Each object is firstly triangularized by `very fine meshing option`.

Figure 2.6, Figure 2.7 and Figure 2.8 show the values of all elements of the approximated first order PT as conductivity increased for the cube, cylinder and hemisphere. By examining Figure 2.6, Figure 2.7 and Figure 2.8, it can be seen that the non-diagonals for each approximated first order PT are small. We now assume that the non-diagonals for every approximated first order PT to be zero so that each approximated first order PT is a diagonal matrix. For $0 < k < 1$, every diagonal element of the approximated first order PT for each object is negative as shown in the figures whereas the diagonal elements of every approximated first order PT when $k > 1$ are positive. In this case, we can now use Theorem 3 and Definition 2 to show that the approximated first order PT for each object is positive definite for $k > 1$ and negative definite for $0 < k < 1$.

2.4 Conclusions

In this chapter, we have reviewed some mathematical properties of the 3D first order PT. In order to achieve this purpose, we first approximate the first order PT for some objects based on the explicit formula given in [8] by using numerical method of integration with *Matlab*. Moreover, we also describe some properties of the first order PT by adapting properties of matrices.

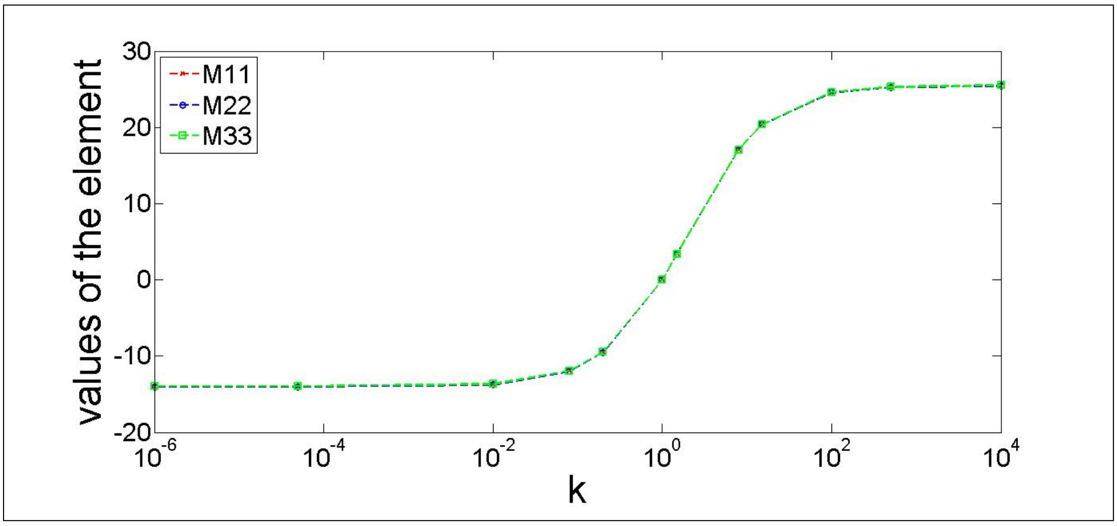

(a)

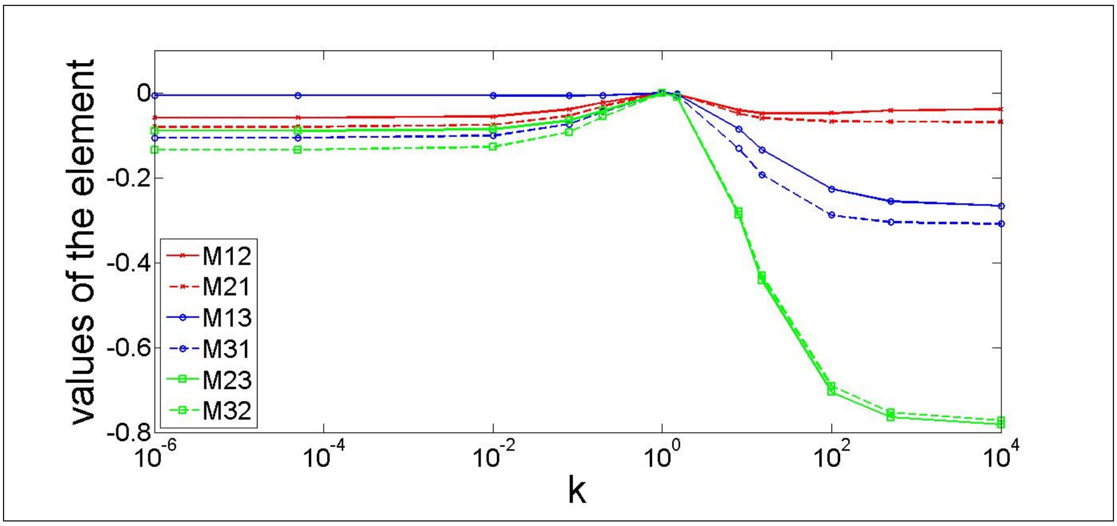

(b)

Figure 2.6: The approximated first order PT for a cube with N=106 at different conductivities, k (a) diagonals (b) non-diagonals

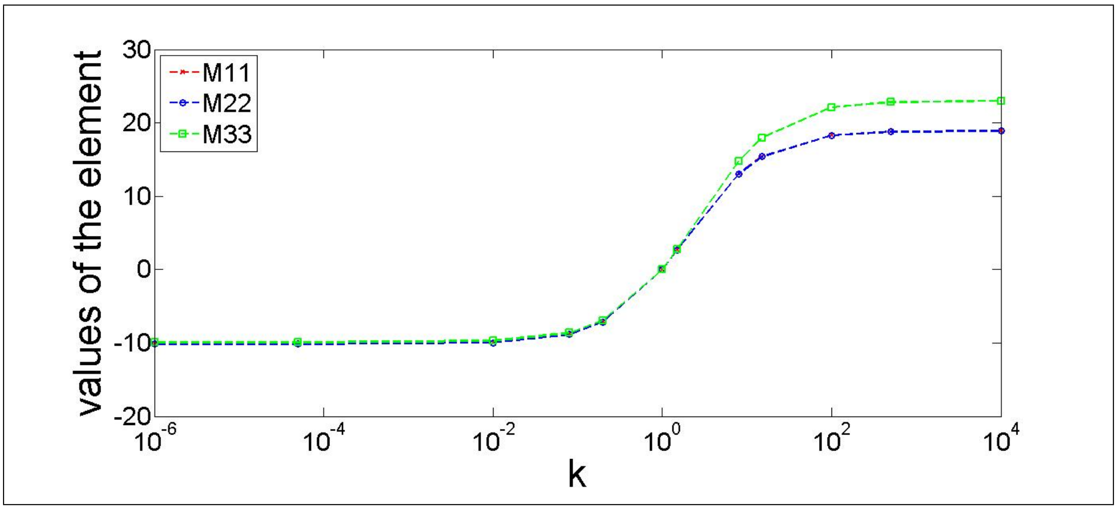

(a)

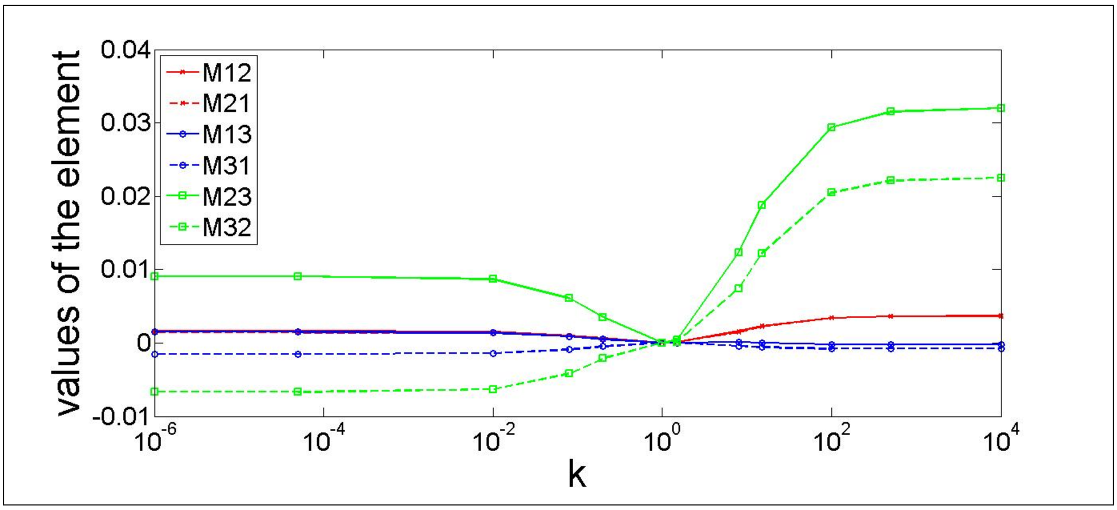

(b)

Figure 2.7: The approximated first order PT for a cylinder with `N`=942 at different conductivities, k (a) diagonals (b) non-diagonals

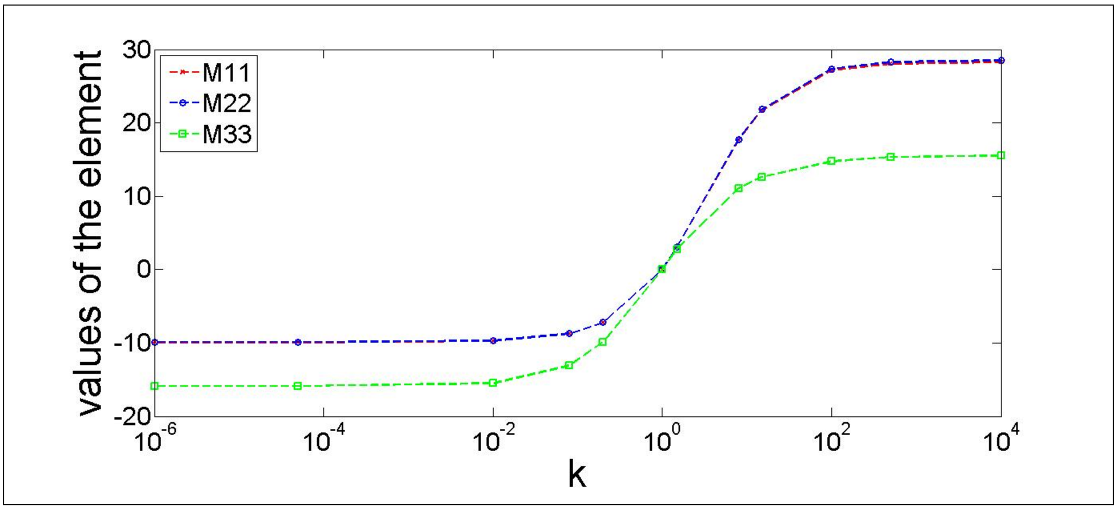

(a)

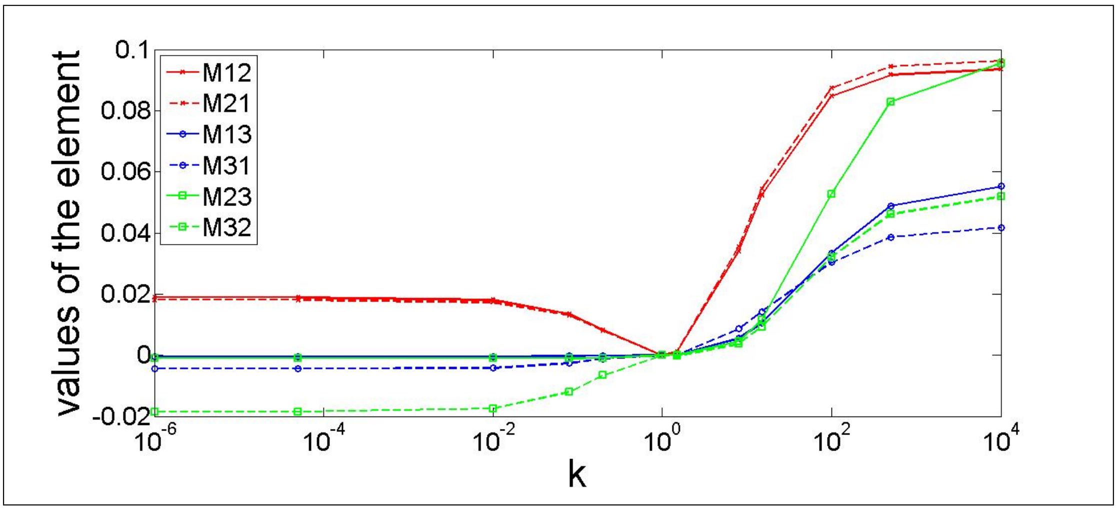

(b)

Figure 2.8: The approximated first order PT for a hemisphere with `N`=458 at different conductivities, k (a) diagonals (b) non-diagonals

Chapter 3

Computing the 3D First Order PT with *BEM++*

In the previous chapter, we have developed a numerical method to compute the 3D first order PT. The results from the method show that the first order PT can be accurately computed at conductivity, k around 1 and is less efficient for other values of k especially when $k \to +\infty$. However, in order to apply it in the related applications for this study, it is neccessary to accurately compute the first order PT at high conductivity. Since the first order PT is defined through boundary integral operators, we then refer to Rjasanow and Steinbach [38] and apply some terminologies of the Boundary Element Method (BEM) to improve our computation. We also use the recent object oriented code for BEM called as *BEM++* [41] to easily execute our new method. Consequently, we have successfully improved the approximated first order PT at any level of conductivity. In this chapter, we will discuss this alternative method to compute the first order PT for 3D domains with *BEM++*.

3.1 Boundary Element Method

BEM is generally used to solve PDEs that can be formulated as boundary integral equations. It emphasizes a few aspects such as expressing a solution of a PDE as boundary integral equations and also methods of approximating the boundary integral equations (see [42] and more recent in [38]). For the purpose of this study, we first restate the following useful lemma from [38].

Lemma 2. *Let $H^{1/2}(\Gamma)$ be the Sobolev space and let $H^{-1/2}(\Gamma)$ be the dual space of $H^{1/2}(\Gamma)$ where Γ is the boundary of a Lipschitz domain Ω. There exist a boundary integral operator $\gamma\tilde{V} : H^{-1/2}(\Gamma) \to H^{-1/2}(\Gamma)$ such that for $w \in H^{-1/2}(\Gamma)$, there holds the representation*

$$\gamma(\tilde{V}w)(x) = \frac{1}{2}w(x) + (K'w)(x)$$

in the sense of $H^{-1/2}(\Gamma)$. Here, $(K'w)(x)$ is the adjoint double layer potential defined by

$$(K'w)(x) = \frac{1}{4\pi} P.V. \int_\Gamma \frac{\langle y - x, v_x \rangle}{|x - y|^3} w(y) ds_y$$

for $x \in \Gamma$.

Note that the Sobolev space in Lemma 2 is defined in [43].

It is given in [38] that the boundary operator $\gamma\tilde{V}w$ is bounded for all $w \in H^{-1/2}(\Gamma)$. This implies that the adjoint double layer potential $(K'w)(x)$ where $K' : H^{-1/2}(\Gamma) \to H^{-1/2}(\Gamma)$ is also bounded for all $w \in H^{-1/2}(\Gamma)$. On the other hand, it is shown in [8] that the boundary integral operator $\mathcal{K}_B^*\phi(x)$ is bounded for all $\phi \in L^2(\partial B)$. For the purpose of this study, we adapt Lemma 2 to extend (1.5) so that $\mathcal{K}_B^*\phi(x) = -(K'w)(x)$ for all $\phi \in H^{-1/2}(\Gamma)$. Similary, $\mathcal{K}_B^* : H^{-1/2}(\Gamma) \to H^{-1/2}(\Gamma)$ is also bounded.

Meanwhile, instead of using (1.3) – (1.5), Ammari and Kang [8] have also proposed to determine the PT (the GPT) by solving transmission boundary value problem of the Laplace's equation. This suggests to implement BEM to compute the PT. However, according to Ammari and Kang [8], solving the transmission problem to find the PT is actually equivalent with using formula (1.3) – (1.5).

3.2 Approximating the First Order PT in *BEM++*

BEM++ is an object oriented code in *C++* for BEM and is developed by Śmigaj et al. [41]. The current version of the code contains many terminologies of BEM, for example as described in [38]. Instead of *C++*, the script for using *BEM++* can also be written in *Python* as an interface to the code. After a mesh for the boundary of an object is loaded to it, the code can then construct, discritize and approximate a few boundary integral operators, at the moment, only for problems in Laplace and Helmholtz equations. Moreover, it can also solve the system of equations. Besides, it offers shorter command to construct and discritize the boundary integral operators than the code for our previous method in *Matlab*. A few examples for constructing and discretizing boundary integral operators with *BEM++* can be found in [41].

In this study, rather than solving the transmission problem step by step, some terminologies of BEM are adapted to numerically compute the first order PT from (1.3) – (1.5) with *BEM++*. First of all, we use the result for BEM in Lemma 2 given by [38] to discritize and approximate (1.5) with *BEM++*. We then proceed by solving (1.5) and finally approximate (1.3) with *BEM++*. The steps to prepare a code in *BEM++* for this purpose will now be explained in this section. For this purpose, we refer to [41] for detail descriptions about our commands in the script to run *BEM++*.

We choose to write a script in *Python* for using the codes of *BEM++* and compute the first order PT for an object at specificied conductivity k. After installing *BEM++* (it is downloaded from *www.bempp.org*), all necessary modules for *BEM++* in the script are set similarly to the script for solving interior Dirichlet problem of the Laplace equation in [41]. We then proceed by loading the mesh of a choosen object with `N` surface elements from a file generated by *Netgen* in the `.msh` format where, the file consists a list of nodes and triangles for the boundary of the object (at the moment, only mesh with linear elements is supported by *BEM++*).

In order to solve for $\phi_i(y)$ from (1.4) with *BEM++*, we first consider (1.4) as

$$(\lambda I - \mathcal{K}_B^*)\phi_i(y) = (v_x \cdot \nabla x^i)(y). \tag{3.1}$$

It is recommended by [38] to approximate a function which is discontinuous on the mesh of the boundary such as $(v_x \cdot \nabla x^i)(y)$ by a piecewise constant basis function. This suggests to approximate $(\lambda I - \mathcal{K}_B^*)^{-1}$ by a piecewise constant basis function as well. Moreover, it is given in [38] that the natural discretisation space for $H^{-1/2}$ is also a piecewise constant basis function. Therefore, we choose to approximate $\mathcal{K}_B^*$ by a piecewise constant basis function since $\mathcal{K}_B^* : H^{-1/2}(\Gamma) \to H^{-1/2}(\Gamma)$.

Now, the boundary integral operator $\mathcal{K}_B^*$ in (1.5) is defined as the negative of adjoint double layer potential in *BEM++*. Both $\mathcal{K}_B^*$ and the identity operator I are then created as `boundary operators` in the script as well as approximated and discretized by space of piecewise constant basis functions. After that, the boundary integral operator $(\lambda I - \mathcal{K}_B^*)$ can then be created at specificied conductivity k. Here, $(\lambda I - \mathcal{K}_B^*)$

is implicitly approximated and discretized by space of piecewise constant basis functions like $\mathcal{K}_B^*$ and I. The steps produce $(\lambda I - \mathcal{K}_B^*)$ as $\mathtt{N} \times \mathtt{N}$ matrix.

Recall that $\phi_i(y)$ of (1.4) for the first order PT reduces to

$$\phi_i(y) = (\lambda I - \mathcal{K}_B^*)^{-1}(\nu_x). \tag{3.2}$$

In order to obtain $\phi_i(y)$ in *BEM++*, each component of ν_x is now defined as `grid functions` and approximated at each element of the boundary by piecewise constant basis function in the script. Using these approximations, (3.2) is rewritten as

$$(\lambda I - \mathcal{K}_B^*)\phi_i(y) = \nu_x \tag{3.3}$$

and for each component of ν_x, (3.3) is solved for $\phi_i(y)$ by using the function `solver` in *BEM++*.

Finally, in order to evaluate and approximate (1.3), we consider y^j as $y^j(y)$ and expand it in a basis of piecewise linear continuous functions $\{g_k(y)\}_1^N$ so that

$$y^j(y) = \sum_k y_{jk} g_k(y). \tag{3.4}$$

Substituting (3.4) in (1.3) gives

$$M_{ij} = \sum_k y_{jk} \int_{\partial B} g_k(y)\phi_i(y)d\sigma(y). \tag{3.5}$$

In *BEM++*'s terminology, the values $\int_{\partial B} g_k(y)\phi_i(y)d\sigma(y)$ are the 'projection' of $\phi_i(y)$ on the basis $\{g_k(y)\}_1^N$ and are called in the script by the function `projections` for each column $\phi_i(y)$. On the other hand, the values y_{jk} are the 'coefficients' of y^j on the basis $\{g_k(y)\}_1^N$ and are called for each y^j in the script by the function `coefficients`. The first order PT, M can then be obtained by multiplying the coefficients and the projections according to (2.1) using the standard function `np.dot` in the script.

3.3 Results and Discussions

We provide several numerical examples about the approximated first order PT by *BEM++* in this section. First of all, the approximated first order PT for a few ellipsoids at $k = 1.5$ are computed and compared where, $k = 1.5$ (k near 1) is choosen to ensure more accurate results for the approximation as shown in the previous chapter. After that, we compare and discuss the approximated first order PT for the sphere by considering the following cases :

i. at $k = 1.5$ on the mesh with different number of elements

ii. at different conductivity k on the mesh consisting 9920 elements

3.3.1 The approximated first order PT for ellipsoids

We start by computing the first order PT for four types of ellipsoid at conductivity 1.5 by using analytical formula (2.2), our previous method in *Matlab* and our recent method in *BEM++*. Each ellipsoid is firstly triangularized with the `fine meshing option` in *Netgen* before numerically computed by *Matlab* and *BEM++* where for each ellipsoid, the same mesh is used in both *Matlab* and *BEM++*. In order to easily compare the first order PT approximated by *Matlab* and *BEM++* with the analaytical solutions, all elements of the first order PT approximated by the two methods and also from the analytical solution (2.2) are plotted in the same graph for each ellipsoid. These are shown in Figure 3.1, Figure 3.2, Figure 3.3 and Figure 3.4 respectively. In these figures, elements of the first order PT are denoted as mij for $i, j = 1, 2, 3$.

Based on Figure 3.1, it can be seen that all elements of the approximated first order PT for $\frac{x^2}{9} + \frac{y^2}{4} + z^2 = 1$ computed either by *Matlab* or *BEM++* are close to the elements of the analytical solutions except for m22 where, m22 is closer to the analytical solution when computed by *BEM++*. For $\frac{x^2}{4} + \frac{y^4}{4} + z = 1$, the diagonals of the first order PT approximated in *Matlab* and *BEM++* differ only slightly with the diagonals of the first order PT for the analytical solution as shown in Figure 3.2. Besides, the diagonals of the approximated first order PT for $x^2 + y^2 + \frac{z^2}{4} = 1$ computed by *BEM++* in Figure 3.3 have only a small difference with the same elements of the analytical and *Matlab*'s solution. In contrast, Figure 3.4 indicates that the diagonals of the first order PT for $x^2 + y^2 + y^2 = 1$ approximated either in *Matlab* or *BEM++* have a big difference with the same elements of the analytical solution but these approximations look closer to the analytical solutions when computed by *BEM++*. We also want to highlight that in each figure, all non-diagonal elements of the approximated first order PT for every ellipsoid computed either by *Matlab* or *BEM++* are zero as required by the analytical solutions.

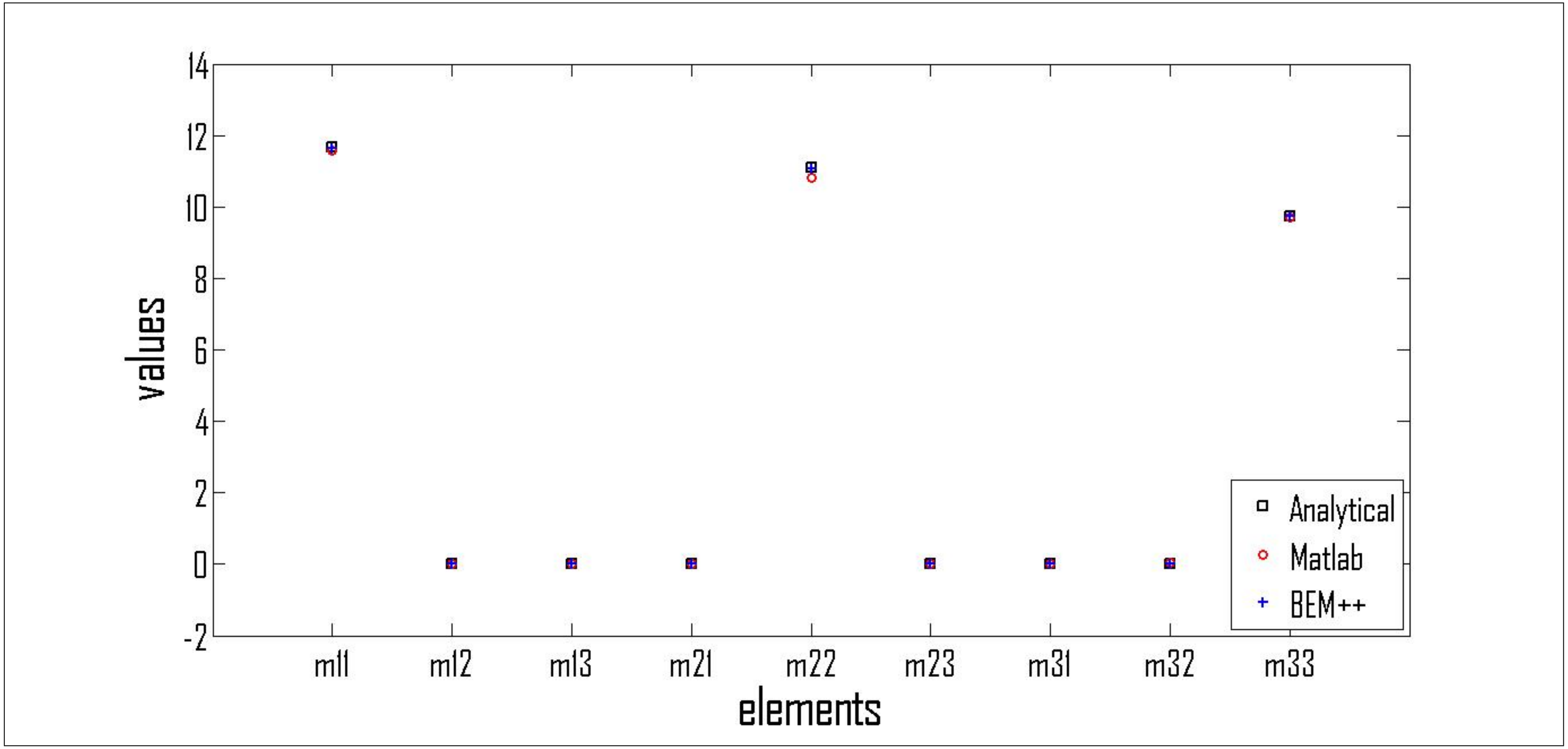

Figure 3.1: The approximated first order PT by *Matlab* and *BEM++* for the scalene ellipsoid $\frac{x^2}{9} + \frac{y^2}{4} + z^2 = 1$ (mesh with 7806 total elements) at $k = 1.5$ and the analytical solution

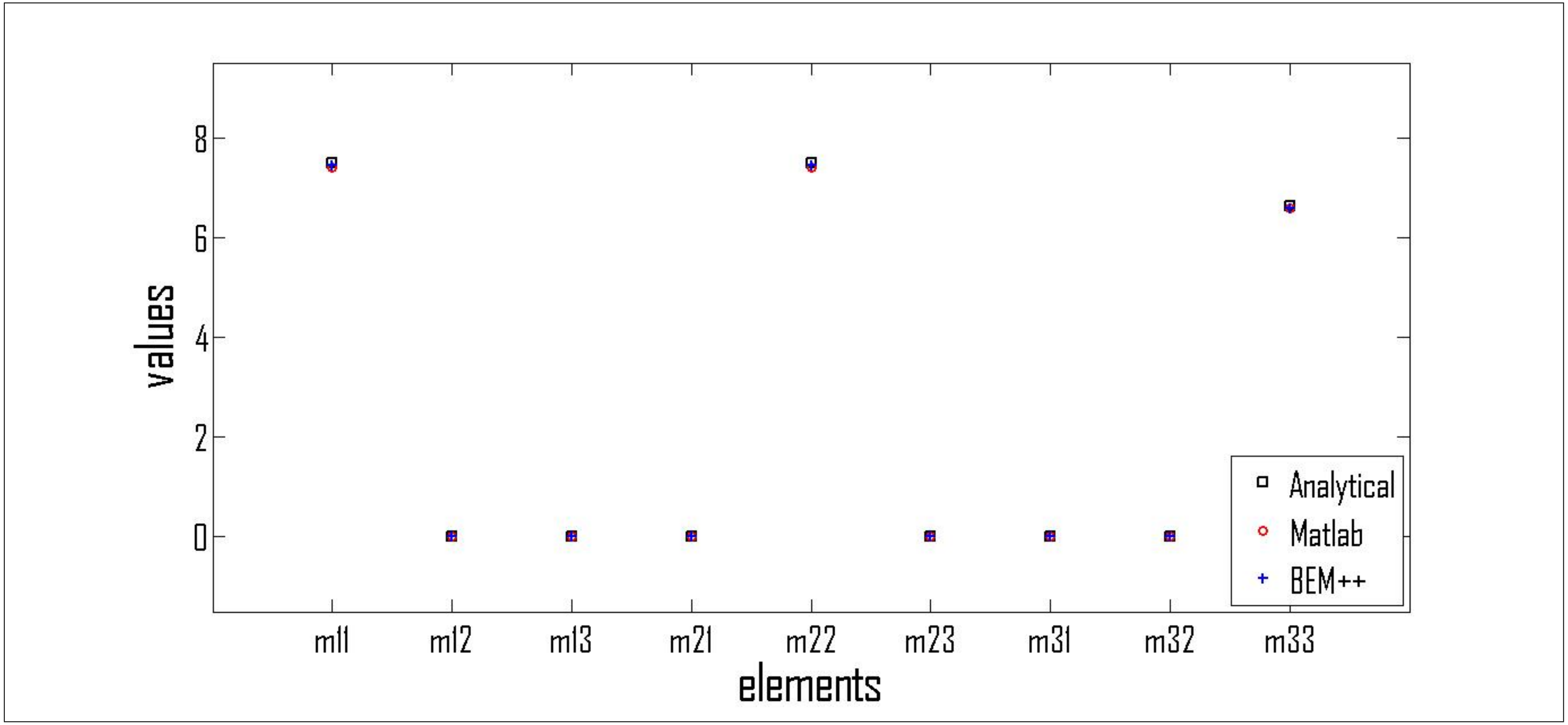

Figure 3.2: The approximated first order PT by *Matlab* and *BEM++* for the oblate ellipsoid $\frac{x^2}{4} + \frac{y^2}{4} + z^2 = 1$ (mesh with 2608 total elements) at $k = 1.5$ and the analytical solution

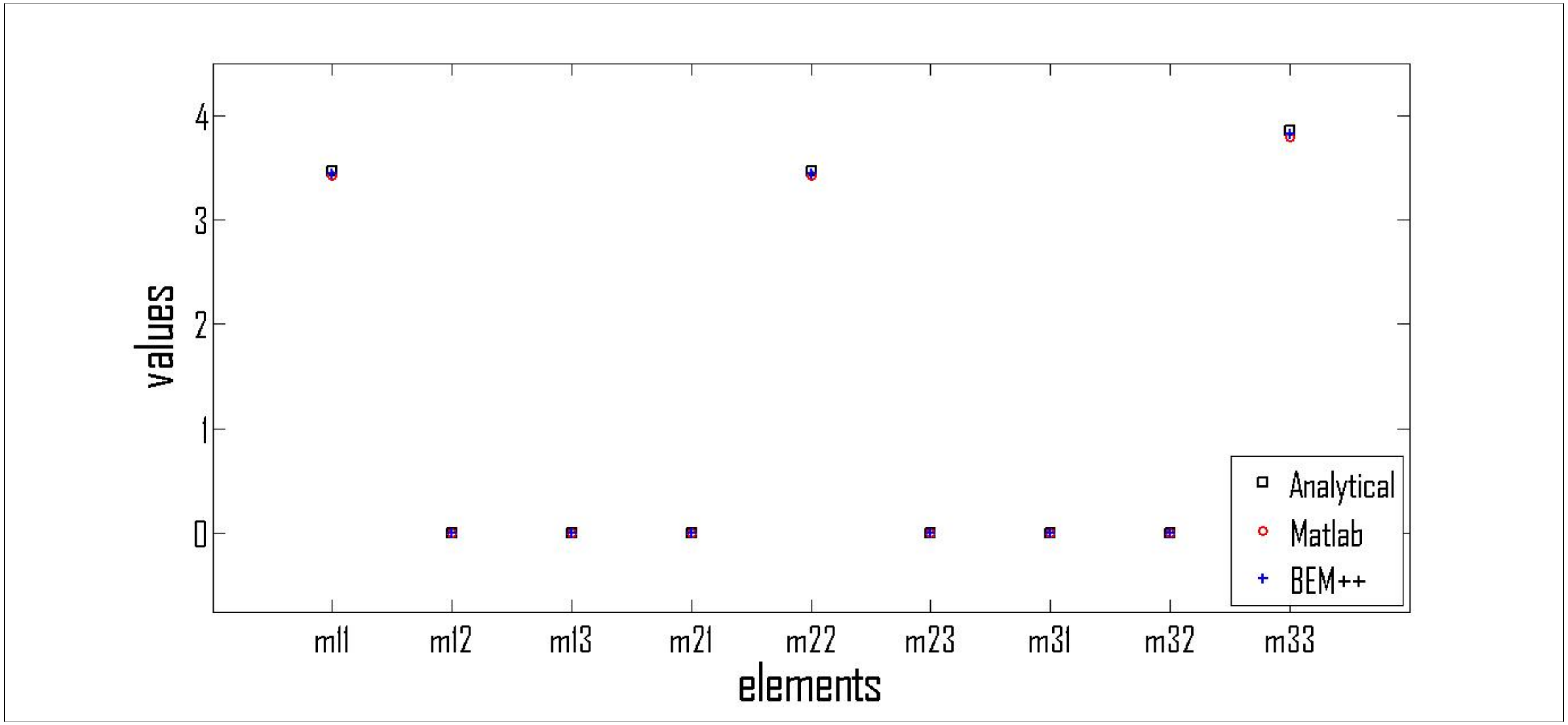

Figure 3.3: The approximated first order PT by *Matlab* and *BEM++* for the prolate ellipsoid $x^2 + y^2 + \frac{z^2}{4} = 1$ (mesh with 1722 total elements) at $k = 1.5$ and the analytical solution

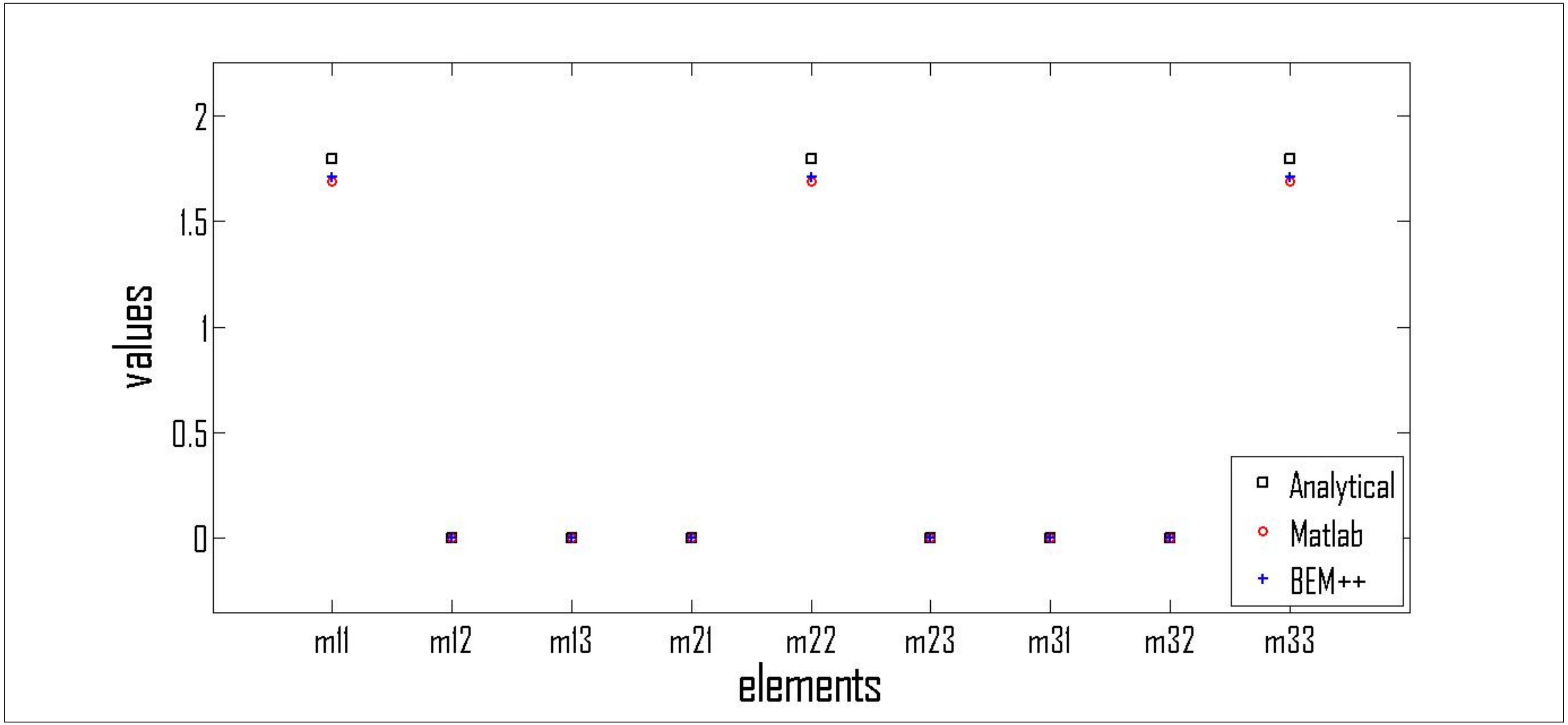

Figure 3.4: The approximated first order PT by *Matlab* and *BEM++* for the sphere $x^2 + y^2 + y^2 = 1$ (mesh with 242 total elements) at $k = 1.5$ and the analytical solution

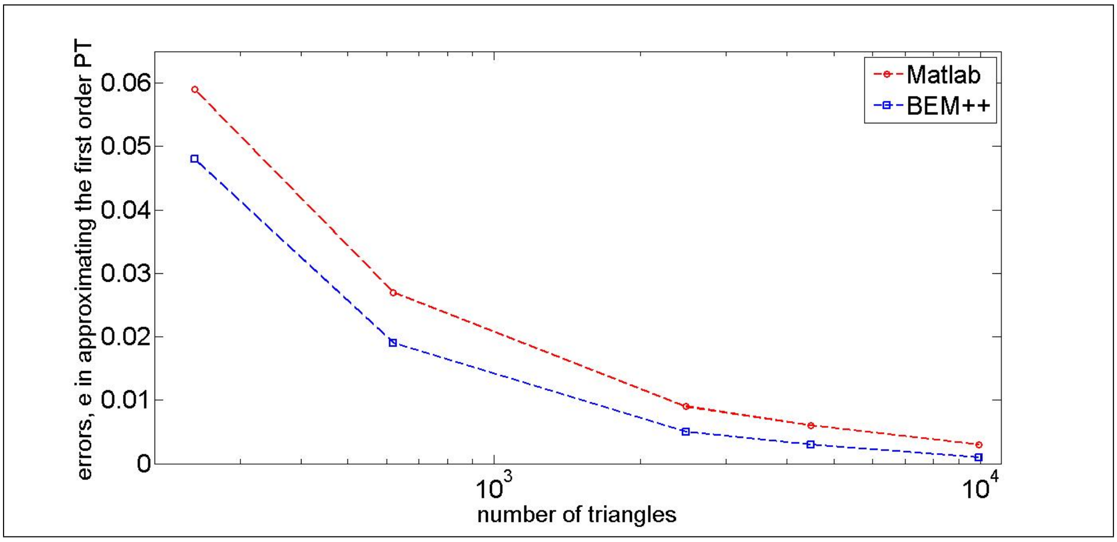

Figure 3.5: The error, e when the first order PT for the sphere of radius 1 is approximated at $k = 1.5$ by both *Matlab* and *BEM++* on the mesh consisting 242, 620, 2480, 4480 and 9920 triangles against the number of triangles

3.3.2 Increasing the number of triangles `N`

One possible way to theoretically improve the approximation of the first order PT for a triangularized object is to increase the number of triangles used during the triangularization. In this section, we compute the first order PT for the sphere $x^2 + y^2 + y^2 = 1$ at conductivity $k = 1.5$ by our previous method in *Matlab* and also by *BEM++* with different number of triangles used for the mesh and compare the results with the analytical solution (2.4). For this purpose, five triangularized spheres $x^2 + y^2 + y^2 = 1$ consisting 242, 620, 2480, 4480 and 9920 triangles are considered where the mesh with 2480, 4480 and 9920 triangles are specifically generated by `refine mesh option` in *Netgen*.

In order to make comparisons, by using the entry-wise norm for the 3×3 matrix A defined by $\|A\|_2 = \sqrt{\sum_{i=1}^{3}\sum_{j=1}^{3}|A_{ij}|^2}$, we compute the error $e = \left\|M - \bar{M}\right\|_2 / \|M\|_2$ between the analytic first order PT, M and the approximated first order PT, $\bar{M}$ (by both *Matlab* and *BEM++*) for each mesh. Here, the analytic M is computed based on (2.4). After that, the error e is then plotted against the number of triangles for each mesh in Figure 3.5. Based on the curves in Figure 3.5, we can see that e decreases as the number of triangles used for the mesh increases when approximating the first order PT for the sphere at $k = 1.5$ by both *Matlab* and *BEM++*. However, e are smaller when the first order PT for the sphere are approximated by *BEM++* for each mesh.

3.3.3 Changing conductivity k

In the previous chapter, we have found that the conductivity of the object also influences its approximated first order PT. Thus, we will compute the first order PT for the sphere $x^2 + y^2 + y^2 = 1$ by *Matlab* and *BEM++* with a mesh of 9920 triangles at different values of conductivity and compare the results with the analytical solution to further investigate the approximated first order PT. In this case, 9920 triangles are used to ensure better approximation both in *Matlab* and *BEM++*. Here, we again evaluate the first order PT for the sphere at conductivities 0.000001, 0.00005, 0.01, 0.08, 0.2, 1.00004, 1.5, 8, 15, 100, 500 and 10000 as in the previous chapter. Figure 3.6 and Figure 3.7 shows the results of our computations.

All diagonal elements of the approximated first order PT (by both *Matlab* and *BEM++*) and also the analytical values for all diagonals against conductivities are given in Figure 3.6. Here, all diagonals from the analytical solution in each graph of Figure 3.6 are the same but only change according to the conductivity based on formula (2.4). According to these graphs, we can see that every diagonal of the approximated first order PT computed either by *Matlab* or *BEM++* is close to the analytical solutions except at some high conductivities when computed by *Matlab*.

On the other hand, the non-diagonal elements of the first order PT for the sphere approximated in both *Matlab* and *BEM++* are only equal to zero as required by the analytical solution at conductivities near to 1 and these are shown in Figure 3.7. However, all non-diagonal elements which are non-zero are symmetrical at four decimal places when approximated by both methods. When computed by *Matlab*, the non-diagonal elements have a small difference with the analytical solution at conductivities less than one and have a greater difference when conductivities are greater than 1. In contrast, although the non-diagonal elements approximated in *BEM++* have a slight difference with the analytical solutions at conductivities greater than 1, they are equal to zero for conductivities less than 1 except for elements (1)(3) (element in the first row and third column) and (3)(1) (element in the third row and first column). Obviously, the non-diagonal elements computed by *BEM++* are closer to zero than the one computed by *Matlab* at all conductivities.

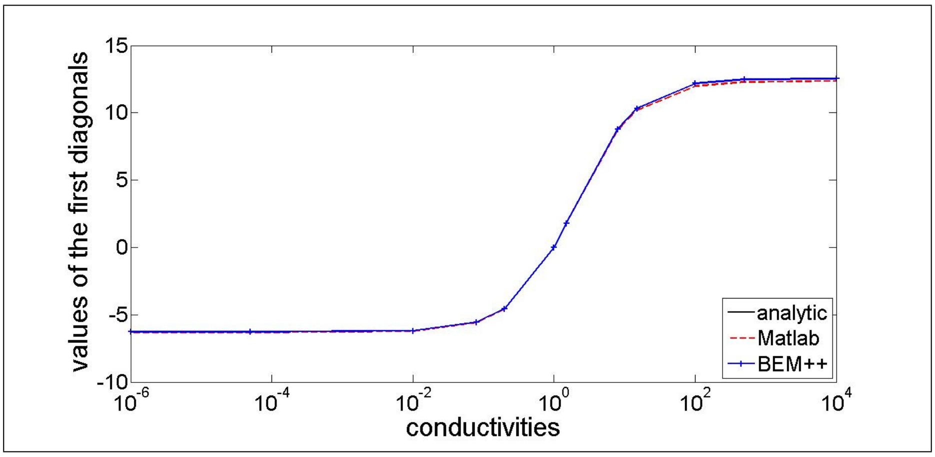

(a)

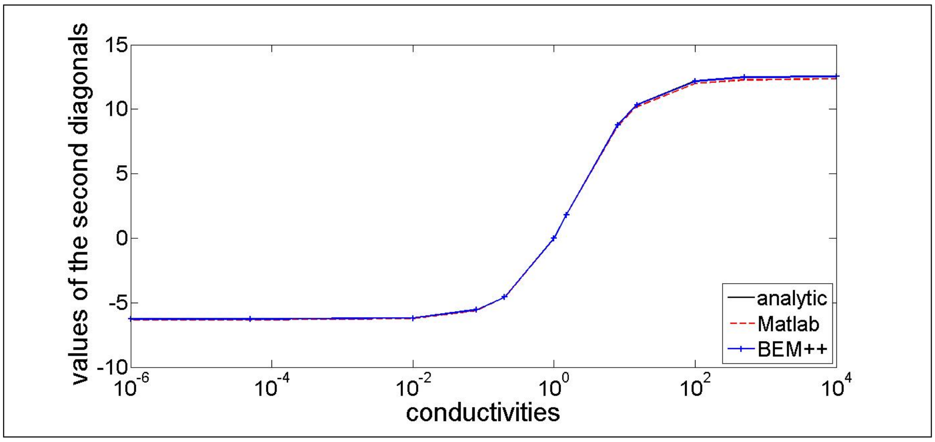

(b)

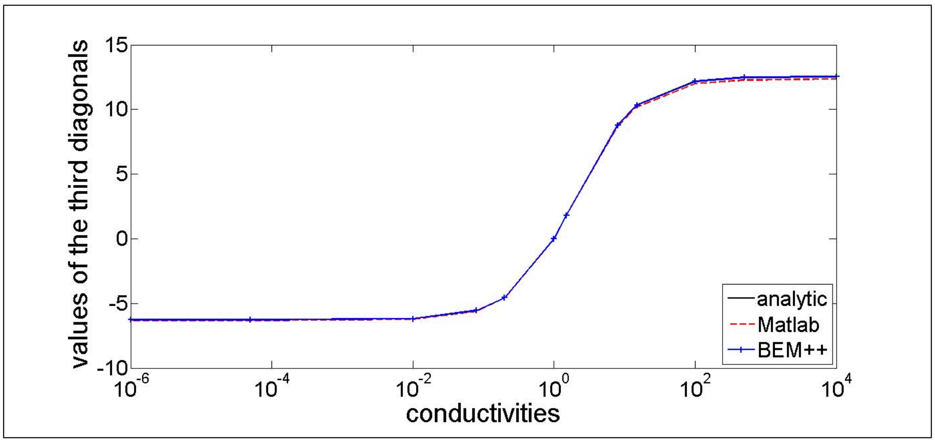

(c)

Figure 3.6: Diagonal elements of the analytical solutions and the approximated first order PT by *Matlab* and *BEM++* for the sphere $x^2 + y^2 + y^2 = 1$ (mesh with 9920 triangles) against conductivities

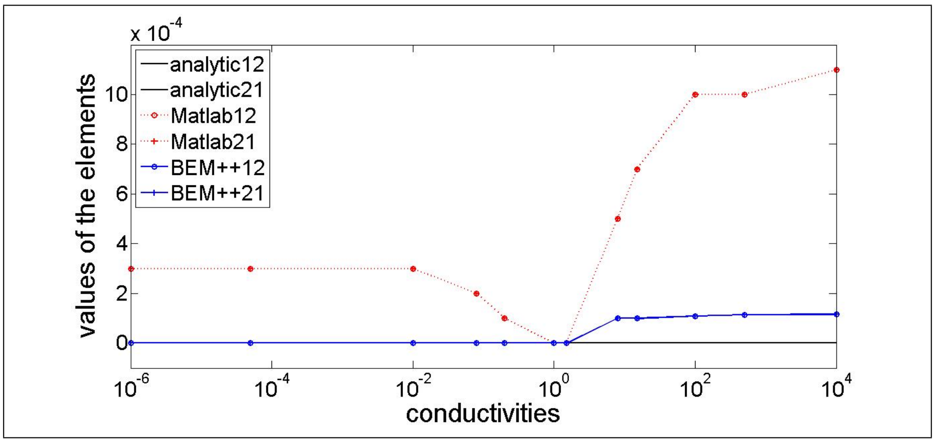

(a)

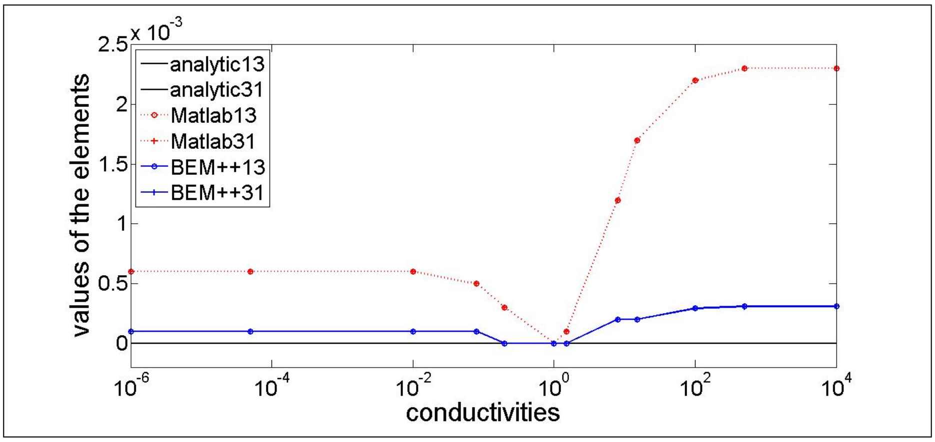

(b)

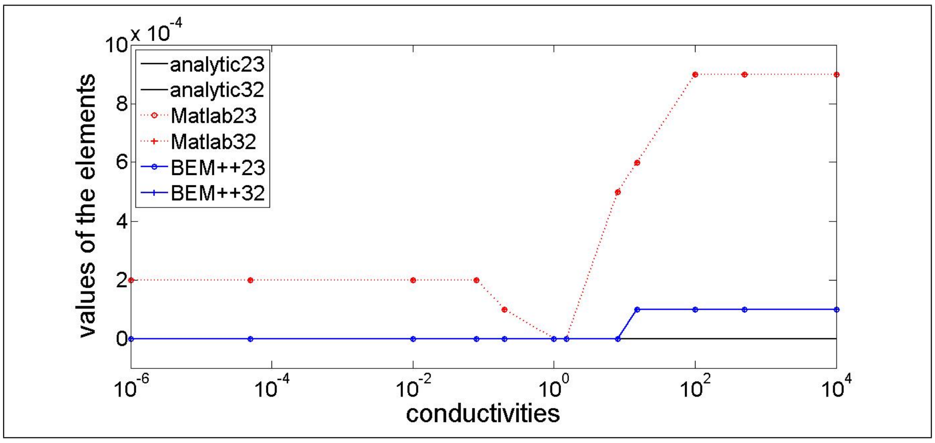

(c)

Figure 3.7: Non-diagonal elements of the analytical solutions and the approximated first order PT by *Matlab* and *BEM++* for the sphere $x^2 + y^2 + y^2 = 1$ (mesh with 9920 triangles) against conductivities

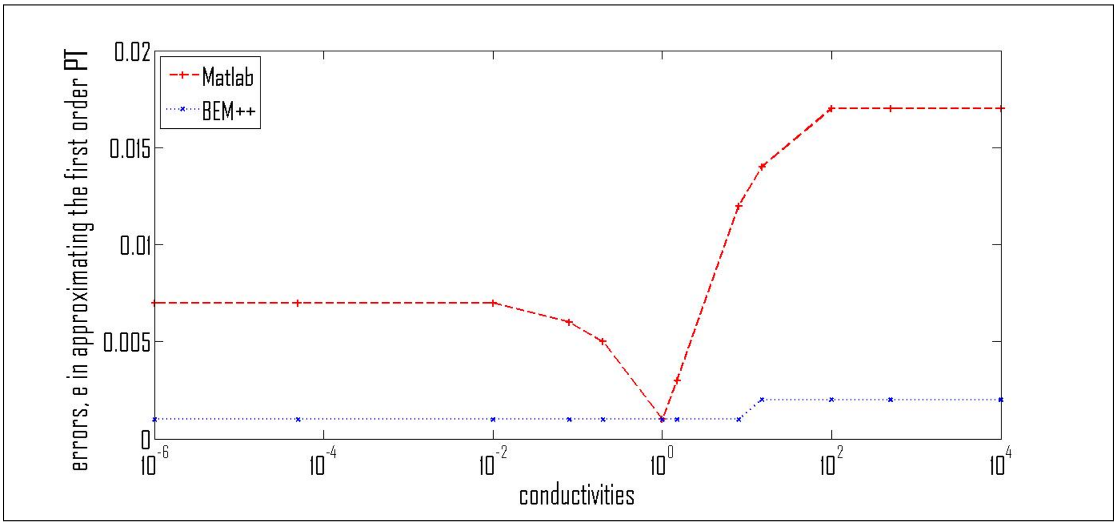

Figure 3.8: The error, e when the first order PT for the sphere of radius 1 is approximated by both *Matlab* and *BEM++* on the mesh with 9920 triangles

Figure 3.8 next shows the error $e = \left\|M - \bar{M}\right\|_2 / \left\|M\right\|_2$ between the analytic first order PT, M as given by (2.4) and the approximated first order PT, $\bar{M}$ (by both *Matlab* and *BEM++*) at every chosen conductivity. Similarly, $\|A\|_2$ denotes the entry-wise norm $\sqrt{\sum_{i=1}^{3}\sum_{j=1}^{3}|A_{ij}|^2}$ for the 3×3 matrix A. Based on Figure 3.8, the approximated first order PT, $\bar{M}$ in both *Matlab* and *BEM++* has larger error when conductivity is greater than 1 but the error is small when the conductivity is less than or near to 1. Obviously, the errors are smaller at every chosen conductivity when $\bar{M}$ is approximated by *BEM++*. Thus, we conclude that *BEM++* provides better approximation of the first order PT for this sphere than *Matlab* at every chosen conductivity (see [44] and [45] for another examples of comparing two numerical methods to compute boundary integral operators for high contrast materials).

In general, with the same number of elements for the mesh, *BEM++* produces closer approximation to the analytical solution for the first order PT of the sphere and ellipsoids than *Matlab* at every chosen conductivity. Obviously, using piecewise linear continuous basis function to approximate y^j in (1.3) with *BEM++* produces better approximation than using barycentre and area of the triangle to approximate y^j with *Matlab*. Moreover, although both codes discritize (1.5) with piecewise constant basis function, *BEM++* gives better approximation to (1.4) than *Matlab*. This is because *BEM++* uses a Galerkin approach to evaluate the singular integrals (1.5) by analytical functions whereas *Matlab* uses the less accurate Lemma 1. Here, Tausch and Wang [46] give further explanation for evaluating a singular integral operator where the methods used by [46] are actually similar with our methods in *Matlab* and *BEM++*.

Based on previous discussion, it is still possible to increase the number of triangles used during triangularization to improve the results either with *Matlab* or *BEM++*. However, larger number of triangles causes slower computation in both codes and the machine needs more memory to compute the first order PT in *Matlab*. Faster computation can be achieved in *BEM++* as it is equipped with iterative solver provided by various components of *Trilinos* (including a *GMRES* and a *CG* solver) whereas *Matlab* uses matrix operation which consumes more memory. For completeness, we include in Table 3.1 the number of triangles, `N` tested to approximate the first order PT for the sphere $x^2 + y^2 + y^2 = 1$ in *BEM++* accurate to three decimal places with the analytical solutions for the cases of low and high conductivity as well as when the conductivity is 1.5. Here, running *Matlab* with the same `N` to approximate the first order PT at the given conductivity will cause our machine to run out of memory.

Table 3.1: `N` for each k

Conductivity, k	`N`
1×10^{-6}	124928
1.5	61952
10000	247808

3.4 Conclusions

In this chapter, an alternative method to approximate the first order PT based on some terminologies of BEM has being discussed. A new software for BEM called as *BEM++* is used as a platform for computing the first order PT based on the method. Here, we also give some results to show that the approach with BEM++ provides a better approximation to the first order PT than the approach with Matlab.

Chapter 4

Fitting Ellipsoids from the First Order PT

Given the first order polarization tensor (PT) for a known or unknown object, it is possible to obtain the three semi principal axes of an ellipsoid so that the ellipsoid will have the same first order PT at a specified conductivity. This is because the explicit formula of the first order PT for an ellipsoid exists [8] as stated in (2.2). Futhermore, in the next chapter, we would like to recommend an experiment to test whether an electrosensing fish can distinguish a pair of objects that have the same first order PT, where the pair can be an ellipsoid and any other object. Therefore, the main purpose of this chapter is to present a strategy to determine such ellipsoid. Basically, the ellipsoid is obtained after all semi principal axes in the analytical formula (2.2) are determined. In order to achieve this, some mathematical properties about the existence and uniqueness of the ellipsoid are firstly given. After that, we will derive three nonlinear equations from (2.2) at a fixed conductivity by equating (2.2) to a given first order PT in the form (2.1) and then simultaneously solve them.

4.1 Mathematical Properties

For the purpose of this study, we denote every integrand in (2.3) of (2.2) as functions $f_1(t,a,b,c)$, $f_2(t,a,b,c)$ and $f_3(t,a,b,c)$ as follows

$$f_1(t,a,b,c) = \frac{1}{t^2\sqrt{t^2-1+(\frac{b}{a})^2}\sqrt{t^2-1+(\frac{c}{a})^2}},$$

$$f_2(t,a,b,c) = \frac{1}{(t^2-1+(\frac{b}{a})^2)^{\frac{3}{2}}\sqrt{t^2-1+(\frac{c}{a})^2}}, \tag{4.1}$$
$$f_3(t,a,b,c) = \frac{1}{\sqrt{t^2-1+(\frac{b}{a})^2}(t^2-1+(\frac{c}{a})^2)^{\frac{3}{2}}},$$

so that

$$P = \frac{bc}{a^2}\int_1^{+\infty} f_1(t,a,b,c)dt,$$
$$Q = \frac{bc}{a^2}\int_1^{+\infty} f_2(t,a,b,c)dt, \tag{4.2}$$
$$R = \frac{bc}{a^2}\int_1^{+\infty} f_3(t,a,b,c)dt.$$

We now prove the following lemma.

Lemma 3. *For any $t > 0$,*

1. *if $0 < a \le b \le c$ then $f_1(t,a,b,c) \le 1/t^4$.*

2. *if $0 < c \le b \le a$ then there exist positive constant K so that $f_1(t,a,b,c) \le K/t^4$.*

Proof. Starting from $a \le b$, it is easy to show that for any $t > 0$

$$t \le \sqrt{t^2-1+(b/a)^2}$$

while $a \le c$ implies

$$t \le \sqrt{t^2-1+(c/a)^2}$$

for any $t > 0$. Multiplying both inequalities gives

$$t^2 \le \sqrt{t^2-1+(b/a)^2}\sqrt{t^2-1+(c/a)^2}$$

and hence $t^4 \le (f_1(t,a,b,c))^{-1}$. This completes the proof of the first part of the lemma.

Similarly, $b \le a$ and $c \le a$ imply that for any $t > 0$

$$\sqrt{t^2-1+(b/a)^2} \le t \text{ and } \sqrt{t^2-1+(c/a)^2} \le t \text{ respectively.}$$

This leads to

$$\sqrt{t^2-1+(b/a)^2}\sqrt{t^2-1+(c/a)^2} \le t^2 \text{ and } 1/t^4 \le f_1(t,a,b,c).$$

As $0 < 1/t^4 \le f_1(t,a,b,c)$, multiply the right hand-sided of $1/t^4 \le f_1(t,a,b,c)$ with some positive constant K to complete the proof of the lemma. □

The above lemma explains that $f_1(t,a,b,c)$ is bounded for both $0 < a \leq b \leq c$ and $0 < c \leq b \leq a$. Similarly, we can also show that $f_2(t,a,b,c)$ and $f_3(t,a,b,c)$ are also bounded by $1/t^4$ for $0 < a \leq b \leq c$ and by K/t^4 for $0 < c \leq b \leq a$. This lemma is important to derive three nonlinear equations from (2.2) and also (2.3).

Besides, it is straight forward that $P = Q = R = (1/3)$ if $a = b = c$. Consequently, the first order PT for a sphere at a fixed conductivity k where $0 < k \neq 1 < +\infty$ is a multiple of the identity of size 3 as given in (2.4). Conversely, we give the following corollary to highlight that any non-zero real matrix which is the multiple of the identity of size 3 is actually the first order PT for some sphere at some specified conductivity k where $0 < k \neq 1 < +\infty$.

Corollary 1. *Let the conductivity k be specified where $0 < k \neq 1 < +\infty$. Let M be any non-zero real matrix such that M is positive definite if $k > 1$ or negative definite if $0 < k < 1$. If M is a multiple of the identity of size 3, then M is the first order PT for some sphere at the specified k.*

Proof. The corollary is actually a direct result from the explicit formula of the first order PT for a sphere and can be shown by expressing the multiple of the identity of size 3, M as (2.4) at the specified k. □

The next lemma explains that there always exist a unique sphere E of radius r with a fixed conductivity k from a 3×3 non-zero real matrix M when M has one distinct eigenvalue. Here, both M and the first order PT for E have one similar eigenvalues. Moreover, if M is a diagonal matrix, then it is also the first order PT for E.

Lemma 4. *Let the conductivity, k be fixed where $0 < k \neq 1 < +\infty$. Assume that a 3×3 non-zero real matrix M is positive definite if $k > 1$ or negative definite if $0 < k < 1$. If M has only one distinct eigenvalue denoted by m, then there exist a unique $r > 0$ satisfying*

$$m = \frac{4(k-1)\pi r^3}{2+k}$$

where r is the radius of a sphere with the fixed conductivity k.

Proof. Let the conductivity, k be fixed where $0 < k \neq 1 < +\infty$. Assume that a 3×3 non-zero real matrix M is positive definite if $k > 1$ or negative definite if $0 < k < 1$. If

M has only one distinct eigenvalue denoted by m, we can construct a matrix M_E by

$$M_E = \begin{bmatrix} m & 0 & 0 \\ 0 & m & 0 \\ 0 & 0 & m \end{bmatrix}$$

such that M_E is a multiple of identity of size 3. Therefore, M_E is the first order PT for a sphere by Corollary 1. By using (2.4), we can then have

$$m = \frac{4(k-1)\pi r^3}{2+k}, \ 0 < k \neq 1 < +\infty$$

where $r > 0$ is the radius of the sphere at the fixed k.

Introduce a function f such that $m = f(r) = \dfrac{4(k-1)\pi r^3}{2+k}$ for $r > 0$, $0 < k \neq 1 < +\infty$ and it can be shown that f is one to one. This means f is also invertible where, the inverse of f denoted by g is given by $f^{-1}(r) = g(m) = \sqrt[3]{\dfrac{m(2+k)}{4(k-1)\pi}}$. Therefore, there is a unique r satisfying $m = f(r)$. □

Corollary 1 and Lemma 4 are special as they give a unique sphere from any 3×3 non-zero real matrix M that has one distinct eigenvalues. Generally, some 3×3 non-zero real matrix can be associated to the first order PT for the ellipsoid as both of them have three eigenvalues. In this case, it might be possible to obtain an ellipsoid with conductivity, k where $0 < k \neq 1 < +\infty$ from the matrix such that the matrix is positive definite if $k > 1$ or negative definite if $0 < k < 1$. Similarly, it might be possible to obtain an ellipsoid from any first order PT since the first order PT is a 3×3 non-zero real matrix as given by (2.1). At this stage, we will discuss the possibility to obtain an ellipsoid from a given first order PT, M by assuming that M is the first order PT for some ellipsoid.

During this study, it is more diffcult to investigate the existence and the uniqueness of an ellipsoid from a given first order PT. This is because we have to deal with the complicated integrals P, Q and R as given in (2.3). By using the substitution $y = a^2(t^2 - 1)$, it can be actually shown that $P = d_1(a, b, c)$, $Q = d_2(a, b, c)$ and $R = d_3(a, b, c)$ such that

$$d_i(a, b, c) = \frac{abc}{2} \int_0^\infty \frac{dy}{(l_i^2 + y)\sqrt{(a^2 + y)(b^2 + y)(c^2 + y)}} \tag{4.3}$$

where $l_1 = a$, $l_2 = b$ and $l_3 = c$ for $i = 1, 2$ and 3. Here, $d_i(a, b, c)$ is called in [6] as the depolarization (demagnetizing) factors for ellipsoid with semi principal axes

a, b and c. It has been shown by [6] that $d_i(a, b, c)$ can also be expressed as elliptic integrals and these integrals are equivalent to the classical integrals given in [47]. Furthermore, Osborn [47] has presented some numerical values for $d_i(a, b, c)$ to suggest that $0 < d_i(a, b, c) \leq 1$. For a non-zero $d_i(a, b, c)$ satisfying $\sum_i^3 d_i(a, b, c) = 1$, it is claimed by Milton [6] that one can always find the semi principal axes a, b and c for an ellipsoid from the triplet $d_i(a, b, c)$.

Now, we will investigate whether a, b and c obtained from the triplet $d_i(a, b, c)$ (denoted by d_i) are unique. For some special cases of the ellipsoid, the explicit formula for d_i is given by [47] and also [6]. In Appendix A.1, we use the explicit formula of d_1 for prolate spheroid (where in this case, the semi principal axes are $a < b = c$ while the depolarization factors are d_1 and $d_2 = d_3 = 1 - d_1$) to find a specific interval for $\psi = \sqrt{1 - (b/a)^2}$ so that ψ is a unique solution to d_1 on the interval. By using ψ and specifying the volume of the prolate spheroid, we then show that a and b are unique. After that, we repeat the same steps and determine an interval for $\varphi = \sqrt{1 - (a/b)^2}$ so that φ is a unique solution to d_1 for oblate spheroid to show that a and b for the oblate spheroid are unique on the interval. For a general ellipsoid, the task is more difficult since we have to determine the derivatives of the complicated integrals given in (4.3) so, we leave this as our future investigation. We believe that this can be done by examining the properties of the elliptic integrals which represent (4.3).

On the other hand, in order to investigate the existence of an ellipsoid from a given first order PT, we substitute $d_i(a, b, c)$ (denoted by d_i) in (2.2). For a fixed conductivity k, $0 < k \neq 1 < +\infty$, we can express

$$d_i = \frac{(k-1)|B| - \lambda_i}{\lambda_i(k-1)}, \ i = 1, 2 \text{ and } 3 \tag{4.4}$$

where λ_i is the eigenvalues of the first order PT for any ellipsoid E denoted by M_E such that M_E is positive definite if $k > 1$ or negative definite if $0 < k < 1$. Note that we can also use the diagonal element instead of λ_i since M_E is a diagonal matrix. Therefore, following the claim by [6], we can always obtain a, b and c for an ellipsoid B for the correspond λ_i from d_i, $i = 1, 2$ and 3 (where $\sum_i^3 d_i(a, b, c) = 1$) if given to us the volume of the ellipsoid, $|B|$. However, we will not investigate whether a, b and c are unique for the given λ_i, $i = 1, 2$ and 3 when $|B|$ is specified due to time constraint during this study. Besides, it is also possible to find an ellipsoid from the given first order PT without specifying the volume of the ellipsoid. For the same reason, we only aim to explore this in the future. So, in order to reflect our results in this chapter, we state the hypothesis in the next conjecture.

Conjecture 1. *Let the conductivity, k be fixed where $0 < k \neq 1 < +\infty$. Let M_S be the first order PT for an arbitrary ellipsoid S where M_S is positive definite if $k > 1$ or negative definite if $0 < k < 1$. There exist semi principal axes a, b and c for the ellipsoid, E so that the eigenvalues of the first order PT for E at the fixed k are equal to the eigenvalues of M_S.*

4.2 Finding an Ellipsoid from the First Order PT

In this section, we present a strategy to determine an ellipsoid from a given first order PT. By assuming the given first order PT is also the first order PT for an ellipsoid, we first specified the conductivity, k for the ellipsoid where $0 < k \neq 1 < +\infty$ so that the given first order PT is positive definite if $k > 1$ or negative definite if $0 < k < 1$. After that we set the given first order PT equal to (2.2) to derive three nonlinear equations with three unknowns a, b and c and simultaneously solve them to obtain a, b and c representing the semi principal axes for the ellipsoid.

4.2.1 Formulating the nonlinear equations

In order to derive three nonlinear equations from a given first order PT by using (2.2), we first observe the integrals in (2.3). Each integral cannot be analytically determined thus, Lemma 3 is firstly used to approximate the integrals. Since all integrals have one infinite interval, a common approach to approximate them is by truncating the limits where the infinite range is replaced by a sufficiently large value L so that the infinite range becomes finite. The integrals can then be approximated by a standard numerical integration method of finite interval [48]. In this case, it is neccessary to properly choose L to avoid inaccurate results if L is underestimated or, expending needless effort if L is overestimated.

Before proceeding further, we first consider a problem to approximate integral with an infinite interval by an integral with a finite interval given by

$$\int_1^{\infty} (20/t^4)dt \approx \int_1^{C} (20/t^4)dt. \tag{4.5}$$

By following [48], the constant $C > 1$ in (4.5) is firstly estimated by evaluating

$$\int_{C}^{+\infty} (20/t^4)dt. \tag{4.6}$$

For $t \geq C$ then $t^4 \geq Ct^3$. Hence,

$$\int_{C}^{+\infty} (20/t^4)dt \leq \int_{C}^{+\infty} (20/Ct^3)dt = 20/2C^3. \tag{4.7}$$

Thus, if $C = 100$ for example, then $20/2C^3 \approx 0.00001$ so, (4.5) can be approximated to four figures of computation by $\int_1^C (20/t^4)dt$ with $C = 100$.

Now, suppose that we want to approximate $\int_1^{+\infty} f_1(t, a, b, c)dt$. Since $f_1(t, a, b, c)$ is integrable according to [8] for $1 < t < +\infty$, $f_1(t, a, b, c)$ is also integrable for $1 < t < C_1$ such that

$$\int_{1}^{+\infty} f_1(t, a, b, c)dt = \int_{1}^{C_1} f_1(t, a, b, c)dt + \int_{C_1}^{+\infty} f_1(t, a, b, c)dt. \tag{4.8}$$

By using Lemma 3, we have

$$\int_{1}^{C_1} f_1(t, a, b, c)dt \leq \int_{1}^{C_1} (1/t^4)dt \tag{4.9}$$

for $0 < a \leq b \leq c$ and

$$\int_{1}^{C_1} f_1(t, a, b, c)dt \leq \int_{1}^{C_1} (K/t^4)dt \tag{4.10}$$

for $0 < c \leq b \leq a$ where K is a positive constant. Furthermore, $\int_1^{C_1} (1/t^4)dt \leq \int_1^{C_1} (K/t^4)dt$. Following the previous explanation to approximate (4.5) by $\int_1^C (K/t^4)dt$ for $K = 20$ and $C = 100$, we now approximate $\int_1^{+\infty} f_1(t, a, b, c)dt$ by sufficiently $\int_1^{C_1} f_1(t, a, b, c)dt$ where $\int_1^{C_1} f_1(t, a, b, c)dt$ is bounded for both $0 < a \leq b \leq c$ and $0 < c \leq b \leq a$. Similarly, $\int_1^{+\infty} f_2(t, a, b, c)dt$ and $\int_1^{+\infty} f_3(t, a, b, c)dt$ are approximated respectively by $\int_1^{C_2} f_2(t, a, b, c)dt$ and $\int_1^{C_3} f_3(t, a, b, c)dt$. Our objective now is to derive the nonlinear equations from (2.2) by approximating the integrals in (4.2) (or (2.3)) with $\int_1^{C_1} f_i(t, a, b, c)dt$ (denoted by $\hat{f}_i(a, b, c)$) for $i = 1, 2$ and 3 as follows

$$\begin{aligned}
\int_{1}^{+\infty} f_1(t, a, b, c)dt &\approx \int_{1}^{C_1} f_1(t, a, b, c)dt = \hat{f}_1(a, b, c), \\
\int_{1}^{+\infty} f_2(t, a, b, c)dt &\approx \int_{1}^{C_2} f_2(t, a, b, c)dt = \hat{f}_2(a, b, c), \\
\int_{1}^{+\infty} f_3(t, a, b, c)dt &\approx \int_{1}^{C_3} f_3(t, a, b, c)dt = \hat{f}_3(a, b, c).
\end{aligned} \tag{4.11}$$

In this study, the trapezoidal rule from numerical integration technique of finite interval is used to develop the desired system of nonlinear equations from (2.2) and (4.11). The method is chosen with the hope to develop a simple set of equations that can be easily and directly solved. By using the trapezoidal rule, we obtain the equations

$$\hat{f}_1(a,b,c) = h_1 \left[\frac{f_1(1,a,b,c) + f_1(C_1,a,b,c)}{2} + \sum_{\kappa=1}^{n_1-1} f_1(1+\kappa h_1, a, b, c) + R_1 \right], \quad (4.12)$$

$$\hat{f}_2(a,b,c) = h_2 \left[\frac{f_2(1,a,b,c) + f_2(C_2,a,b,c)}{2} + \sum_{\kappa=1}^{n_2-1} f_2(1+\kappa h_2, a, b, c) + R_2 \right], \quad (4.13)$$

$$\hat{f}_3(a,b,c) = h_3 \left[\frac{f_3(1,a,b,c) + f_3(C_3,a,b,c)}{2} + \sum_{\kappa=1}^{n_3-1} f_3(1+\kappa h_3, a, b, c) + R_3 \right], \quad (4.14)$$

where for $i = 1, 2, 3$, R_i is the small error in the approximation and $h_i = (C_i - 1)/n_i$ must be very small to increase the accuracy of the computation [48]. Then, if given the first order PT of any object S (denoted by $M(k, S)$) as diagonal matrix of size 3, the desired system of nonlinear equation is obtained by comparing the diagonals of (2.2) with the diagonals of $M(k, S)$. Finally, by using (2.3) with (4.11) and rearrange, the system will be in the form

$$m_{ii} + (k-1) \left[m_{ii} \frac{bc}{a^2} \hat{f}_i(a,b,c) - |B| \right] = 0 \quad (4.15)$$

where m_{ii} is the diagonal element of the given $M(k, S)$ for $i = 1, 2, 3$ and $|B| = (4/3)\pi abc$.

4.2.2 Solving system of nonlinear equations

In this study, given the first order PT for an object, the system of nonlinear equations (4.15) is numerically solved at a fixed conductivity k to obtain the desired ellipsoid. For this purpose, the values C_i and h_i for $\hat{f}_i(a,b,c)$ in (4.15) must firstly be specified where, in general, the value C_i is large and can be set like C in (4.5) (due to (4.9) and (4.10)). In this case, it is impossible to estimate C_i (like we did in (4.5)) since $\int_{C_i}^{+\infty} f_i(t,a,b,c)dt$ cannot be analytically integrated. On the other hand, h_i is set to be sufficiently small. At this stage, the function `fsolve.m` of *Matlab* is used to solve (4.15) for $a, b,$ and c with the initial values $a = b = c = 0$. The resulting a, b and c can then be used in the analytical formula (2.2) to ensure that the first order PT for the determined ellipsoid at the fixed k agress with the given first order PT. The computation can be repeated with different values of C_i and h_i until the results agree at some degree of accuracy.

4.2.3 Limitations

There are some limitations of this strategy especially since this method is designed for our specific application in the study. First of all, the ellipsoid can only be obtained if the given first order PT, M is a diagonal matrix such that M has the same form with the first order PT for some ellipsoid as given by (2.2). This is possible because the first order PT for most objects that we have encountered so far are diagonal matrices at certain decimal places. Moreover, the conductivity k of the ellipsoid must be specified so that the given first order PT satisfies Theorem 3 (see Chapter 2). Otherwise, the system (4.15) cannot be solved by `fsolve.m` or it can be solved but the values $a, b, c < 0$.

We also do not have any result about the existence and the uniqueness of the solutions for (4.15) which are equivalent to (4.4) as they are out of the scope of the study at this moment. So far, we only know based on the claim by [6] that we can obtain an ellipsoid E from the first order PT if the volume of E is given. However, we generalize the system of nonlinear equations (4.15) and solve them for some E that have some unspecified volume. The steps taken to solve (4.15) without specifying the volume are also consistent with the proposed Conjecture 1. In this case, the diagonals of the given first order PT for some objects are used instead of the eigenvalues so that the determined ellipsoid and the object will have the same first order PT.

In addition, according to [49], at least n nonlinear equations are needed if we want to find a unique solution for n independent variables provided the solution exists. This seems to be true if the system is solved by analytical techniques. However, our system (4.15) can only be solved by numerical method. Furthermore, some authors such as [50] and [51] have also claimed that there is no guarantee to find the unique or all solutions for the system of nonlinear equations by numerical method because of the difficulties in analyzing the existence and uniqueness of the solutions for the system. Therefore, following the claim by Press et. al [52] that there is no particular ‘good method’ in solving the system of nonlinear equations, only the standard method in the function `fsolve.m` of *Matlab* is used to solve (4.15) to achieve our purpose.

4.3 Results and Discussion

In order to provide numerical examples, given the first order PT for an object S denoted by $M(k, S)$, the conductivity k for the to be determined ellipsoid E in (4.15) is firstly fixed so that the given first order PT satisfies Theorem 3 (see Chapter 2). Moreover, the conductivity in (4.15) for E here is set to be equal to the conductivity of S (in this case, we may say that both E and S are constructed from the same material). We now assume small error in the approximations (4.12), (4.13) and (4.14) such that $R_1 \approx 0$, $R_2 \approx 0$ and $R_3 \approx 0$. By choosing $C_1 = C_2 = C_3 = 50$ and $h_1 = h_2 = h_3 = 0.00001$ for (4.12), (4.13) and (4.14), the system (4.15) can be solved in *Matlab* by using the function `fsolve.m` to determine a, b and c of E. Table 4.1 shows a few common objects S and every semi axes of ellipsoids E at four decimal places which are obtained by solving (4.15) equal to $M(k, S)$ at the same conductivity k for both S and E.

In addition, it is more useful to represent the first order PT for an object with three of its eigenvalues. Since the eigenvalues of the first order PT of ellipsoids are just the diagonals as given by (2.2), we can then determine an ellipsoid E from all eigenvalues of $M(k, S)$ by solving (4.15) equal to the corresponds eigenvalues of $M(k, S)$. By doing this, instead of having the same first order PT, the ellipsoid E and the object S will have similar eigenvalues of their first order PT (see Table 4.2 for examples). Furthermore, by using (2.2) and Theorem 2 (see Chapter 2), if an object S is rotated, we can show that the eigenvalues of the first order PT for E are still similar to the eigenvalues of $M(k, S)$ for some rotation on S. In this case, the first order PT for E does not necessary equal to $M(k, S)$.

We also want to highlight that by using a, b and c for ellipsoid E in Table 4.1 with the given k in (2.2), the first order PT for E is exactly the same as $M(k, S)$ in the table at two decimal places. Besides, after the first order PT for ellipsoid E in Table 4.2 and its eigenvalues are recomputed with (2.2), the eigenvalues for the first order PT for E are exactly equal at two decimal places to the eigenvalues of $M(k, S)$ except for the shaft where the eigenvalues for the first order PT for E are only equal to the eigenvalues of the first order PT for the shaft after they are rounded to three significant figures. This suggests good agreements between the first order PT for the determined ellipsoid and the given $M(k, S)$ in the results.

Table 4.1: Ellipsoid and object with the same first order PT

Object, S	k	$M(k,S)$	Ellipsoid, E $(\frac{x}{a})^2+(\frac{y}{b})^2+(\frac{z}{c})^2=1$
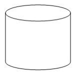 **Cylinder** $d=3$, $h=3$	5×10^{-5}	$\begin{bmatrix} -33.80 & 0.00 & 0.00 \\ 0.00 & -33.80 & 0.00 \\ 0.00 & 0.00 & -33.52 \end{bmatrix}$	$a=1.7425$ $b=1.7425$ $c=1.7669$
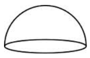 **Hemisphere** $d=3$	1×10^{-2}	$\begin{bmatrix} -9.70 & 0.00 & 0.00 \\ 0.00 & -9.70 & 0.00 \\ 0.00 & 0.00 & -15.42 \end{bmatrix}$	$a=1.5240$ $b=1.5240$ $c=0.7699$
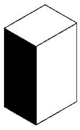 **Cuboid** $2\times4\times1$	1.5	$\begin{bmatrix} 27.95 & 0.00 & 0.00 \\ 0.00 & 29.90 & 0.00 \\ 0.00 & 0.00 & 25.05 \end{bmatrix}$	$a=2.5212$ $b=4.3181$ $c=1.4064$
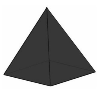 **Pyramid** $2\times2\times2$	500	$\begin{bmatrix} 12.85 & 0.00 & 0.00 \\ 0.00 & 12.85 & 0.00 \\ 0.00 & 0.00 & 8.50 \end{bmatrix}$	$a=1.0775$ $b=1.0775$ $c=0.7569$
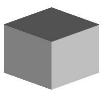 **Cube** $2\times2\times2$	10000	$\begin{bmatrix} 28.90 & 0.00 & 0.00 \\ 0.00 & 28.90 & 0.00 \\ 0.00 & 0.00 & 28.90 \end{bmatrix}$	$a=1.3201$ $b=1.3201$ $c=1.3201$

note : d = diameter, h = height

Table 4.2: The similar eigenvalues of the first order PT for S and E

Object, S	k	Eigenvalues of $M(k,S)$	Ellipsoid, E $(\frac{x}{a})^2+(\frac{y}{b})^2+(\frac{z}{c})^2=1$
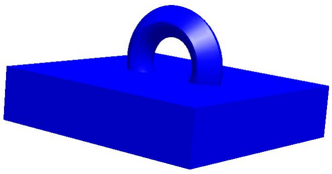 **half-Ring on Cuboid**	1.5	56.50 56.50 46.62	$a = 4.4860$ $b = 4.4860$ $c = 1.4607$
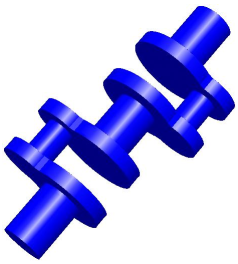 **Shaft**	500	30.90×10^5 12.42×10^5 8.40×10^5	$a = 84.8042$ $b = 41.8165$ $c = 29.2011$
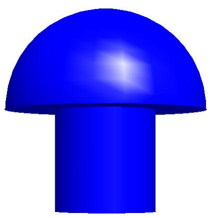 **Mushroom**	10000	87.42 79.00 79.00	$a = 1.9735$ $b = 1.8144$ $c = 1.8144$

4.4 Conclusions

In this chapter, an approach to determine an ellipsoid from a given first order PT at some fixed conductivity has being highlighted. In this case, based on the analytical formula (2.2) and (2.4), we firstly discuss some existences and uniquenesses of the ellipsoid from the first order PT. Numerical examples are also given to show that an object and the ellipsoid can have the same first order PT.

Chapter 5

The First Order PT with Complex Conductivity

An asymptotic formula representing the perturbation in the electromagnetic field for the complete time harmonic Maxwell's equations due to the presence of isolated conducting and magnetic objects has been derived by Ammari et al. [33]. This formula could be useful to describe the isolated objects for examples in microwave tomography, radar and ground penetrating radar (GPR). Moreover, in their recent works on GPR, Watson and Lionheart [53] have claimed that the PT derived from the asymptotic formula [33] is equivalent to the first order PT (the Pólya-Szegő PT). In this case, k of the first order PT is the relative complex permittivity of the isolated object. This motivates us to investigate the first order PT for complex conductivity $k = a + b\mathrm{i}$ where i is the standard imaginary unit. In this chapter, the first order PT for a few objects at complex conductivity are numerically evaluated and presented. Since complex permittivity depends on the frequency of the electromagnetic field, by setting k equal to the relative complex permittivity as suggested by [53], we also investigate the first order PT at a few different frequencies.

5.1 Some Known Properties

The first order PT for an object B at complex conductivity $k = a + b\mathrm{i}$ in the form (2.1) can be determined by solving the same (1.3)-(1.5). In addition, the analytical solutions (2.2) and (2.4) for ellipsoids and spheres are also applicable. Following Theorem 1 (see

Chapter 2), it is easy to see that the first order PT in this case is complex symmetric. Therefore, the first order PT can then be expressed as $\mathcal{R} + \mathcal{J}\mathrm{i}$ such that $\mathcal{R}$ and $\mathcal{J}$ are the real and imaginary parts of the first order PT. In this case, both $\mathcal{R}$ and $\mathcal{J}$ are 3×3 symmetrical real matrices.

In addition, we also define the relative complex permittivity of B denoted by ϵ_r as

$$\epsilon_r = \frac{1}{\epsilon_0}\left(\epsilon_B - \frac{\sigma_B}{\omega}\mathrm{i}\right) \tag{5.1}$$

where $\epsilon_0 = 8.854 \times 10^{-12}$ F/m (Farads per meter) is the permittivity of the free space and ω (rad/s) is the frequency while ϵ_B and σ_B each is the permittivity and conductivity of B. Note that $\mathcal{J}$ for the first order PT is a non-zero matrix only if $b \neq 0$ for k. Thus, by setting k equal to ϵ_r of an object B, $\mathcal{J}$ of the first order PT for B depends on σ_B and ω as given by (5.1).

5.2 Approximating the First Order PT at Complex Conductivity and Complex Permittivity

First of all, to numerically compute the first order PT for the object B at complex conductivity k (or complex permittivity) by solving (1.3)-(1.5), our previous codes in both *Matlab* and *BEM++* (see Appendix B.2 and Chapter 3) are modified. In *Matlab*, we only have to assign complex value for k (*Matlab* then will automatically define and solve functions (1.3) and (1.4) as complex-valued). However, for *BEM++*, besides specifying complex value for k in the *Python* script, we also need to specify the `quadStrategy` of *BEM++* (see [41] for details) so that it produces and solves complex-valued functions for each (1.3) and (1.4). After that, both codes can be used to approximate the first order PT for an object B by using the mesh of the boundary of B. Similarly, the computation is repeated by uniformly increasing the number of elements for the mesh with *Netgen* until there is no relative difference at six decimal places between the current and the previous solutions where the current computed solution is then chosen to approximate the first order PT.

5.3 Results and Discussions

In this section, we firstly approximate the first order PT for a sphere and an ellipoid with complex conductivity k in *BEM++* so that we can compare the results to the analytical solutions (2.4) and (2.2). After that, we approximate the first order PT for an object (no analytical solution for the first order PT) by our codes in both *Matlab* and *BEM++* at the same complex conductivity k to describe the object. Finally, by setting the relative complex permittivity equal to complex conductivity k, we investigate the first order PT for two objects with a fixed real part and a few different imaginary parts of k where the imaginary parts are generated according to a few frequencies for the relative complex permittivity.

5.3.1 The first order PT for some geometric objects

Figure 5.1 shows the agreement between the elements of the approximated first order PT computed by *BEM++* with the analytical solution (2.4) for the sphere of radius 1 centimeters (cm) at $k = 3.4 + 0.02\mathrm{i}$. Here, the approximated first order PT is obtained on the mesh with 14720 triagular elements. It can be seen that the approximated first order PT for the sphere is a complex diagonal matrix at six decimal places where the diagonal are all equal.

On the other hand, an agreement between the elements of the approximated first order PT computed by *BEM++* with the analytical solution (2.2) for the ellipsoid $\dfrac{x^2}{a^2} + \dfrac{y^2}{b^2} + \dfrac{z^2}{c^2} = 1$ where $a = 0.3$, $b = 0.2$, $c = 0.1$ cm at $k = 1.9 - 0.3\mathrm{i}$ is shown in Figure 5.2. Here, the mesh for the ellipsoid consists of 14272 triangular elements. Similarly, it can be seen that the approximated first order PT for the ellipsoid is a complex diagonal matrix at five decimal places.

We are also motivated to investigate the first order PT for the vs50 landmine. This is due to the recent study conducted by [53] with the purpose of locating a buried vs50 landmine from the soil by using the GPR. The model of the landmine is given in Figure 5.3 (see [31] for its actual diagram) while its dimension is according to [54]. By setting $k = 2.9 - 0.0052\mathrm{i}$ (which is the complex permittivity of the explosive TNT at frequency 3 GHz as given in [32]), the first order PT is computed with *BEM++* on the mesh with 1033 triangles. Since the first order PT in this case has no analytical

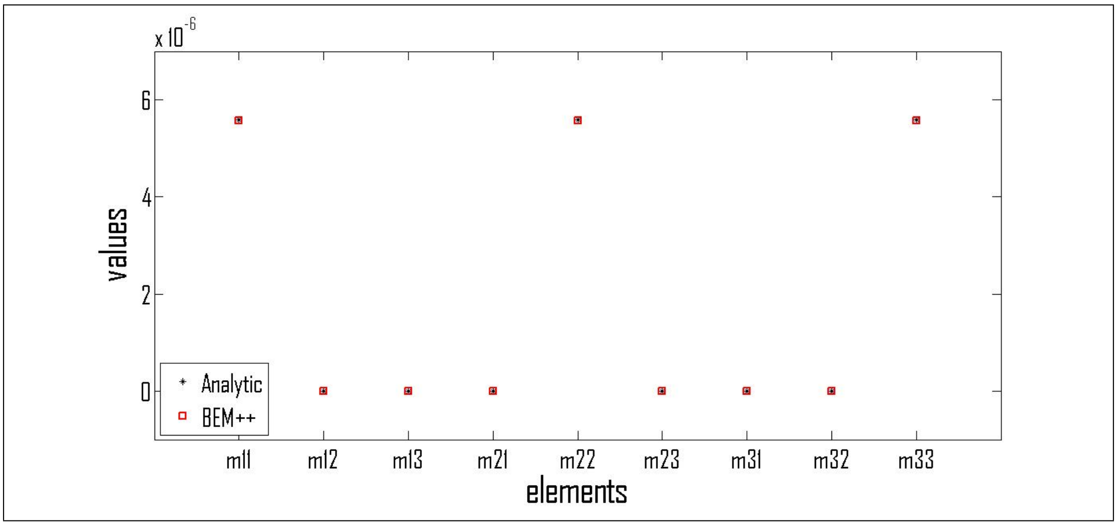

(a)

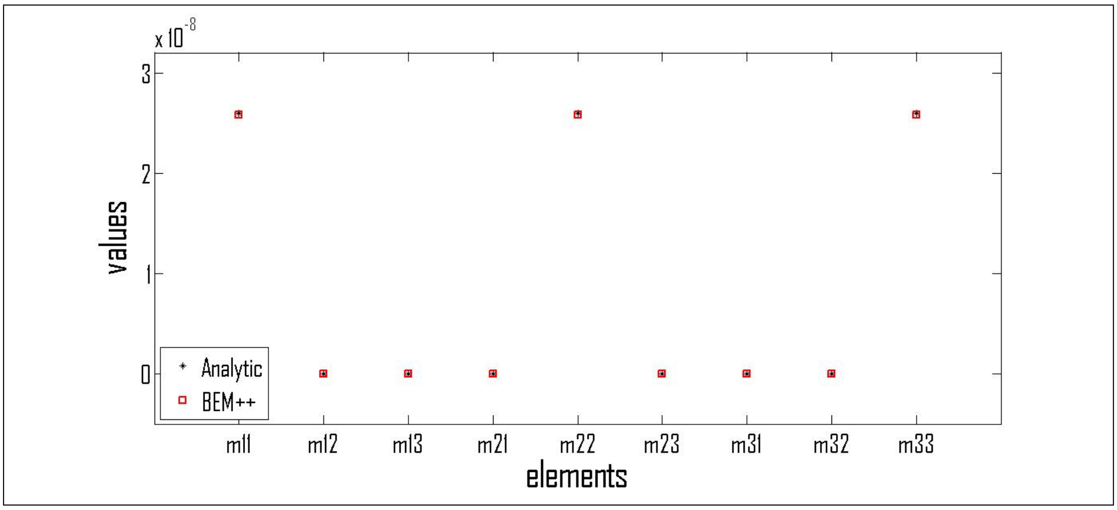

(b)

Figure 5.1: A comparison between the elements of the approximated first order PT obtained with *BEM++* and the analytical solution (2.4) for the sphere of radius 1 cm at $k = 3.4 + 0.02\mathrm{i}$ (a) real part (b) imaginary part

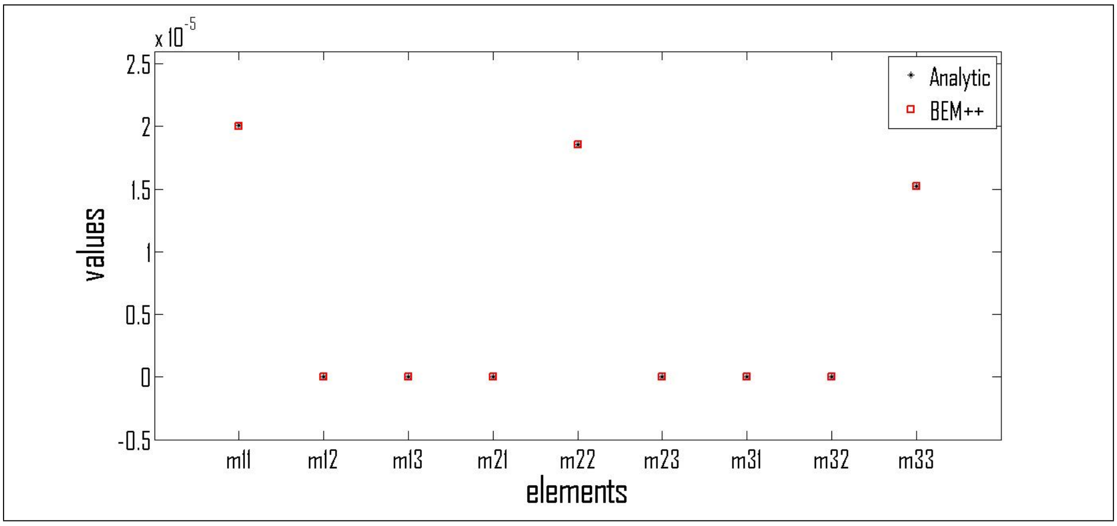

(a)

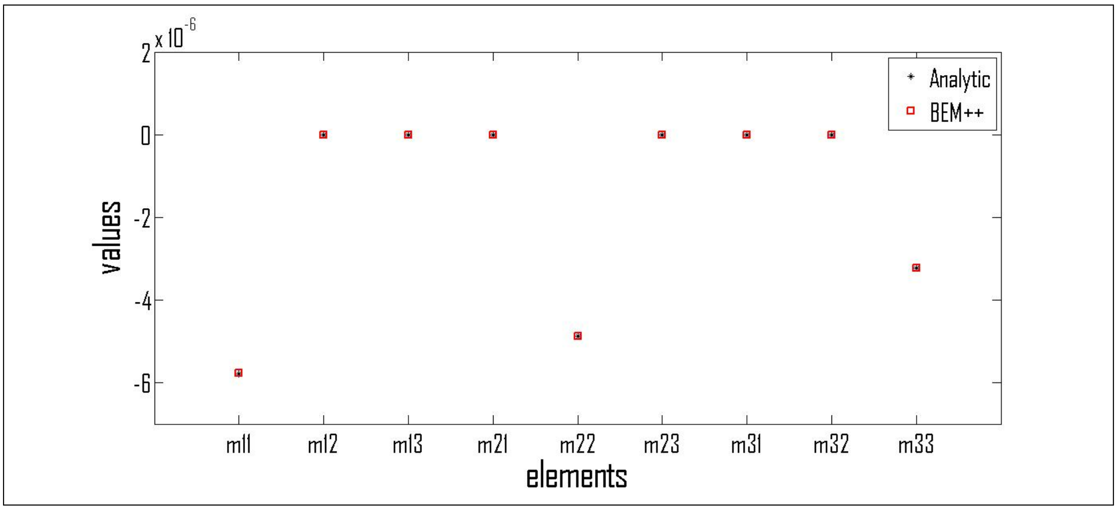

(b)

Figure 5.2: A comparison between the elements of the approximated first order PT obtained with *BEM++* and the analytical solution (2.2) for $\frac{x^2}{a^2} + \frac{y^2}{b^2} + \frac{z^2}{c^2} = 1$ ($a = 0.3$, $b = 0.2$, $c = 0.1$ cm) at $k = 1.9 - 0.3\mathrm{i}$ (a) real part (b) imaginary part

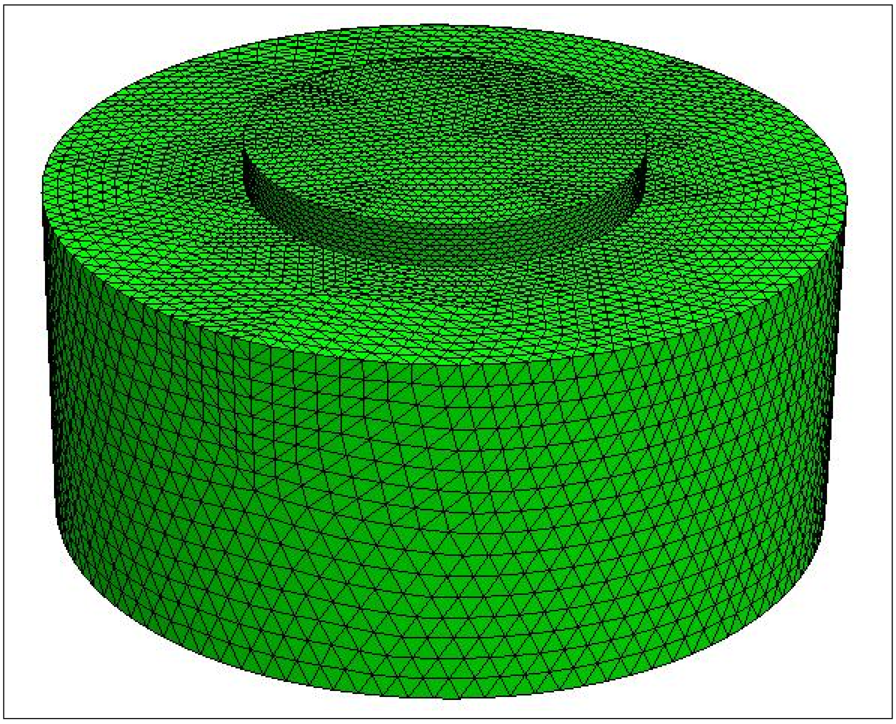

Figure 5.3: A model for a vs50 landmine [31]

solution, the same mesh is used to recompute the first order PT this time with our code in *Matlab* for later comparison.

In order to show an acceptable agreement between the two approximated first order PT for vs50, all elements for the real and imaginary parts of both approximated first PT are plotted in the same graph in Figure 5.4. Based on these graphs, both approximated first order PT for vs50 are complex diagonal matrices at four decimal places. Moreover, the first diagonal is equal to the second diagonal for both approximations. Not only that, by using Definition 2 (see Chapter 2), it can be shown that the real part of the approximated first order PT is a positive definite matrix whereas the imaginary part is a negative definite matrix. These results could be very useful to identify the vs50 landmine from the GPR later on.

5.3.2 The first order PT at a few different frequencies

Previously, Rehim et al. [55] presented the capability to determine the magnetic polarizibility tensor from a metal detector for landmine detection by investigating frequency response for the polarizibility tensor. Moreover, Ledger and Lionheart [30] has recently showed that the frequency response of the polarizibility tensor in [55]

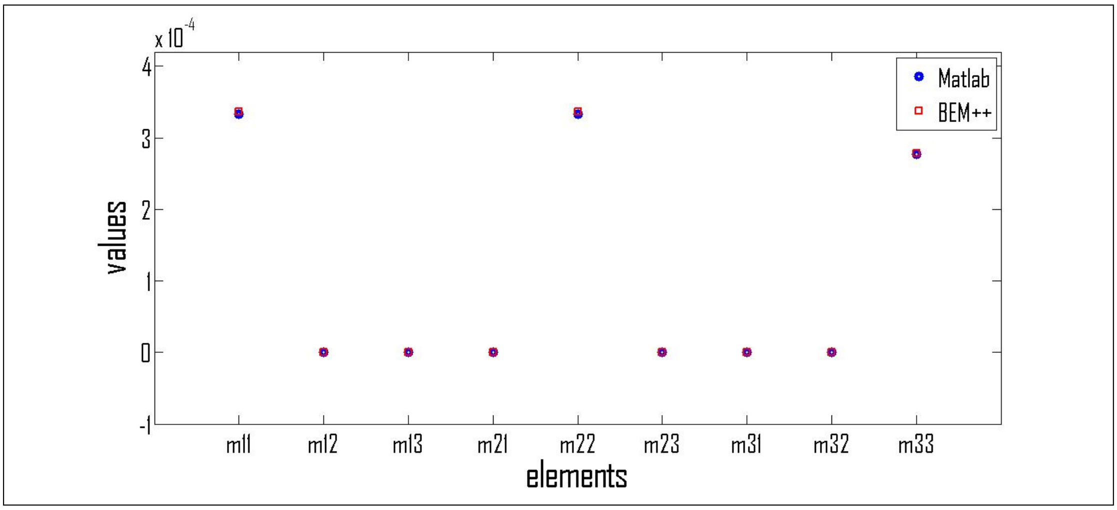

(a)

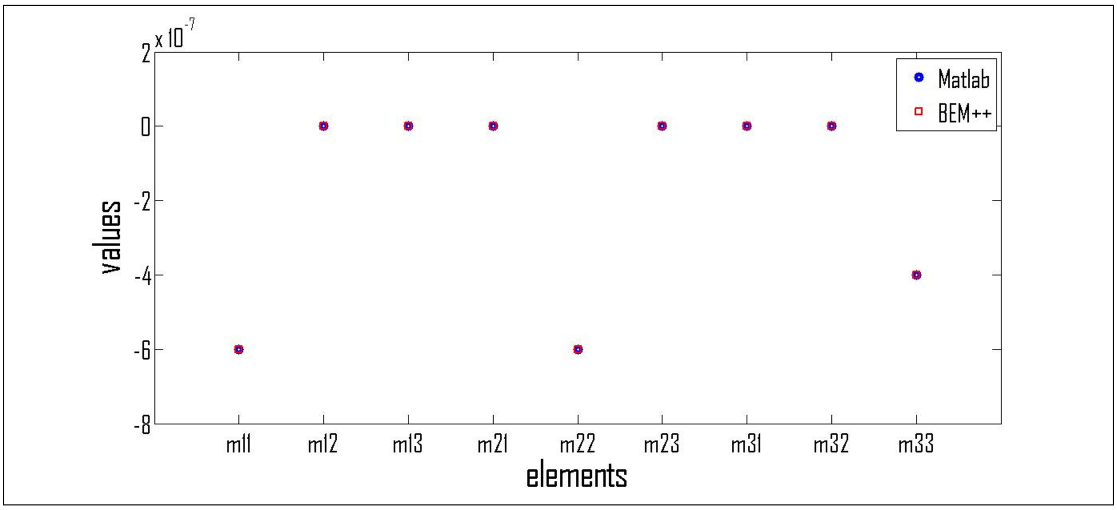

(b)

Figure 5.4: A comparison between the elements of the approximated first order PT obtained by *Matlab* with the elements of the approximated first order PT obtained by *BEM++* for the model of vs50 landmine at $k = 2.9 - 0.0052\mathrm{i}$ (a) real part (b) imaginary part

actually agrees with the expilicit formula of the PT for metal detection, where, the PT for metal detection will be discussed during this study in Chapter 7. Similarly, this motivates us to investigate frequency response for the first order PT with a relative complex permittivity with the hope to improve the GPR in the future for locating and describing landmine.

In this section, we investigate the first order PT at different frequencies ω for a few complex permittivities. First of all, we show the agreements between the approximated first order PT and the analytical solution (2.4) for the sphere of radius 1 cm at a few complex permittivities. The real part of the permittivities are fixed to be equal but the imaginary part are changed according to a few chosen frequency, ω (rad/s) where $1 \leq \omega \leq 4.7124 \times 10^{11}$. After that, by using the same permittivities, we investigate for different ω, the approximated first order PT for the model of vs50 landmine as it is one of objects of interest for landmine clearance by using the GPR. Note that the complex permittivities with different ω considered here are actually generated based on the actual complex permittivity of the explosive TNT as given in [32].

The first order PT for the sphere of radius 1 cm is computed with *BEM++* and also by using the analytical formula (2.4) at various complex permittivities, $k = 2.9 - (9.8216 \times 10^7)\omega^{-1}\mathrm{i}$ where $1 \leq \omega \leq 4.7124 \times 10^{11}$. Here, the mesh consisting 9920 triangular elements for the sphere is used in *BEM++*. Next, the first order PT obtained from the formula (2.4) and also *BEM++* are plotted against ω where the agreements between every element of the first order PT obtained from (2.4) and *BEM++* at all ω are shown in Figure 5.5 until Figure 5.8. Obviously, all graphs in Figure 5.5 are equal to each other and the same thing happens to the graphs in Figure 5.7 since the diagonal elements for both real and imaginary parts of the first order PT for the sphere are equal (the diagonal elements for both real and imaginary parts of the approximated first order PT for the sphere are equal to each other at six decimal places). Moreover, for all chosen ω, the approximated first order PT for the sphere are complex diagonal matrices at six decimal places since all non-diagonal elements for the real and imaginary parts of the approximated first order PT are zero at six decimal places as given by the graphs in Figure 5.6 and Figure 5.8.

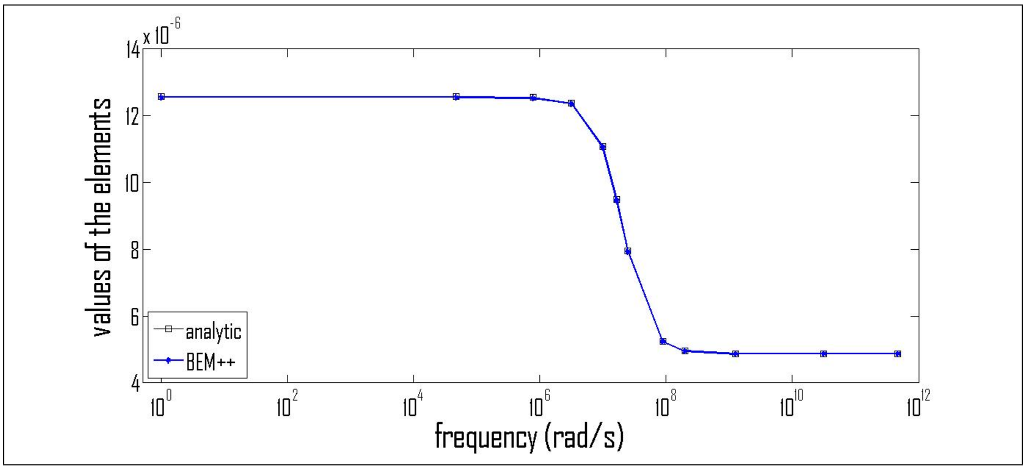

(a)

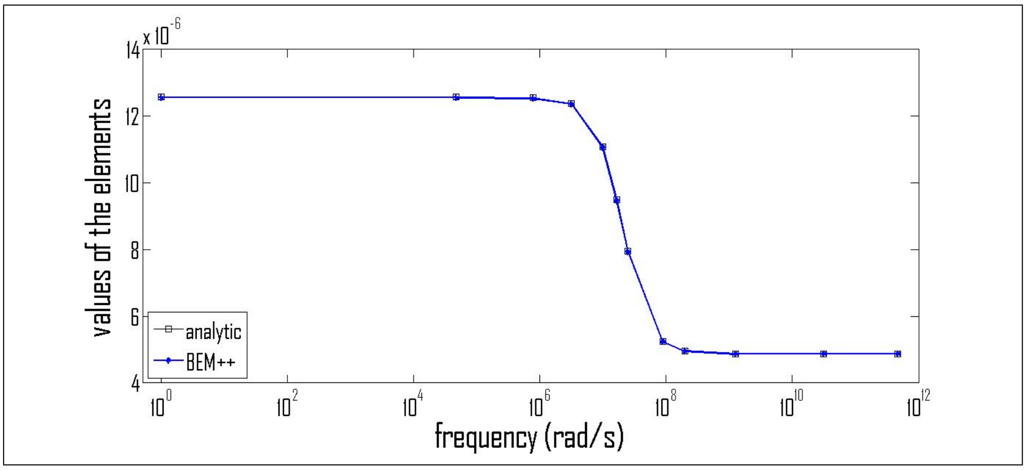

(b)

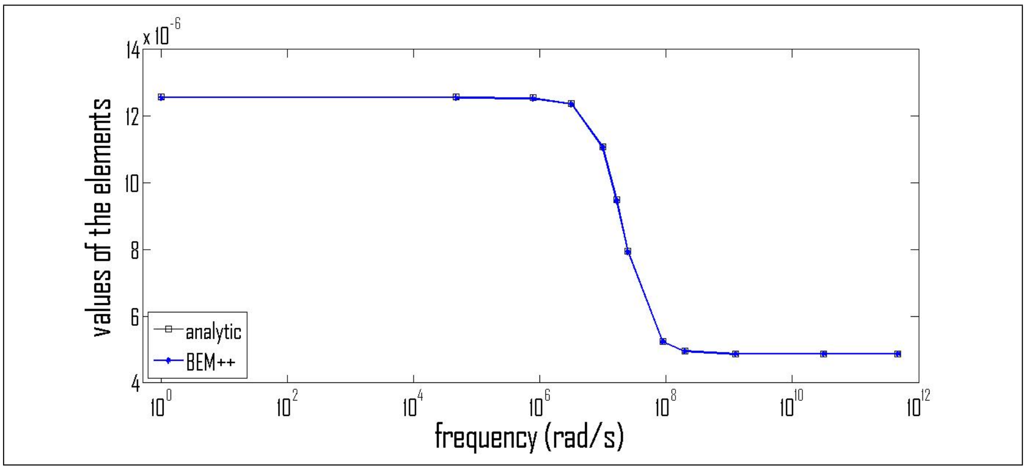

(c)

Figure 5.5: Diagonal elements (real part) of the analytical solution and the approximated first order PT by *BEM++* for the sphere of radius 1 cm against frequencies ω (a) first diagonal (b) second diagonal (c) third diagonal

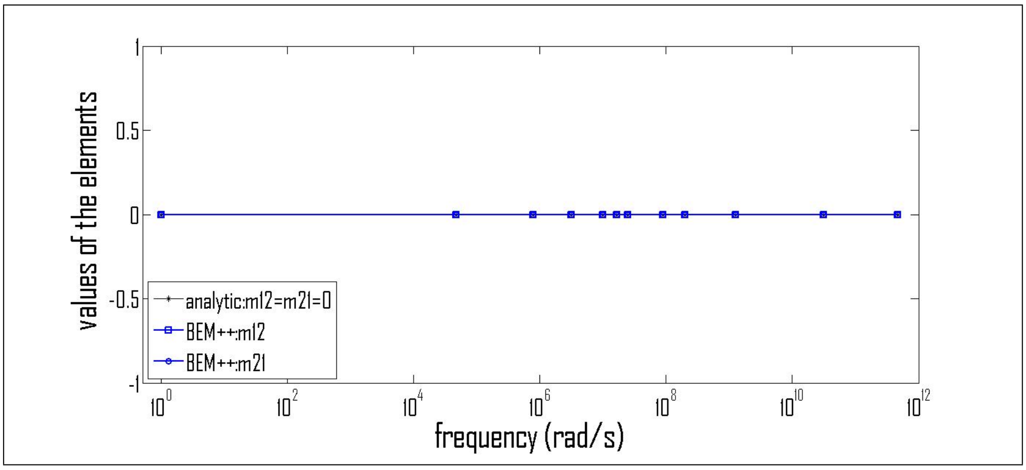

(a)

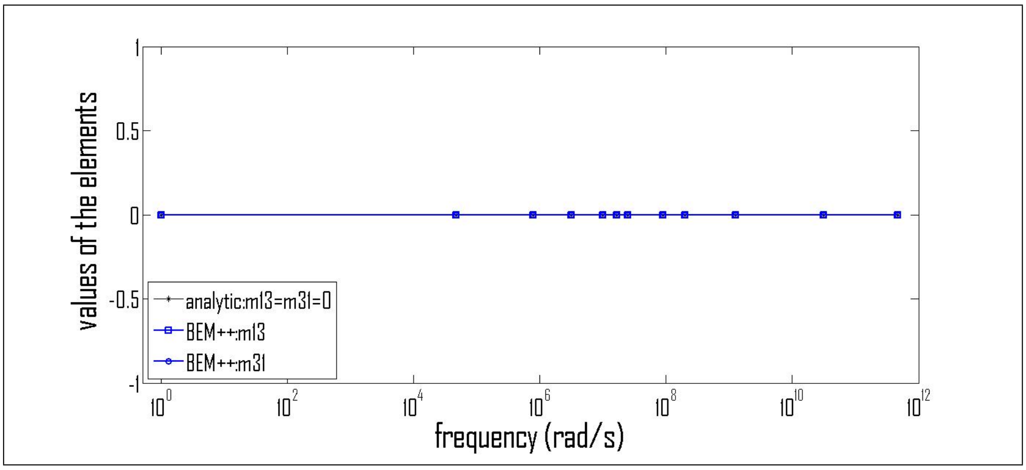

(b)

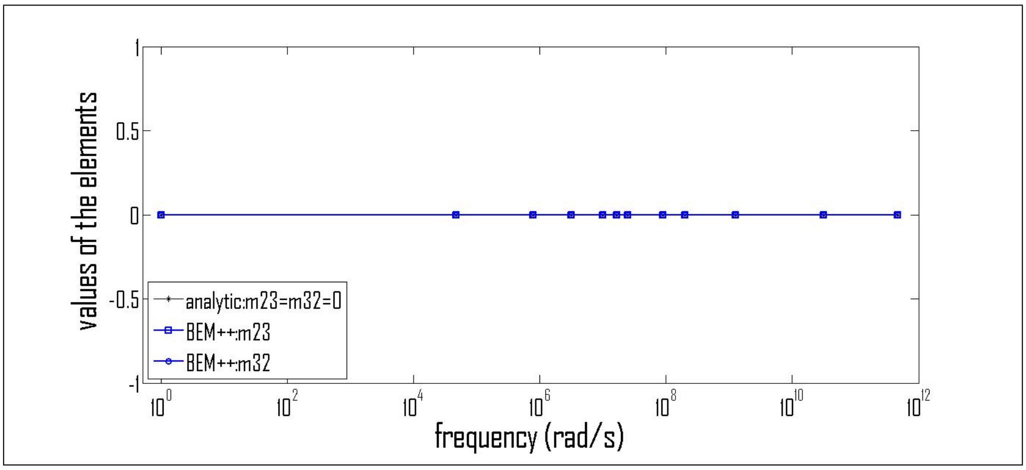

(c)

Figure 5.6: Non-diagonal elements (real part) of the analytical solution and the approximated first order PT by *BEM++* for the sphere of radius 1 cm against frequencies ω

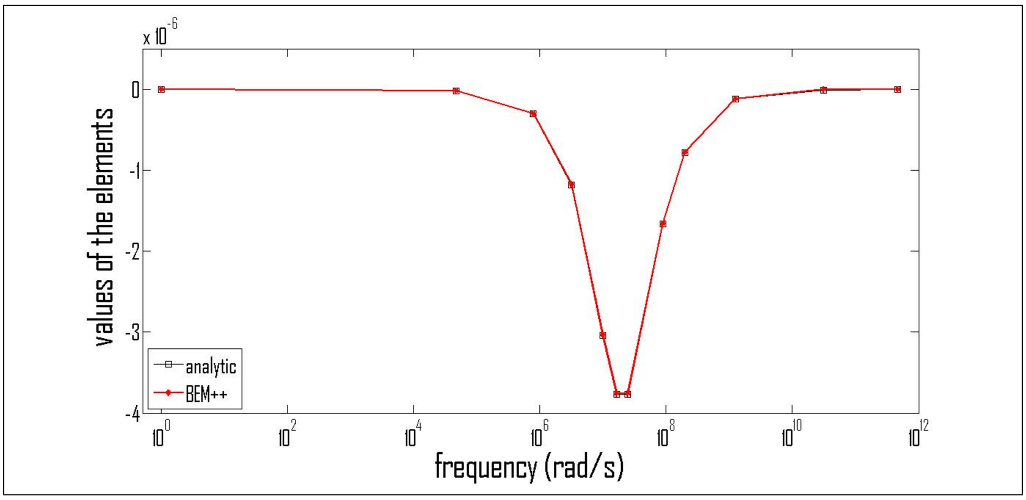

(a)

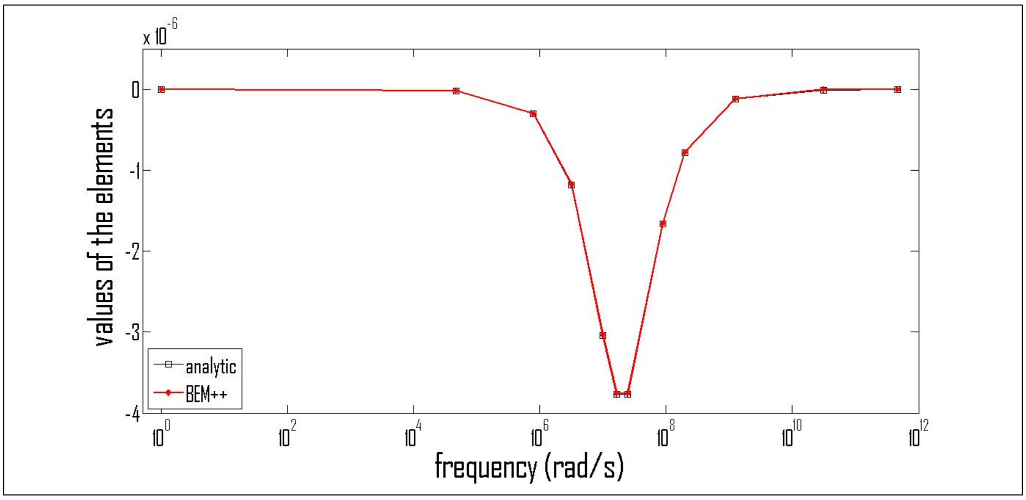

(b)

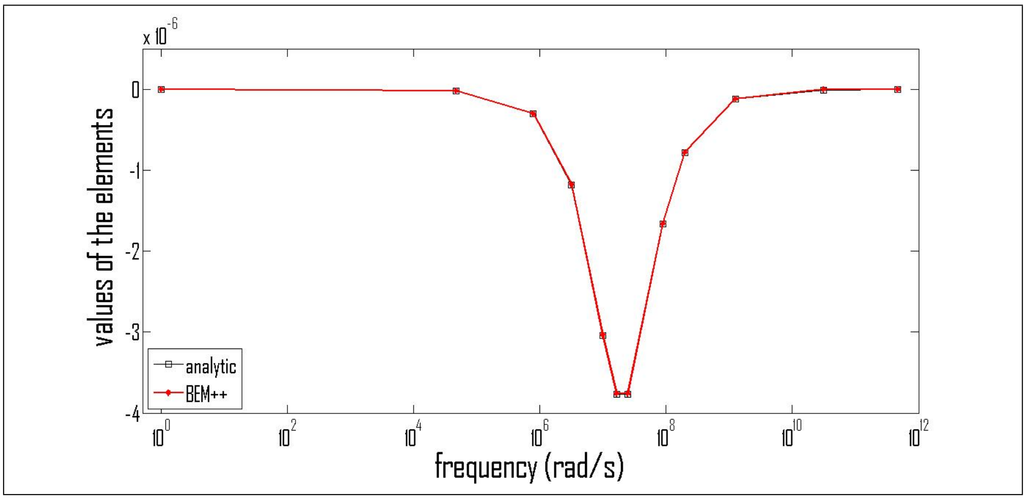

(c)

Figure 5.7: Diagonal elements (imaginary part) of the analytical solution and the approximated first order PT by *BEM++* for the sphere of radius 1 cm against frequencies ω (a) first diagonal (b) second diagonal (c) third diagonal

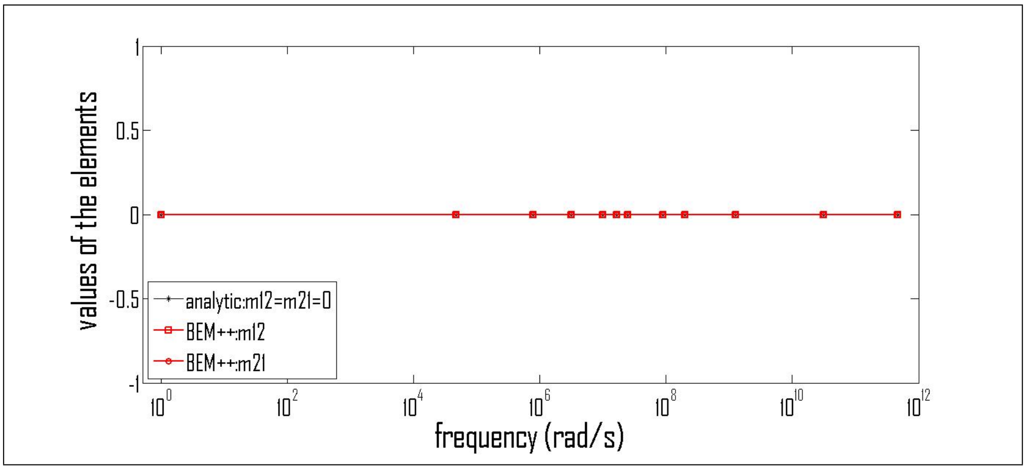

(a)

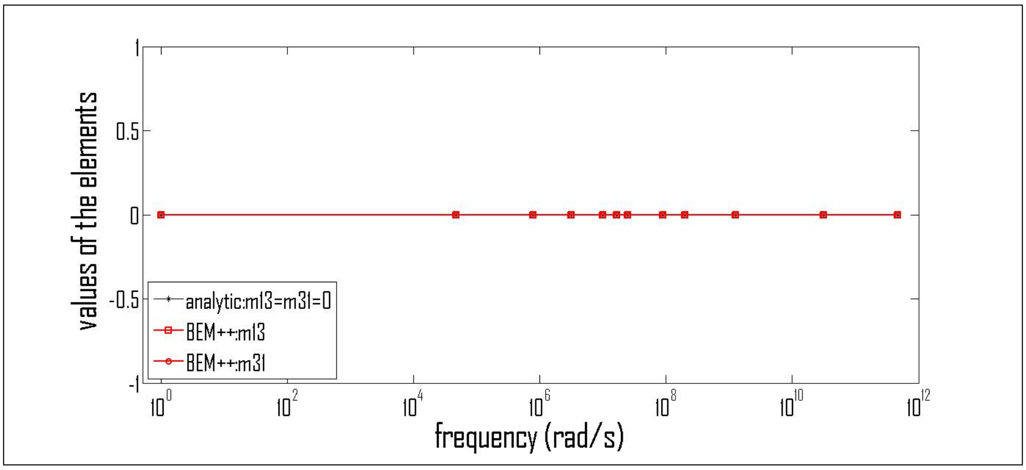

(b)

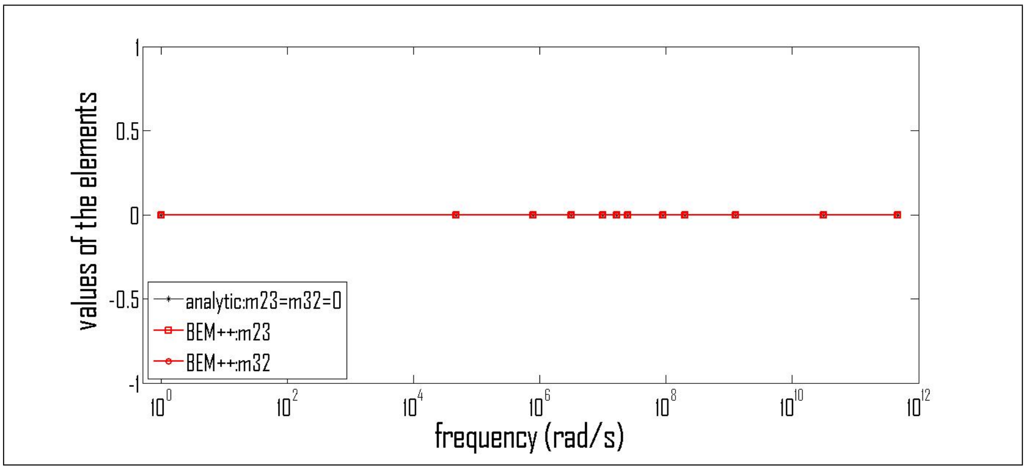

(c)

Figure 5.8: Non-diagonal elements (imaginary part) of the analytical solution and the approximated first order PT by *BEM++* for the sphere of radius 1 cm against frequencies ω

On the other hand, Figure 5.9 until Figure 5.12 show the elements of the approximated first order PT computed by *BEM++* against ω for the model of vs50 landmine (the mesh consists 4132 triangular elements) also at complex permittivities, $k = 2.9 - (9.8216 \times 10^7)\omega^{-1}\mathrm{i}$ where $1 \leq \omega \leq 4.7124 \times 10^{11}$. Based on the graphs in Figure 5.9 and Figure 5.11, we can see that the first and the second diagonal for both real and imaginary parts of the approximated first order PT are equal at four decimal places for every ω. Furthermore, for every ω, the approximated first order PT for the model of vs50 landmine are also complex diagonal matrices at four decimal places since all non-diagonal elements for both real and imaginary parts of the approximated first order PT are zero at four decimal places as given by the graphs in Figure 5.10 and Figure 5.12.

Moreover, based on Figure 5.5 and Figure 5.9, every diagonal element for the real part of the approximated first order PT for both objects remains a constant at frequency, ω between 1 and 10^6 before drop significantly to another constant when ω is between around 10^6 and 10^9. The value for each diagonal remains at the constant as ω inceases from 10^9 to 4.7124×10^{11}. In contrast, every diagonal element for the imaginary part of the approximated first order PT for both objects has non-zero value only at ω between 10^5 and 10^{11} as shown in 5.7 and Figure 5.11. Not only that, every diagonal element for the imaginary part of the approximated first order PT for both objects has a minimum value at ω around 3×10^8. As the same complex relative permittivities are used for both objects, the curves for graphs in Figure 5.5 are similar to the curves for graphs in Figure 5.9 while the curves for graphs in Figure 5.7 are similar to the curves for graphs in Figure 5.11.

Although the curves of the graphs are similar for each real and imaginary part, the absoulte values of the diagonals for the approximated first order PT for vs50 are larger than the absoulte values of the diagonals for the approximated first order PT for the sphere probably because vs50 has larger volume. Furthermore, by combining the real and the imaginary parts in the figures, the graphs also provide a unique diagonal for the objects at each different frequency. These values can then be used to further identify the objects from their first order PT in the future related applications by using the appropriate tools.

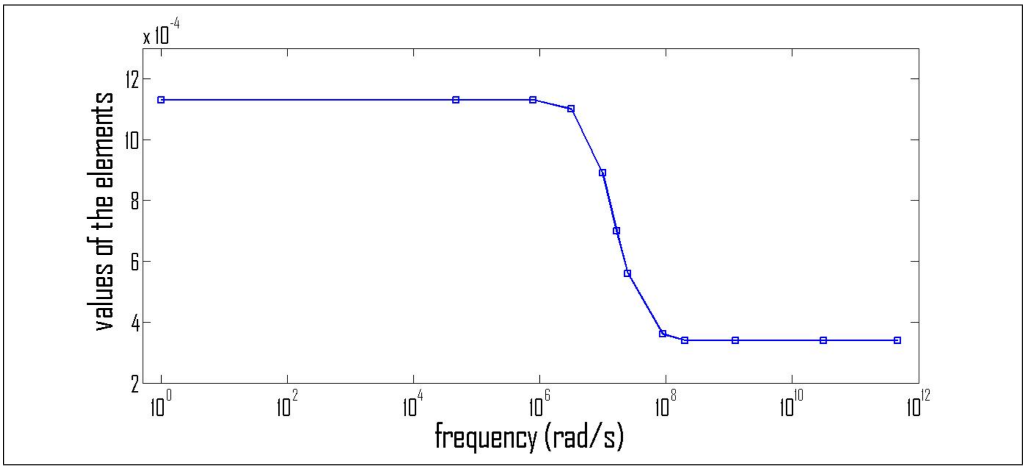

(a)

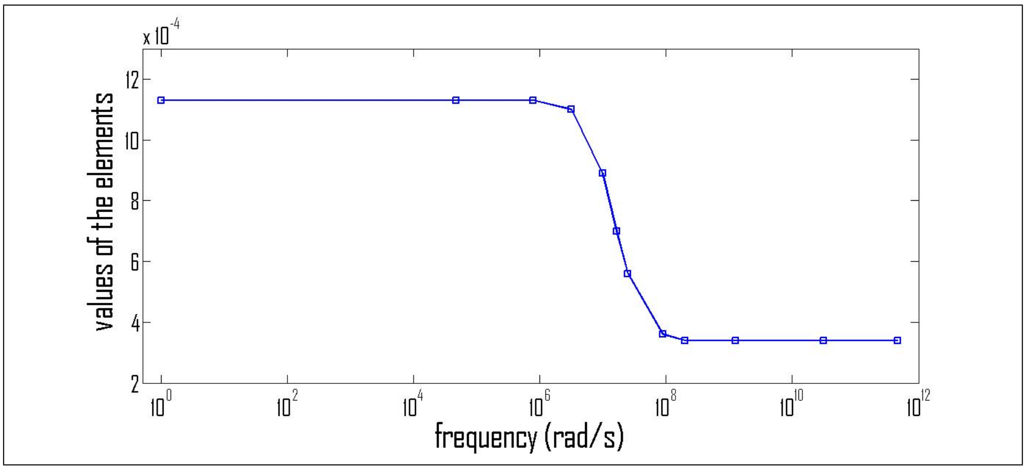

(b)

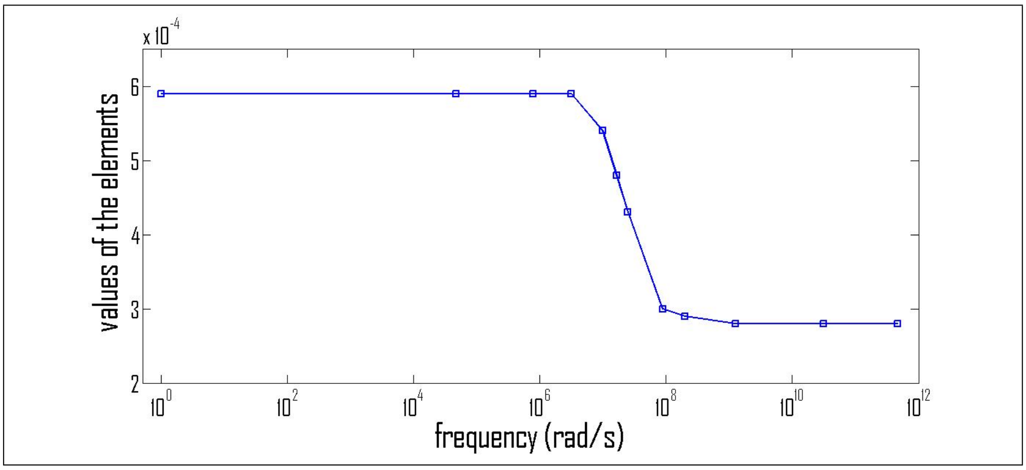

(c)

Figure 5.9: Diagonal elements (real part) of the approximated first order PT by *BEM++* for the model of vs50 landmine against frequencies ω (a) first diagonal (b) second diagonal (c) third diagonal

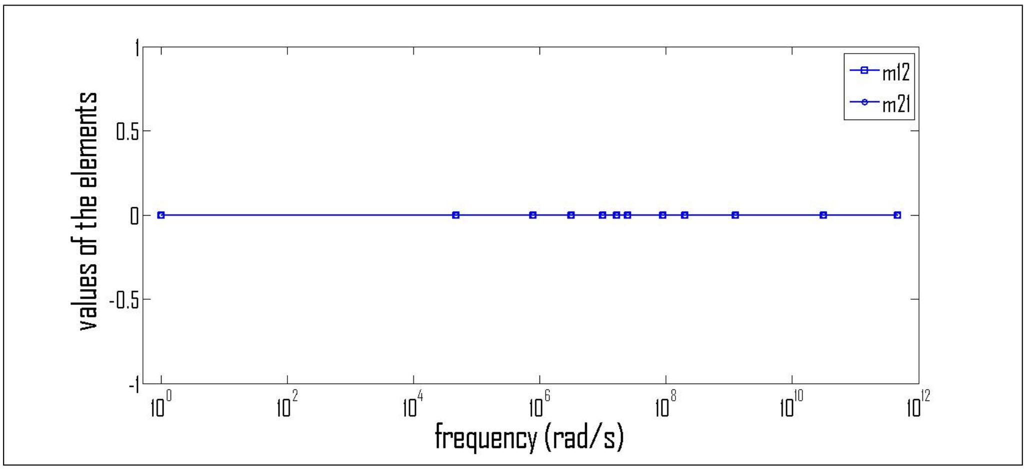

(a)

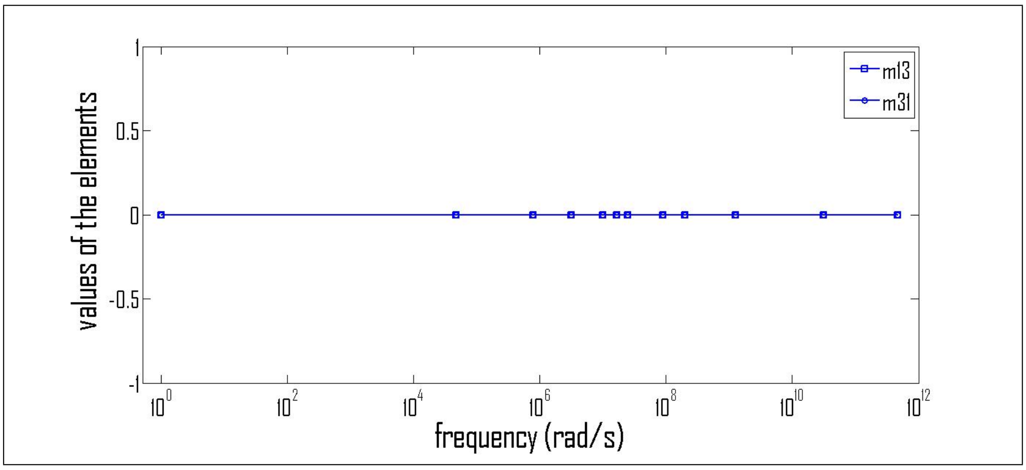

(b)

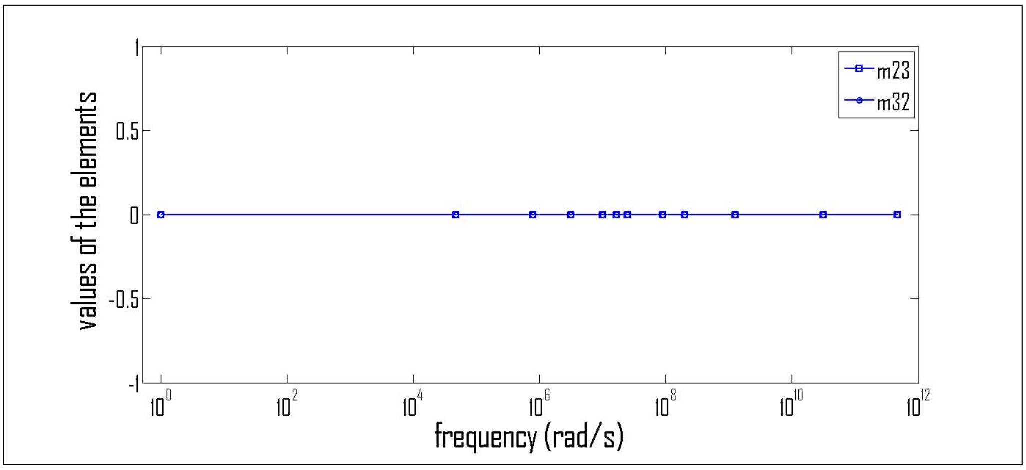

(c)

Figure 5.10: Non-diagonal elements (real part) of the approximated first order PT by *BEM++* for the model of vs50 landmine against frequencies ω

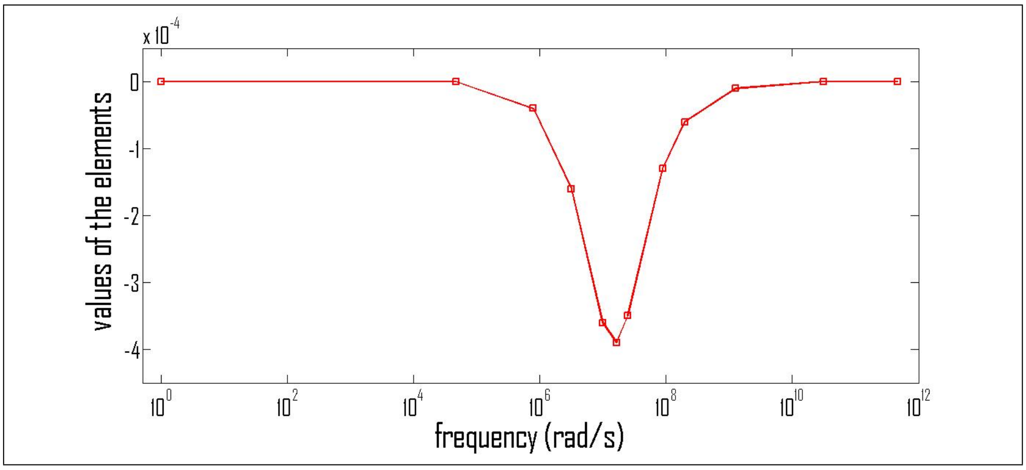

(a)

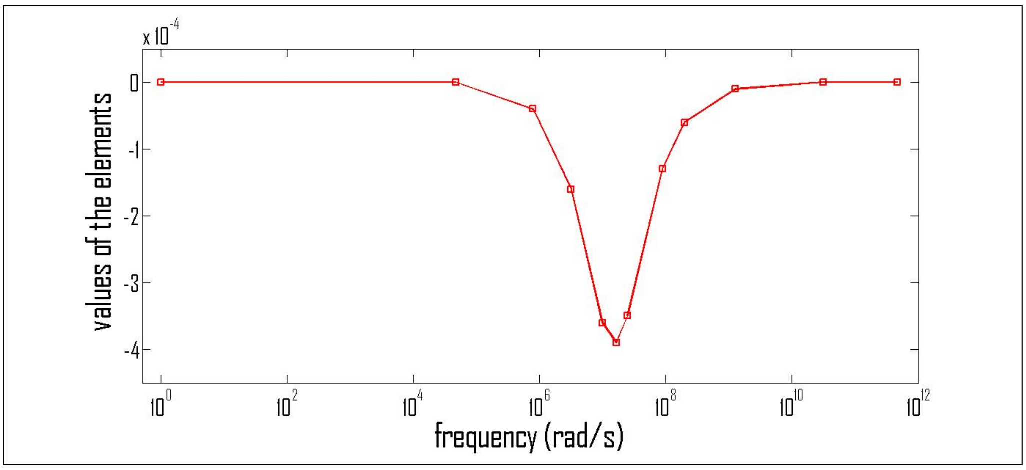

(b)

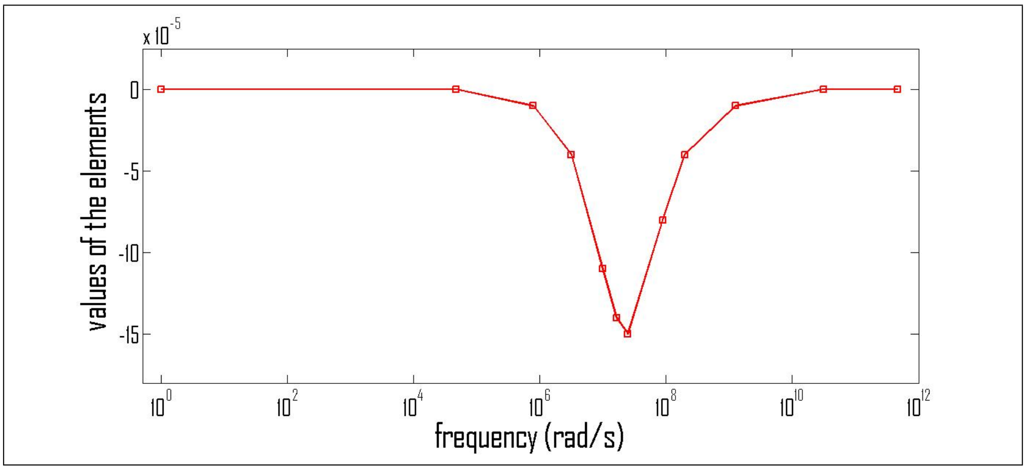

(c)

Figure 5.11: Diagonal elements (imaginary part) of the approximated first order PT by *BEM++* for the model of vs50 landmine against frequencies ω (a) first diagonal (b) second diagonal (c) third diagonal

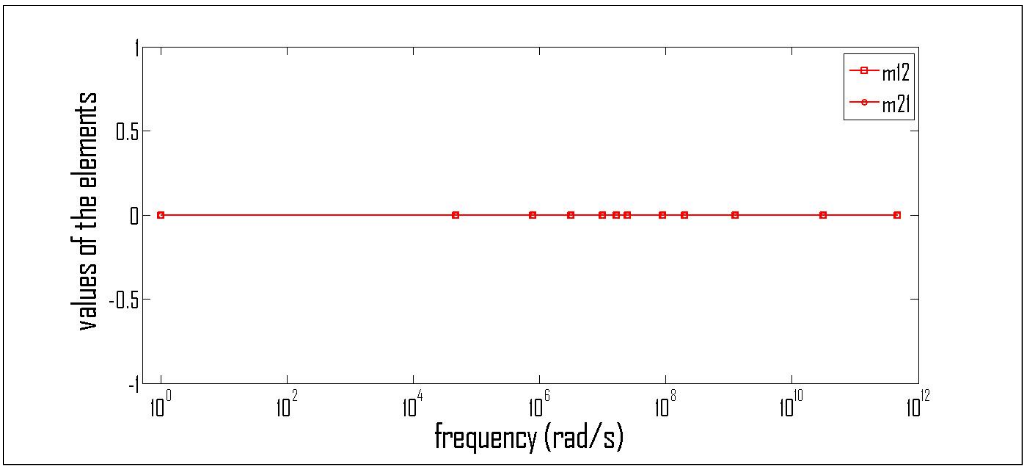

(a)

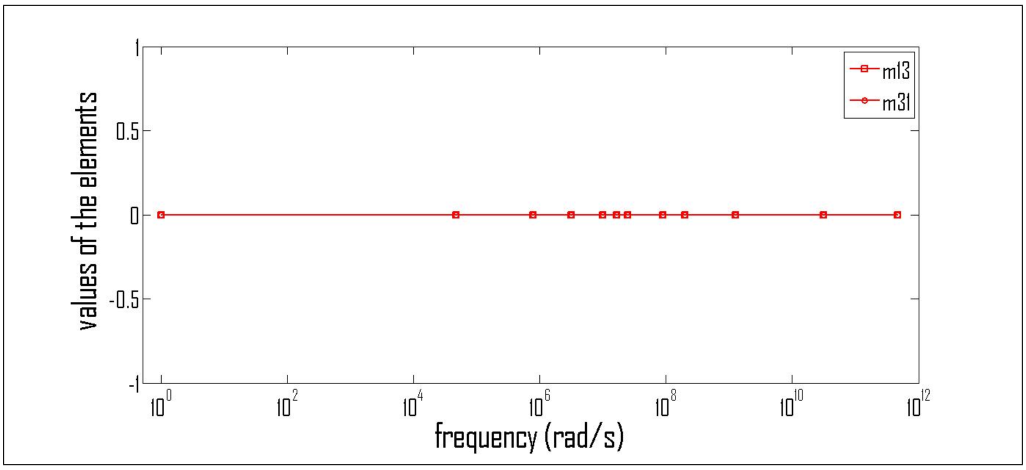

(b)

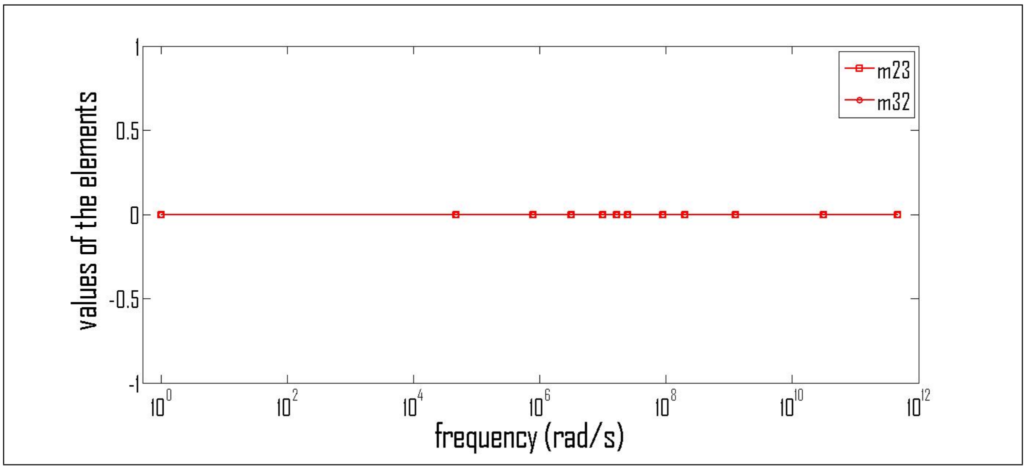

(c)

Figure 5.12: Non-diagonal elements (imaginary part) of the approximated first order PT by *BEM++* for the model of vs50 landmine against frequencies ω

5.4 Conclusions

In this chapter, we have investigated the first order PT for some objects with complex conductivities. We give numerical examples to show that the explicit formula of the first order PT with the real conductivity can also be used if the conductivity is complex. Here, we also investigate the frequency response of the first order PT with the hope to apply it in the future potential applications such as radar and GPR.

Chapter 6

The First Order PT in Electrosensing Fish

Weakly electric fish can be found in the rivers of South America and Africa. They perform electrosensing for navigation as well as to characterize objects and locate prey. Given that electrical imaging is a nonlinear and illposed inverse problem of considerable computational complexity, it would be surprising if electrosensing fish are able to perform a complete three dimensional spatial image reconstruction in real time. Experimental studies by von der Emde and Fetz [11] have shown that the fish *Gnathonemus petersii* can be trained to recognize and discriminate between conducting and insulating objects with variety kinds of shapes. Here, one possible mechanism for the fish to recognize shapes of objects from electrical data at some distance without using the image is to use the GPT of the object. In this chapter, we evaluate numerically the first order GPT for several objects used in the experiments. We then examine the first order GPT (or the first order PT) to provide evidences from the experimental study to support our hypothesis that it is used by weakly electric fish as part of their characterization algorithm.

6.1 Mathematical Model

Let the conductivity of the water or other objects in the water in the region exterior to a weakly electric fish be σ. The electrical voltage u due to electrical current generated by the fish in the region is assumed to satisfy the equation

$$\nabla \cdot (\sigma \nabla u) = 0 \tag{6.1}$$

to indicate that there is no other current source exterior to the fish. Consider the domain $\Omega = \mathbb{R}^3 - F$ where F is the fish. Suppose that there is an isolated object $B \subset \Omega$ which is assumed to be a Lipschitz bounded domain in $\mathbb{R}^3$ at some distance from the fish and for any point $\mathbf{x} \in \Omega$,

$$\sigma(\mathbf{x}) = \begin{cases} k & \text{for } \mathbf{x} \in B \\ 1 & \text{for } \mathbf{x} \in \Omega - B \end{cases} \tag{6.2}$$

where k constant. According to Ammari and Kang [8], the perturbation in the voltage due to a small object in the region Ω can be approximated by an asymptotic expansion where the dominant term of the expanison is determined by the PT.

Let H be the voltage inside the water without the object B such that $\nabla \cdot H = 0$ (H harmonic) from (6.1). Then, from [8] we have

$$(u - H)(x) = -\nabla \Gamma(\mathbf{x}) \cdot M \nabla H(0) + O(1/|\mathbf{x}|^2) \text{ as } |x| \to \infty \tag{6.3}$$

where the origin $O \in B$, $\Gamma(\mathbf{x}) = -(4\pi|\mathbf{x}|)^{-1}$ and M is the first order PT. Thus, instead of using the voltage in (6.3), one can now consider the first order PT, M to describe B. Here M of an object B is a 3×3 matrix in the form of (2.1) and can be determined by solving the similar integral equation (1.3), (1.4) and (1.5). Furthermore, M is independent of position B from the fish, F as given by (6.3) and it is shown in [8] that M is symmetry. In addition, M of an object rotates when the object rotates as given by Theorem 2 (see Chapter 2) and this suggests that the eigenvalues of M describe the shape while the eigenvectors tell the orientation of the object. At the same time, this also means shape of two objects might not be discriminated if both objects have the same first order PT. We also assume that the shape is independent of position when discriminated by the electrosensing fish through M.

In their series of experiments, von der Emde and Fetz [12] suggested that weakly electric fish *Gnathonemus petersii* were actually able to perform complex objects recognition tasks. However, they did not consider the PT of the objects in their findings. In this study, the PT of objects used in [12] are calculated and used to reexamine the experiments to support our hypothesis and stimulate further research for investigating the role of the PT in object characterization by the fish.

6.2 Experimental Biology and the First Order PT

In order to investigate the role of the first order PT in electrosensing by weakly electric fish, we have considered a few experiments done by von der Emde and Fetz [12]. Previously, they conducted a series of experiments to the fish to investigate the ability of the fish to recognize shape and conductivity contrast of a few objects. During their study [12], eight fish were trained to accept or reject two different objects. Each fish was rewarded for choosing the correct object and punished for choosing the wrong object until they were able to choose the correct object with 75% succession rate in three consecutive days. Some controls were also used to ensure that the fish depended only on their electrical sense in making decision. The period taken by each fish to complete the training was then recorded. In this study, only five fish from the study are used. For later convenient, we have renamed Fish 1, Fish 2, Fish 3, Fish 7 and Fish 8 in [12] as Fish B, Fish A, Fish E, Fish C and Fish D respectively.

For the purpose of this study, we compute the first order PT for the objects used in the chosen experiments with *BEM++* according to Chapter 3. In order to make computation, mesh of triangular elements for each object is firstly generated by *Netgen*. After that, we repeat the computation in *BEM++* by uniformly increasing the number of elements for the mesh with *Netgen* until there is no relative difference at six decimal places between the current and the previous solutions where the current computed solution is then chosen to approximate the first order PT for each object.

The resulting first order PT as matrices for all objects are then analyzed to achieve our purpose. Here, for the first order PT of an object, B denoted by M_B, all three eigenvalues of M_B are firstly determined. Each eigenvalues of M_B is then normalized by taking its ratio to the largest eigenvalue of M_B. After that, the average of the normalized eigenvalues is computed to measure M_B. In this case, if the fish use the first order PT to recognize objects in the previous experiment, we say that two objects are electrically similar to the fish if the average of the normalized eigenvalues of M_B for both objects are the same.

Table 6.1: The first order PT for a few objects presented in [12]

Object, B	Dimension (cm)	The First Order PT, M_B	$\hat{e}_{M_B}$	$\hat{c}$
Cone	$d = h = 3$	$10^{-5} \times \begin{bmatrix} 0.28 & 0 & 0 \\ 0 & 0.28 & 0 \\ 0 & 0 & 0.31 \end{bmatrix}$	0.9032 0.9032 1.0000	0.9355
Cube	$l = w = h = 3$	$10^{-5} \times \begin{bmatrix} 0.98 & 0 & 0 \\ 0 & 0.98 & 0 \\ 0 & 0 & 0.98 \end{bmatrix}$	1.0000 1.0000 1.0000	1.0000
Pyramid	$l = w = h = 3$	$10^{-5} \times \begin{bmatrix} 0.42 & 0 & 0 \\ 0 & 0.42 & 0 \\ 0 & 0 & 0.32 \end{bmatrix}$	0.7619 1.0000 1.0000	0.9206

note : cm = centimeter, d = diameter, h = height, l = length, w = width

Table 6.2: Results for the training in [12]

Fish	Accept, S+	Reject, S-	Period (Days)	v
A	Pyramid	Cube	4	0.0794
B			7	
C	Cone	Cube	8	0.0645
D			10	
E	Cone	Pyramid	19	0.0149

6.3 Results and Discussion

Since objects from [12] considered here are made from high conducting metal, the first order PT of each object, M_B is calculated at conductivity 10^7 in this study. Each M_B is shown accurately at six decimal places in Table 6.1 together with its normalized eigenvalues, $\hat{e}_{M_B}$. The average of the normalized eigenvalues of M_B denoted by $\hat{c}$ is also included in the table. Based on Table 6.1, we can see that each M_B is a diagonal matrix. Furthermore, cone and pyramid have two distinct eigenvalues while cube has only one.

Table 6.2 then shows the time taken by the fish in [12] to complete their training in accepting and rejecting two objects (denoted by S+ and S- respectively) based on the explanation in the previous section. Here, we extend these results by finding the absolute difference of $\hat{c}$ for S+ and S- denoted by v to deduce the role of the first order PT in this training. According to this table, Fish E takes the longest time to discriminate cone and pyramid and we can see that these two objects have the smallest v between them. Furthermore, Fish A and Fish B are able to achieve their tasks in

Table 6.3: The similar first order PT for S and B

Object, S	Ellipsoid, B	The First Order PT for S and B
Cone $d = h = 3$	$a = 1.28$ $b = 1.28$ $c = 1.40$	$10^{-5} \times \begin{bmatrix} 0.28 & 0 & 0 \\ 0 & 0.28 & 0 \\ 0 & 0 & 0.31 \end{bmatrix}$
Cube $l = w = h = 3$	$a = 1.98$ $b = 1.98$ $c = 1.98$	$10^{-5} \times \begin{bmatrix} 0.98 & 0 & 0 \\ 0 & 0.98 & 0 \\ 0 & 0 & 0.98 \end{bmatrix}$
Cylinder $d = h = 3$	$a = 1.69$ $b = 1.69$ $c = 1.99$	$10^{-5} \times \begin{bmatrix} 0.67 & 0 & 0 \\ 0 & 0.67 & 0 \\ 0 & 0 & 0.82 \end{bmatrix}$
Hemisphere $d = 3$	$a = 1.50$ $b = 1.50$ $c = 0.82$	$10^{-5} \times \begin{bmatrix} 0.31 & 0 & 0 \\ 0 & 0.31 & 0 \\ 0 & 0 & 0.15 \end{bmatrix}$
Pyramid $l = w = h = 3$	$a = 1.56$ $b = 1.56$ $c = 1.24$	$10^{-5} \times \begin{bmatrix} 0.42 & 0 & 0 \\ 0 & 0.42 & 0 \\ 0 & 0 & 0.32 \end{bmatrix}$

note : dimensions are in centimeter (cm), d = diameter, h = height, l = length, w = width

a shorter period than Fish C and Fish D. At the same time, v between pyramid and cube differentiated by Fish A and Fish B is larger than v between cone and cube differentiated by Fish C and Fish D. This suggests that the fish use the first order PT as part of their recognition algorithm where they need more time to complete the training when the objects have almost similar first order PT. In this case, the similarity between the first order PT for both objects is represented by v.

However, our findings here are not yet conclusive. In order to conclude whether the first order PT has a role in the way fish perform this task, further experiments to test whether fish can distinguish two objects with similar first order PT need to be carried out. If the fish can discriminate these two objects then we can conclude that it uses not just the first order PT. It might be that it uses higher order PT as well for example. Table 6.3 shows a few ellipsoids with semi principal axes a, b and c that have similar first order PT with the given objects, S where the ellipsoids are determined based on the method in the previous chapter. Here, the conductivity of all objects and the ellipsoids are fixed to 10^7 to indicate that in this example, all of them are made by the same high conducting metal. A pair of objects with similar first order PT from this table can then be used during the experiment to the fish in the future.

Besides, another easy future test that can be performed is by giving, for example, a pair of a cone pointing up and down for the fish to discriminate since both cone pointing up and down have the same first order PT. This can be quickly shown by using Theorem 2 (see Chapter 2) and appropriate rotation matrix to find the first order PT for the cone pointing down from the first order PT for the cone pointing up where cone pointing down is a result after cone pointing up is rotated 180°. Indeed, as the first order PT in some sense is the best electrically in fitting ellipsoid, it is probably insufficient to only test whether the fish can discriminate between a cone pointing up and down. Since two similar ellipsoids can be constructed from both cones, asking the fish to electrically distinguish cone pointing up and down might be similar with asking whether it can discriminate two equal ellipsoids. This is a false test in our case as we want to investigate how the first order PT characterizes different objects.

In addition, when investigating electrosensing fish, it might be useful to consider the PT with complex conductivity $k = \sigma + \omega\epsilon \mathrm{i}$ (as defined by [56]) where σ and ϵ are object's conductivity and permittivity while ω (rad/s) is the frequency. During electrosensing, black ghost knife fish use almost pure sine wave whereas elephant nose fish use something more like a square wave with a wider range of frequencies (see [14] and [15]). Here, the knife fish have to use a pure frequency to not interfere with each other but the elephant nose fish do not have that restriction. Thus, the PT with complex conductivity which depends on frequency might discriminate between objects of interest for different fish. In this case, for example, it might be worth to conduct experiments to test whether the elephant nose fish can distinguish objects that cannot be discriminated by the black ghost knife fish.

Furthermore, by considering fictional complex conductivity $k = 1.5 + 0.1\omega\mathrm{i}$ for ellipsoid with semi-principal axes 3 cm, 2 cm and 1 cm, we evaluate using (2.2) its first order PT at a few frequencies, f Hz (Hertz) denoted by M_f where $\omega = 2\pi f$. As in Chapter 5, each M_f is now a complex matrix and thus can be expressed as $\mathcal{R} + \mathcal{J}\mathrm{i}$ such that the 3×3 symmetrical real matrices $\mathcal{R}$ and $\mathcal{J}$ are the real and imaginary parts of M_f. Similarly, for every M_f, the three eigenvalues of $\mathcal{R}$ are normalized by dividing each of them with the largest eigenvalues of $\mathcal{R}$ while the three eigenvalues of $\mathcal{J}$ are also normalized by dividing each of them with the largest eigenvalues of $\mathcal{J}$. In Table 6.4, the normalized eigenvalues of both $\mathcal{R}$ and $\mathcal{J}$ denoted by $\hat{e}^{M_{f_{\mathcal{R}}}}$ and $\hat{e}^{M_{f_{\mathcal{J}}}}$ are

Table 6.4: M_f for an ellipsoid at a few frequencies, f (Hz)

Frequency, f (Hz)	$\hat{e}^{M_{f_{\mathcal{R}}}}$	$\hat{c}^{M_{f_{\mathcal{R}}}}$	$\hat{e}^{M_{f_{\mathcal{J}}}}$	$\hat{c}^{M_{f_{\mathcal{J}}}}$
20	0.3370 0.6778 1.0000	0.6716	0.0927 0.3998 1.0000	0.4975
50	0.2821 0.6015 1.0000	0.6279	0.0766 0.3524 1.0000	0.4763
120	0.2730 0.5880 1.0000	0.6203	0.0740 0.3441 1.0000	0.4727
250	0.2715 0.5857 1.0000	0.6191	0.0736 0.3427 1.0000	0.4721
500	0.2712 0.5852 1.0000	0.6188	0.0735 0.3424 1.0000	0.4720

Table 6.5: The average between $\hat{c}^{M_{f_{\mathcal{R}}}}$ and $\hat{c}^{M_{f_{\mathcal{J}}}}$ for each M_f

Frequency, f (Hz)	$\hat{c}^{M_f}$
20	0.5846
50	0.5521
120	0.5465
250	0.5456
500	0.5454

shown for each M_f. In addition, for each M_f, we also include in the same table the average for both $\hat{e}^{M_{f_{\mathcal{R}}}}$ and $\hat{e}^{M_{f_{\mathcal{J}}}}$ and denoted them respectively by $\hat{c}^{M_{f_{\mathcal{R}}}}$ and $\hat{c}^{M_{f_{\mathcal{J}}}}$.

Next, in order to further describe each M_f, we also evaluate $\hat{c}^{M_f}$, the average between $\hat{c}^{M_{f_{\mathcal{R}}}}$ and $\hat{c}^{M_{f_{\mathcal{J}}}}$ as shown in Table 6.5. From this table, we can see that the values of $\hat{c}^{M_f}$ are different for each f. In this case, if $\hat{c}^{M_f}$ is used to represent the ellipsoid, the ellipsoid will be described distinctly for each frequency. Thus, there is a possibility of differently recognizing one same ellipsoid by electrosensing fish with different generating frequencies. This could be a very useful strategy that can be learned from the fish to describe eletrical objects for the related applications in the future.

Finally, as the expansion (6.3) is asymptotic in distance, the tests should be performed in such a way that the fish are at least a certain distance from the object. Some controls need to be made to ensure that the distance is not too close to ensure formula (6.3) is mathematically valid. On the other hand, the object also must not be too far from the fish so that it can be eletrically sensed by the fish.

6.4 Conclusions

In this chapter, the role of the first order PT in electrosensing fish has being presented, where, we first discuss the related mathematical background that is similar to the EIT. After that, we study some experiments conducted by the biologists to find some evidences to suggest that the first order PT for an object is considered by the fish when characterizing the object. We also recommend future researches that can be conducted to the fish to further investigate this by considering the first order PT with both real and complex conductivities.

Chapter 7

Investigating the PT for Metal Detection

In the eddy current approximation to Maxwell's equations, Ammari et al. [27] derived an asymptotic formula that represented the perturbation of the magnetic field due to the presence of an isolated conducting (could also be magnetic) object. Based on this foundation, Ledger and Lionheart [29] applied tensor operations to introduce a new rank 2 polarization tensor (PT) by combining the magnetic and conductivity polarization tensors given in [27]. Furthermore, it is shown by [29, 30] that the magnetic polarizibilty tensor from engineering literatures for metal detection in [24, 25, 26, 55] is equivalent to the rank 2 polarization tensor in [29]. Therefore, instead of experimental works or simulations, the polarizibility tensor [24, 25, 26, 55] can be alternatively determined for the first time from an explicit formula of the rank 2 polarization tensor [29]. In this chapter, we compute the rank 2 polarization tensor according to [29] and compare it to the polarizibility tensor from engineering works in [24] and [26] in order to numerically justify the agreements between the two tensors.

7.1 Mathematical Formulation and Some Properties of the PT

Metal detectors use low frequency electromagnetic field to locate a high conducting target in a low conducting background from electromagnetic induction data. By neglecting the displacement currents in the Maxwell's equations, metal detection can be modelled by the eddy current equations (see [27, 29]). In this case, a mathematical justification for approximating Maxwell's equations by the eddy current model can be found in [57] and [58]. Now, the mathematical formulation of the PT for metal detection is discussed here by considering first the eddy current model presented in [27, 29]. We assume the presence of an object in the form $B_\alpha = \boldsymbol{z} + \alpha B$ where B is a unit object centered at the origin, α denotes a scaling for B and $\boldsymbol{z}$ denotes a translation vector. Introduce

$$\mu_\alpha = \begin{cases} \mu_* & \text{in } B_\alpha \\ \mu_0 & \text{in } \mathbb{R}^3 \setminus B_\alpha \end{cases}, \ \sigma_\alpha = \begin{cases} \sigma_* & \text{in } B_\alpha \\ 0 & \text{in } \mathbb{R}^3 \setminus B_\alpha \end{cases} \tag{7.1}$$

where $\mu_0 = 4\pi \times 10^{-7}$ NA^{-2} (Newton per Ampere^{-2}) is permeablitiy of the free space while both μ_* and σ_* denote the permeability and conductivity of the inclusion B_α. In this case, μ_* and σ_* are just constants and we drop the subscript α when considering B later on. Moreover, the conductivity contrast between the object and the background has been assumed to be sufficiently high such that the background can be approximated by a zero conductivity.

Let $\boldsymbol{E}_\alpha$ and $\boldsymbol{H}_\alpha$ be the time harmonic eddy current fields (electric and magnetic) in the presence of conducting object B_α that result from a current source $\boldsymbol{J}_0$ located outside B_α. Suppose that $\nabla \cdot \boldsymbol{J}_0 = 0$ in $\mathbb{R}^3$. Both fields $\boldsymbol{E}_\alpha$ and $\boldsymbol{H}_\alpha$ satisfy the eddy current equations

$$\begin{aligned} \nabla \times \boldsymbol{E}_\alpha &= \mathrm{i}\omega\mu_\alpha \boldsymbol{H}_\alpha \text{ in } \mathbb{R}^3, \\ \nabla \times \boldsymbol{H}_\alpha &= \sigma_\alpha \boldsymbol{E}_\alpha + \boldsymbol{J}_0 \text{ in } \mathbb{R}^3, \\ \boldsymbol{E}_\alpha(\boldsymbol{x}) = O(|\boldsymbol{x}|^{-1}),\ & \boldsymbol{H}_\alpha(\boldsymbol{x}) = O(|\boldsymbol{x}|^{-1}) \text{ as } |\boldsymbol{x}| \to \infty, \end{aligned} \tag{7.2}$$

where i is the standard imaginary unit and ω is a fixed angular frequency of the current source. The depth of penetration of the magnetic field in the conducting object is desribed by its skin depth, $s = \sqrt{2/(\omega\mu_*\sigma_*)}$. On the other hand, without the object B_α, the fields $\boldsymbol{E}_0$ and $\boldsymbol{H}_0$ that result from the time varying current source satisfy

$$\begin{aligned} \nabla \times \boldsymbol{E}_0 &= \mathrm{i}\omega\mu_0 \boldsymbol{H}_0 \text{ in } \mathbb{R}^3, \\ \nabla \times \boldsymbol{H}_0 &= \boldsymbol{J}_0 \text{ in } \mathbb{R}^3, \\ \boldsymbol{E}_0(\boldsymbol{x}) = O(|\boldsymbol{x}|^{-1}),\ & \boldsymbol{H}_0(\boldsymbol{x}) = O(|\boldsymbol{x}|^{-1}) \text{ as } |\boldsymbol{x}| \to \infty. \end{aligned} \tag{7.3}$$

By introducing $\nu = 2\alpha^2/s^2$, the related asymptotic formula for the above model that describes the pertubation in the magnetic field at a position $\boldsymbol{x}$, away from $\boldsymbol{z}$, due to the presence of B_α when $\nu = O(1)$ and $(\mu_*/\mu_0) = O(1)$ as $\alpha \to 0$ is given by Ammari et al. [27] in the form

$$
\begin{aligned}
(\boldsymbol{H}_\alpha - \boldsymbol{H}_0)(\boldsymbol{x}) = -\tfrac{\mathrm{i}\nu\alpha^3}{2} \textstyle\sum_{i=1}^{3} \boldsymbol{H}_0(\boldsymbol{z})_i (\int_B \boldsymbol{D}_{\boldsymbol{x}}^2 G(\boldsymbol{x},\boldsymbol{z})\boldsymbol{\xi} \times \\
(\boldsymbol{\theta}_i + \hat{\boldsymbol{e}}_i \times \boldsymbol{\xi}) \mathrm{d}\boldsymbol{\xi}) + \alpha^3 \left(1 - \tfrac{\mu_0}{\mu_*}\right) (\textstyle\sum_{i=1}^{3} \boldsymbol{H}_0(\boldsymbol{z})_i \boldsymbol{D}_{\boldsymbol{x}}^2 G(\boldsymbol{x},\boldsymbol{z}) \\
\textstyle\int_B \left(\hat{\boldsymbol{e}}_i + \frac{1}{2}\nabla \times \boldsymbol{\theta}_i\right) \mathrm{d}\boldsymbol{\xi}) + \boldsymbol{R}(\boldsymbol{x})
\end{aligned}
\tag{7.4}
$$

where $\boldsymbol{\xi}$ is measured from the center of B. Here, $G(\boldsymbol{x},\boldsymbol{z}) = (4\pi|\boldsymbol{x}-\boldsymbol{z}|)^{-1}$ is the free space Laplace Green's function and $\boldsymbol{R}(\boldsymbol{x}) = O(\alpha^4)$ is a small remainder term. Furthermore, for $i = 1,2,3$, $\hat{\boldsymbol{e}}_i$ is a unit vector for the i-th Cartesian coordinate direction, $\boldsymbol{H}_0(\boldsymbol{z})_i$ denotes the i-th element of $\boldsymbol{H}_0(\boldsymbol{z})$ and $\boldsymbol{\theta}_i$ is the solution to the transmission problem

$$
\begin{cases}
\nabla_{\boldsymbol{\xi}} \times \mu^{-1} \nabla_{\boldsymbol{\xi}} \times \boldsymbol{\theta}_i - \mathrm{i}\omega\sigma\alpha^2 \boldsymbol{\theta}_i = \mathrm{i}\omega\sigma\alpha^2 \hat{\boldsymbol{e}}_i \times \boldsymbol{\xi} & \text{in } B \cup B^c, \\
\nabla_{\boldsymbol{\xi}} \cdot \boldsymbol{\theta}_i = 0 & \text{in } B^c, \\
[\boldsymbol{\theta}_i \times \hat{\boldsymbol{n}}]_\Gamma = \boldsymbol{0} & \text{on } \Gamma, \\
[\mu^{-1} \nabla_{\boldsymbol{\xi}} \times \boldsymbol{\theta}_i \times \hat{\boldsymbol{n}}]_\Gamma = -2[\mu^{-1}]_\Gamma \hat{\boldsymbol{e}}_i \times \hat{\boldsymbol{n}} & \text{on } \Gamma, \\
\boldsymbol{\theta}_i(\boldsymbol{\xi}) = O(|\boldsymbol{\xi}|^{-1}) & \text{as } |\boldsymbol{\xi}| \to \infty
\end{cases}
\tag{7.5}
$$

where $\hat{\boldsymbol{n}}$ is the outward normal vector to Γ, the boundary of B. Based on (7.4) and (7.5), the *conductivity polarization tensor* (CPT) and the *magnetic* (or *permeability*) *polarization tensor* (MPT) have been introduced in [27].

Using this framework, Ledger and Lionheart [29] have applied tensor operations to combine both CPT and MPT as well as reformulate (7.4) in the alternative form

$$
(\boldsymbol{H}_\alpha - \boldsymbol{H}_0)(\boldsymbol{x}) = \boldsymbol{D}_{\boldsymbol{x}}^2 G(\boldsymbol{x},\boldsymbol{z}) \check{\check{M}} \boldsymbol{H}_0(\boldsymbol{z}) + \boldsymbol{R}(\boldsymbol{x}) \tag{7.6}
$$

where $\check{\check{M}}$ is the new polarization tensor for a conducting and magnetic inclusion B_α. Importantly, they show that $\check{\check{M}}$ is a complex symmetric rank 2 tensor defined by six complex coefficients after reducing (7.4) to (7.6). The *hp*-finite element method presented in [59] is also used in [29] to numerically compute $\check{\check{M}}$ and some analysis for the errors in the method are also given. In this study, the same $\check{\check{M}}$ is considered, where our main motivation for choosing this is because it agrees with the engineering prediction about the polarization tensor for metal detector [29]. The rank 2 tensor $\check{\check{M}}$ is given by [29] as

$$\check{\check{M}} = N_{ji} - C_{ji} \tag{7.7}$$

where

$$N_{ji} = \alpha^3 \left(1 - \frac{\mu_0}{\mu_*}\right) \int_B \left(\hat{\boldsymbol{e}}_j \cdot \hat{\boldsymbol{e}}_i + \frac{1}{2}\hat{\boldsymbol{e}}_j \cdot \nabla \times \boldsymbol{\theta}_i\right) \mathrm{d}\boldsymbol{\xi} \tag{7.8}$$

and

$$C_{ji} = \left(-\frac{\mathrm{i}\nu\alpha^3}{4}\right) \hat{\boldsymbol{e}}_j \cdot \int_B \boldsymbol{\xi} \times (\boldsymbol{\theta}_i + \hat{\boldsymbol{e}}_i \times \boldsymbol{\xi}) \mathrm{d}\boldsymbol{\xi} \tag{7.9}$$

for $j = 1, 2, 3$ and θ_i is the solution to the previous (7.5) for $i = 1, 2, 3$. Note that N_{ji} (denoted as N) is an equivalent form of the original rank 2 tensor MPT in [27]. Furthermore, the rank 2 tensor C_{ji} (denoted as C) is a reduction of the original rank 4 tensor CPT in [27] introduced by [29] using tensor operations.

After some manipulations, it can be shown that the coefficients (or elements) of the rank 2 tensor $\check{\check{M}}$ can be expressed as 3×3 complex matrix and if $\check{\check{M}}$ is expressed as $\check{\check{M}} = \mathcal{R} + \mathcal{J}\mathrm{i}$, each $\mathcal{R}$ and $\mathcal{J}$ has three real eigenvalues. For a conducting (magnetic) sphere, the analytical formula for $\check{\check{M}}$ is also given in [29] on page 13. In addition, [29] also explain that $\check{\check{M}} = N$ when B_α has $\sigma_* = 0$ such that B_α is a magnetic non-conducting object. Therefore, $\check{\check{M}} = N$ for a magnetic non-conducting object B_α is real symmetric as given by (7.8). Moreover, according to [29], N for a magnetic non-conducting object B_α here reduces to the first order GPT so $\check{\check{M}} = N$ can now be determined by solving the previous boundary integral equations (1.3)-(1.5) where the parameter k is now the contrast μ_*/μ_0 (or the relative permeability of B_α).

7.2 Polarizibility Tensor and the Rank 2 PT

In the engineering literatures (for examples [24, 25, 26]), the polarization (polarizibility) tensor $\bar{\bar{M}}$ for a metallic object was expressed as

$$\boldsymbol{V}_{ind} = \boldsymbol{H}^T \cdot (\bar{\bar{M}} \boldsymbol{H}^R) \tag{7.10}$$

where $\boldsymbol{V}_{ind}$ were measurements of induced voltage in a coil due to the presence of an object while both $\boldsymbol{H}^T$ and $\boldsymbol{H}^R$ were the fields generated by the transmitting and receiving coil respectively. Rather than using the explicit formula, the coefficients of $\bar{\bar{M}}$ in [24] and [26] were approximated after simulating or measuring $\boldsymbol{V}_{ind}$, $\boldsymbol{H}^T$ and $\boldsymbol{H}^R$. Recently, the equivalence between $\bar{\bar{M}}$ and $\check{\check{M}}$ was established in [30] and for the first time, an explicit formula of $\bar{\bar{M}}$ was given and equal to (7.7) of $\check{\check{M}}$.

In Dekdouk et al. [26], electromagnetic induction data due to the presence of a few objects were simulated in two systems namely the trial axial Helmholtz coil system (TAHC) and the electromagnetic induction plannar sensor (EMIPS, which is a type of metal detector). An optimization technique was then applied by [26] to (7.10) based on the simulated data from both systems to estimate $\bar{\bar{M}}$ for the objects. Two sets of $\bar{\bar{M}}$ for each object were obtained for both systems and hence were then compared in [26].

On the other hand, Marsh et al. [24] conducted several experiments for a walk-through metal detector (WTMD) to determine $\bar{\bar{M}}$ for a few test objects in security screening. Measurements from an array of coils in WTMD were taken following the passage of a candidate carrying the tested object. These measurements were then used in their proposed algorithm to determine $\bar{\bar{M}}$ for the object and its location from (7.10).

In order to compare $\bar{\bar{M}}$ for objects in [24] and [26] to the rank 2 tensor $\check{\check{M}}$ in (7.6), the same *hp*-FEM method described in [29] will be used to numerically compute $\check{\check{M}}$ for the object by approximating the solution to (7.5) and then using (7.7)-(7.9). Three objects each from [24] and [26] are considered where they are listed in Table 7.1 together with their material properties, μ_* in NA^{-2} (Newton per ampere^2) and σ_* in Sm^{-1} (Siemens per meter). The objects from [26] are aluminium sphere (AS) and two metal components of two landmines (ring of elsie mine (REM) and detonator analogue of type 72 AP mine (DA72)) while ferrite sphere and two models of gun are from [24].

Before computing the rank 2 tensor $\check{\check{M}}$ for an object B_α, a finite domain $\tilde{B}^c$ at a finite distance from the unit object, B of B_α must be created as required by the method where $\tilde{B}^c$ can be any suitable domain. Next, the software *Netgen* is used to create the mesh with `N` tetrahedral elements for the union $B \cup \tilde{B}^c$ (the mesh in Table 7.1 represents the unit object, B for each B_α). Either linear or quadratic elements for representing the geometry can be used in the method. In our study, after setting α according to the actual dimension of B_α, the method proposed by [29] is repeatedly run by uniformly increasing the polynomial degree, p of the *hp*-FEM or alternatively, fixing the polynomial degree and refining the mesh in order to approximate $\check{\check{M}}$ for the object

Table 7.1: A few objects from [24, 26] with their type of material and dimension

<table>
<tr><th>Object, B_α</th><th>Material</th><th>μ_* (NA^{-2})</th><th>σ_* (Sm^{-1})</th><th>Dimensions</th></tr>
<tr><td rowspan="2">Sphere
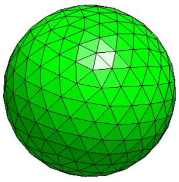</td><td>Ferrite</td><td>$12\mu_0$</td><td>0</td><td>$d = 3.7$</td></tr>
<tr><td rowspan="4">Aluminium</td><td rowspan="4">μ_0</td><td rowspan="4">3.5×10^7</td><td>$d = 1$</td></tr>
<tr><td>REM
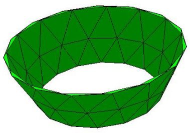</td><td>$d_{max} = 5.2$
$h_{max} = 1.5$</td></tr>
<tr><td>DA72
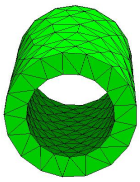</td><td>$d_{max} = 0.6$
$h_{max} = 1$</td></tr>
<tr><td rowspan="2">Gun
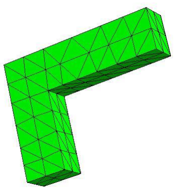</td><td>$l_{max} = 7.5$
$w_{max} = 5.8$
$h_{max} = 1.4$</td></tr>
<tr><td>Steel</td><td>$100\mu_0$</td><td>6×10^6</td><td>$l_{max} = 7.5$
$w_{max} = 5.8$
$h_{max} = 1.8$</td></tr>
</table>

note : dimensions are in centimeter (cm), d = diameter, h = height, l = length, w = width

Table 7.2: The setting in hp-FEM to compute $\check{\check{M}}$ for objects in [26]

Object, B_α	Geometry Representation	`N`	p
AS	Quadratic	2425	3
REM	Linear	10473	3
DA72	Quadratic	5629	3

B_α. The former procedure is called p-refinement while the latter is called h-refinement. These are done until there is no relative difference at some decimal places (depending on the object B_α) between the latest computed solution and the previous computed solution. The latest computed solution is then chosen to approximate $\check{\check{M}}$.

7.3 Results and Discussions

In this section, $\check{\check{M}}$ for each B_α in Table 7.1 are firstly approximated by the hp-FEM method. After that, we compare the coefficients of $\bar{\bar{M}}$ obtained from simulations in the systems TAHC and EMIPS to the coefficients of the approximated $\check{\check{M}}$ and analyze the results. Then, the coefficients of $\bar{\bar{M}}$ determined from experiments by using the WTMD are compared to the coefficients of $\check{\check{M}}$.

7.3.1 $\bar{\bar{M}}$ and $\check{\check{M}}$ for systems TAHC and EMIPS

Besides μ_* and σ_* of the object, Table 7.2 shows settings employed in the hp-FEM method to approximate every coefficient of $\check{\check{M}}$ for the object, B_α presented in [26] at the same frequency as [26]. In the table, `N` is the number of tetrahedral elements for $B \cup \tilde{B}^c$ in *Netgen* and for each object B_α, p of the hp-FEM is equal to 3. Computation to ten decimal places in the hp-FEM produces a complex diagonal matrix for the approximated $\check{\check{M}}$ for the AS where the diagonals are all equal, which also agrees with the analytical solution given in [29].

For convenience of later comparisons, the polarizibility tensor for the object obtained by [26] from the systems TAHC and EMIPS are now respectively denoted by $\bar{\bar{M}}_{\text{TAHC}}$ and $\bar{\bar{M}}_{\text{EMIPS}}$. In this case, each object B_α is represented by three tensors which are the approximated $\check{\check{M}}$, $\bar{\bar{M}}_{\text{TAHC}}$ and $\bar{\bar{M}}_{\text{EMIPS}}$. By arranging their coefficients, all three tensors are complex symmetric matrices so, we express each $\check{\check{M}}$, $\bar{\bar{M}}_{\text{TAHC}}$ and $\bar{\bar{M}}_{\text{EMIPS}}$

Table 7.3: $c_{\check{\check{M}}}$, $c_{\bar{\bar{M}}_{\text{TAHC}}}$ and $c_{\bar{\bar{M}}_{\text{EMIPS}}}$ for object B_α

Object, B_α	$c_{\check{\check{M}}}$		$c_{\bar{\bar{M}}_{\text{TAHC}}}$		$c_{\bar{\bar{M}}_{\text{EMIPS}}}$	
	$\mathcal{R}$	$\mathcal{J}$	$\mathcal{R}$	$\mathcal{J}$	$\mathcal{R}$	$\mathcal{J}$
AS	1.500	1.500	1.500	1.500	1.570	1.575
REM	2.624	2.236	2.791	2.513	2.489	2.343
DA72	1.505	1.500	1.503	1.502	1.926	1.969

for all object B_α as $\mathcal{R} + \mathcal{J}\text{i}$ where $\mathcal{R}$ and $\mathcal{J}$ are real and imaginary parts of the tensor.

In order to compare the approximated $\check{\check{M}}$ to $\bar{\bar{M}}_{\text{TAHC}}$ and $\bar{\bar{M}}_{\text{EMIPS}}$ for the same object B_α, the absolute value of the ratio between the standard deviation of the coefficient to the mean of the coefficient of $\mathcal{R}$ and $\mathcal{J}$ for each $\check{\check{M}}$, $\bar{\bar{M}}_{\text{TAHC}}$ and $\bar{\bar{M}}_{\text{EMIPS}}$ are determined to three decimal places. These ratios are denoted by $c_{\check{\check{M}}}$, $c_{\bar{\bar{M}}_{\text{TAHC}}}$ and $c_{\bar{\bar{M}}_{\text{EMIPS}}}$ respectively, and are shown for each object, B_α in Table 7.3. For an object B_α, we say $\check{\check{M}} = \bar{\bar{M}}_{\text{TAHC}}$ (or $\check{\check{M}} = \bar{\bar{M}}_{\text{EMIPS}}$ or $\bar{\bar{M}}_{\text{TAHC}} = \bar{\bar{M}}_{\text{EMIPS}}$) if $c_{\check{\check{M}}} = c_{\bar{\bar{M}}_{\text{TAHC}}}$ (or $c_{\check{\check{M}}} = c_{\bar{\bar{M}}_{\text{EMIPS}}}$ or $c_{\bar{\bar{M}}_{\text{TAHC}}} = c_{\bar{\bar{M}}_{\text{EMIPS}}}$) for both $\mathcal{R}$ and $\mathcal{J}$. Based on the values in Table 7.3, $\check{\check{M}} = \bar{\bar{M}}_{\text{TAHC}}$ for AS since $c_{\check{\check{M}}} = c_{\bar{\bar{M}}_{\text{TAHC}}} = 1.500$ at three decimal places for both $\mathcal{R}$ and $\mathcal{J}$ (since each $\mathcal{R}$ and $\mathcal{J}$ for $\check{\check{M}}$ and $\bar{\bar{M}}_{\text{TAHC}}$ for AS is actually the multiple of the identity matrix). However, there are no $\check{\check{M}} = \bar{\bar{M}}_{\text{EMIPS}}$ and $\bar{\bar{M}}_{\text{TAHC}} = \bar{\bar{M}}_{\text{EMIPS}}$ for the object in Table 7.3.

For further comparisons, the absolute difference between $c_{\check{\check{M}}}$ and $c_{\bar{\bar{M}}_{\text{TAHC}}}$ denoted by $|c_{\check{\check{M}}} - c_{\bar{\bar{M}}_{\text{TAHC}}}|$ for $\mathcal{R}$ and $\mathcal{J}$ are also determined to three decimal places and shown in the first row of Table 7.4. Obviously, there is no difference at three decimal places between $c_{\check{\check{M}}}$ and $c_{\bar{\bar{M}}_{\text{TAHC}}}$ for both $\mathcal{R}$ and $\mathcal{J}$ for AS since $\check{\check{M}}$ and $\bar{\bar{M}}_{\text{TAHC}}$ for AS are equal. In addition, the resuts also suggest that $\check{\check{M}}$ and $\bar{\bar{M}}_{\text{TAHC}}$ for DA72 are almost similar but $\check{\check{M}}$ and $\bar{\bar{M}}_{\text{TAHC}}$ for REM are slightly different where for each $\mathcal{R}$ and $\mathcal{J}$, $|c_{\check{\check{M}}} - c_{\bar{\bar{M}}_{\text{TAHC}}}|$ for DA72 is less than $|c_{\check{\check{M}}} - c_{\bar{\bar{M}}_{\text{TAHC}}}|$ for REM. When comparing $\check{\check{M}}$ and $\bar{\bar{M}}_{\text{EMIPS}}$ from $|c_{\check{\check{M}}} - c_{\bar{\bar{M}}_{\text{EMIPS}}}|$, the smallest difference between $c_{\check{\check{M}}}$ and $c_{\bar{\bar{M}}_{\text{EMIPS}}}$ for both $\mathcal{R}$ and $\mathcal{J}$ occur also for the AS. However, the largest difference between $c_{\check{\check{M}}}$ and $c_{\bar{\bar{M}}_{\text{EMIPS}}}$ for both $\mathcal{R}$

Table 7.4: The absolute difference between $c_{\check{\check{M}}}$, $c_{\bar{\bar{M}}_{\mathrm{TAHC}}}$ and $c_{\bar{\bar{M}}_{\mathrm{EMIPS}}}$ for object B_α

Difference	AS		REM		DA72	
	$\mathcal{R}$	$\mathcal{J}$	$\mathcal{R}$	$\mathcal{J}$	$\mathcal{R}$	$\mathcal{J}$
$\lvert c_{\check{\check{M}}} - c_{\bar{\bar{M}}_{\mathrm{TAHC}}}\rvert$	0.000	0.000	0.167	0.277	0.002	0.002
$\lvert c_{\check{\check{M}}} - c_{\bar{\bar{M}}_{\mathrm{EMIPS}}}\rvert$	0.070	0.075	0.135	0.107	0.421	0.469
$\lvert c_{\bar{\bar{M}}_{\mathrm{TAHC}}} - c_{\bar{\bar{M}}_{\mathrm{EMIPS}}}\rvert$	0.070	0.075	0.302	0.170	0.423	0.467

and $\mathcal{J}$ are now happen for DA72 and not REM.

In the study by [26], the polarizibility tensor for B_α obtained from simulated data in a metal detector, $\bar{\bar{M}}_{\mathrm{EMIPS}}$ is compared to $\bar{\bar{M}}_{\mathrm{TAHC}}$ to identify the object. The system TAHC is used to build a library of the polarizibility tensor for metal components of landmine so that it can be referred to identify the objects later on. Because of this, we now determine the absolute difference between $c_{\bar{\bar{M}}_{\mathrm{TAHC}}}$ and $c_{\bar{\bar{M}}_{\mathrm{EMIPS}}}$ for AS, REM and DA72 and compare them with the absolute difference between $c_{\check{\check{M}}}$ and $c_{\bar{\bar{M}}_{\mathrm{EMIPS}}}$ to decide whether $\check{\check{M}}$ or $\bar{\bar{M}}_{\mathrm{TAHC}}$ gives better approximation to $\bar{\bar{M}}_{\mathrm{EMIPS}}$. Based on Table 7.4, at three decimal places, the values of $\lvert c_{\check{\check{M}}} - c_{\bar{\bar{M}}_{\mathrm{EMIPS}}}\rvert$ are less than or equal to the values of $\lvert c_{\bar{\bar{M}}_{\mathrm{TAHC}}} - c_{\bar{\bar{M}}_{\mathrm{EMIPS}}}\rvert$ except for $\mathcal{J}$ of DA72 but $\lvert c_{\check{\check{M}}} - c_{\bar{\bar{M}}_{\mathrm{EMIPS}}}\rvert$ and $\lvert c_{\bar{\bar{M}}_{\mathrm{TAHC}}} - c_{\bar{\bar{M}}_{\mathrm{EMIPS}}}\rvert$ for $\mathcal{J}$ of DA72 are almost equal, where, they are actually equal at two decimal places. These results suggest that for each B_α, $\check{\check{M}}$ are closer to $\bar{\bar{M}}_{\mathrm{EMIPS}}$ than $\bar{\bar{M}}_{\mathrm{TAHC}}$ so $\check{\check{M}}$ which are computed according to (7.5), (7.8) and (7.9) by the *hp*-FEM method can be an alternative to create the library of the polarizibility tensor for B_α in the future.

7.3.2 $\bar{\bar{M}}$ and $\check{\check{M}}$ for WTMD

Similarly, Table 7.5 shows the setting employed in the *hp*-FEM method besides μ_* and σ_* of the object to approximate every coefficient of $\check{\check{M}}$ for the object, B_α presented in [24] at the same frequency with [24]. Computation in the *hp*-FEM gives the approximated $\check{\check{M}}$ for the ferrite sphere with only real coefficients as it is a magnetic but non-conducting object. Moreover, the approximated $\check{\check{M}}$ for the ferrite sphere computed by the *hp*-FEM

Table 7.5: The setting in hp-FEM to compute $\check{\check{M}}$ for objects in [24]

Object, B_α	Geometry Representation	N	p
Ferrite Sphere	Quadratic	2425	3
Aluminium Gun	Quadratic	8002	5
Steel Gun	Quadratic	4913	5

at eight decimal places is a multiple of the identity matrix and equal to the analytical solution given in [29] (and also (2.4) as $\check{\check{M}}$ here reduces to the first order GPT).

According to [25], the WTMD in [24] was callibrated to produce the identity matrix as the polarizibility tensor, $\bar{\bar{M}}$ for the ferrite sphere of diameter 3.7 cm. This means $\bar{\bar{M}}$ for the objects given in Table 7.5 are scaled according to the $\bar{\bar{M}}$ for the ferrite sphere of diameter 3.7 cm. Theoretically, the real matrix $\check{\check{M}}$ as in (2.4) for the ferrite sphere of diameter 3.7 cm can be scaled by multiplying $\check{\check{M}}$ to the reciprocal of the diagonal coefficient of $\check{\check{M}}$ so that the resulting $\check{\check{M}}$ is the identity. Thus, for consistency when making comparison, the approximated $\check{\check{M}}$ for every B_α is also scaled by multiplying each coefficient of the approximated $\check{\check{M}}$ (the coefficients are complex valued for both guns) to the reciprocal of the diagonal coefficient of $\check{\check{M}}$ for the ferrite sphere of diameter 3.7 cm. This reduces the approximated $\check{\check{M}}$ for the ferrite sphere of diameter 3.7 cm to the identity at eight decimal places.

We now denote for every B_α, the scaled $\bar{\bar{M}}$ generated in [24] from WTMD by $\bar{\bar{\mathcal{M}}}_{WTMD}$ while the scaled version of the approximated $\check{\check{M}}$ as $\check{\check{\mathcal{M}}}$. Similarly, since both $\check{\check{\mathcal{M}}}$ and $\bar{\bar{\mathcal{M}}}_{WTMD}$ for all B_α are complex symmetric, each of them can be expressed as $\mathcal{R} + \mathcal{J}\mathrm{i}$ where $\mathcal{R}$ and $\mathcal{J}$ are real and imaginary parts of the tensor (in this case, $\mathcal{J}$ for $\check{\check{\mathcal{M}}}$ for the ferrite sphere is a zero matrix). In order to compare $\check{\check{\mathcal{M}}}$ to $\bar{\bar{\mathcal{M}}}_{WTMD}$ for the same object B_α, the standard deviation of the coefficients for $\mathcal{R}$ and $\mathcal{J}$ for each $\check{\check{\mathcal{M}}}$ and $\bar{\bar{\mathcal{M}}}_{WTMD}$ are determined to three decimal places and are shown in Table 7.6 by $\hat{c}_{\check{\check{\mathcal{M}}}}$ and $\hat{c}_{\bar{\bar{\mathcal{M}}}_{WTMD}}$. Note that the ratio standard deviation to the mean as in the comparison for systems TAHC and EMIPS is not used here since it is undefined for the zero matrix $\mathcal{J}$ for $\check{\check{\mathcal{M}}}$ for the ferrite sphere. For further comparisons, for each B_α, the absolute difference $|\hat{c}_{\check{\check{\mathcal{M}}}} - \hat{c}_{\bar{\bar{\mathcal{M}}}_{WTMD}}|$ for $\mathcal{R}$ and $\mathcal{J}$ are also determined to three decimal places and shown in Table 7.7.

From Table 7.6, the value 0.5 for $\hat{c}_{\check{\check{\mathcal{M}}}}$ for $\mathcal{R}$ for the ferrite sphere is obviously the

Table 7.6: $\hat{c}_{\check{\check{\mathcal{M}}}}$ and $\hat{c}_{\bar{\bar{\mathcal{M}}}_{WTMD}}$ for object B_α

Object, B_α	$\hat{c}_{\check{\check{\mathcal{M}}}}$		$\hat{c}_{\bar{\bar{\mathcal{M}}}_{WTMD}}$	
	$\mathcal{R}$	$\mathcal{J}$	$\mathcal{R}$	$\mathcal{J}$
Ferrite Sphere	0.500	0.000	0.431	0.021
Aluminium Gun	0.668	0.062	0.868	0.077
Steel Gun	0.375	0.272	0.359	0.577

Table 7.7: The absolute difference between $\hat{c}_{\check{\check{\mathcal{M}}}}$ and $\hat{c}_{\bar{\bar{\mathcal{M}}}_{WTMD}}$ for object B_α

Object, B_α	$\lvert\hat{c}_{\check{\check{\mathcal{M}}}} - \hat{c}_{\bar{\bar{\mathcal{M}}}_{WTMD}}\rvert$	
	$\mathcal{R}$	$\mathcal{J}$
Ferrite Sphere	0.069	0.021
Aluminium Gun	0.200	0.015
Steel Gun	0.016	0.305

absolute value of the standard deviation for the coefficients of the identity (identity has 9 coefficients : six of them are zero while the other three are equal to one). On the other hand, $\hat{c}_{\check{\check{\mathcal{M}}}}$ for $\mathcal{J}$ for the ferrite sphere is zero since $\mathcal{J}$ is a zero matrix of size three ($\check{\check{\mathcal{M}}}$ is a scaling version of $\check{\check{M}}$ so $\check{\check{\mathcal{M}}}$ also has only real coefficients). In addition, although WTMD is already callibrated, it does not produce the identity for $\bar{\bar{\mathcal{M}}}_{WTMD}$ for the ferrite sphere since $\hat{c}_{\bar{\bar{\mathcal{M}}}_{WTMD}}$ for $\mathcal{R}$ is not 0.5 and $\hat{c}_{\bar{\bar{\mathcal{M}}}_{WTMD}}$ for $\mathcal{J}$ is not 0. In this case, $\bar{\bar{\mathcal{M}}}_{WTMD}$ for the ferrite sphere generated has imaginary coefficients. This suggests errors in the system when estimating $\bar{\bar{\mathcal{M}}}_{WTMD}$.

Furthermore, we can see that in Table 7.7, there are significant differences between $\hat{c}_{\check{\check{\mathcal{M}}}}$ and $\hat{c}_{\bar{\bar{\mathcal{M}}}_{WTMD}}$ of both $\mathcal{R}$ and $\mathcal{J}$ for all B_α. Here, quite large differences occur in $\mathcal{R}$ for aluminium gun and $\mathcal{J}$ for steel gun. Generally, both $\check{\check{\mathcal{M}}}$ and $\bar{\bar{\mathcal{M}}}_{WTMD}$ computed have their own errors. The error in the system might cause by errors during field measurements and also errors in the inversion algorithm for computing $\bar{\bar{\mathcal{M}}}_{WTMD}$ from the measurements. Moreover, errors also occur when approximating $\check{\check{\mathcal{M}}}$ from the explicit formula by using the numerical method *hp*-FEM. The approximated $\check{\check{\mathcal{M}}}$ here is also less accurate since we do not know the exact value of μ_* and σ_* for each B_α used. However, for each B_α, $\bar{\bar{\mathcal{M}}}_{WTMD}$ is equal to $\check{\check{\mathcal{M}}}$ at zero decimal place since $|\hat{c}_{\check{\check{\mathcal{M}}}} - \hat{c}_{\bar{\bar{\mathcal{M}}}_{WTMD}}| = 0$ for both $\mathcal{R}$ and $\mathcal{J}$ at zero decimal place.

7.3.3 Further discussions

The explicit formula in (7.7)-(7.9) can be directly used to find the rank 2 PT $\check{\check{M}}$ for an object if the geometry (dimension and orientation) and material properties of the object are known. However, there are also several other parameters which will influence the values of $\check{\check{M}}$ if it is determined from field measurements or experimental works such as in [24] and [26]. Notice that the asymptotic formula for the PT in (7.4) is derived for $\alpha \to 0$ and $\nu = 2\alpha^2/s^2 = O(1)$ where $s = \sqrt{2/(\omega\mu_*\sigma_*)}$ so, the rank 2 PT $\check{\check{M}}$ is actually for a small object (target) inclusion where the depth of penetration of the magnetic field in the object, s must be at the same order with the size of the object, α. In our case, the values for s and α are not comparable in TAHC and EMIPS since they are the same for both systems but, in WTMD, $\check{\check{M}}$ (and also $\bar{\bar{M}}$) for objects with non-zero s and α (aluminium and steel guns) are scaled from a non-conducting magnetic sphere that has an undefined s ($\sigma* = 0$) but a non-zero α. So, it is possible that $\bar{\bar{\mathcal{M}}}_{WTMD}$ and $\check{\check{\mathcal{M}}}$ in the previous section are closer to each other if both of them are scaled from $\bar{\bar{M}}_{WTMD}$ and $\check{\check{M}}$ of a conducting (or conducting magnetic) object.

Moreover, the electromagnetic field generated by a metal detector has a wide range of penetration when using a low frequency. But, the formula of the rank 2 PT $\check{\check{M}}$ is for a small target inclusion. Therefore, there must be some distance between the target and metal detector so that the depth of penetration in the target is not large than the size of the target.

Besides, the model for the PT in (7.1)-(7.3) and the asymptotic formula (7.4) show the interaction between the transmitting coil and the inclusion only while the interaction between the inclusion and the receiving coil is given in (7.10) by letting $\bar{\bar{M}}$=$\check{\check{M}}$ as shown by [29]. Nevertheless, no direct interaction between transmitting and receiving coil stated in the model which suggest that there must be a certain distance between both coils so that they do not interact with each other when the inclusion is close to both of them. However, in reality, both coils have physical (electromagnetic) effect to the nearby inclusion and this makes field measurements about the inclusion to be less accurate. Therefore, the inclusion can be moved away from both coils to improve $\bar{\bar{M}}$ from the field measurements where, at the new further distance, the inclusion still generates eddy current by using the field from the transmitting coil and then, the generated eddy current is detected by the receiving coil. From our previous results based on the experiments conducted by [26], we can see that $\bar{\bar{M}}$ is closer to $\check{\check{M}}$ in EMIPS than in TAHC where the distance between the inclusion and the coils as given in [26] are larger in EMIPS than TAHC.

In addition, there are numerical errors in the method for computing the rank 2 PT $\check{\check{M}}$ either from the explicit formula or field measurements by using metal detectors. The computation is even less accurate in the field measurement due to errors in the measurement itself when there are other conducting objects nearby the metal detectors that have wide range of field penetration. Therefore, it might be possible to improve this computation by performing experimental works for field measurements in a less conducting environment. However, in the real complex situation such as during airport security screening, it will not be easy to reduce the errors in computing the PT when making real field measurements. This is because metal detection in that particular situation generally is more complicated and sometimes less efficient.

7.4 Conclusions

In this chapter, the polarization tensor computed from the recently introduced explicit formula has being compared with the polarization tensor from the engineering literatures (engineers called it as the polarizibility tensor) for metal detection. Here, the explicit formula as a rank 2 tensor is firstly given. Our results suggest that computing the polarization tensor based on the explicit formula can be an alternative to performing field measurements for determining the polarizibility tensor to improve metal detection.

Chapter 8

Some Properties of the Eddy Current PT

Previously, we have discussed the polarization tensor (PT) specifically for metal detection based on the new explicit formula introduced by [29]. The formula which is given as the rank 2 tensor $\check{\check{M}}$ in (7.7) enables us to compute the PT for a target according to the shape and material properties of the target. Besides, it is possible that $\check{\check{M}}$ can also be used in any other applications of the eddy current such as magnetic resonance imaging (MRI) [61] and nondestructive testing [62, 19]. For example, the polarizibility tensor is used to describe ellipsoidal defect on layered media in Orlowsky [62] so, it might be interesting to investigate whether $\check{\check{M}}$ is the same as the polarizibility tensor in [62]. Therefore, for the purpose of future applications, we will numerically explore a few properties of $\check{\check{M}}$ in this chapter. For this purpose, the same *hp*-FEM method as in the previous is again used to compute $\check{\check{M}}$. Furthermore, unless stated otherwise and by following [29], the frequency ω is fixed to 133.5 rad/s in this chapter.

8.1 $\check{\check{M}}$ for Translated and Rotated Objects

It can be seen from (7.5)−(7.9) that $\check{\check{M}}$ for an object B_α depends on the size, geometry as well as material of B_α and also the value of ω being used. In addition, by following [8] and [28], it can be shown that $\check{\check{M}}$ for B_α depends on the orientation of B_α but is independent of the position of B_α. Thus, our aim now is to numerically investigate $\check{\check{M}}$ for B_α with the fixed size, material and ω at different orientations and positions.

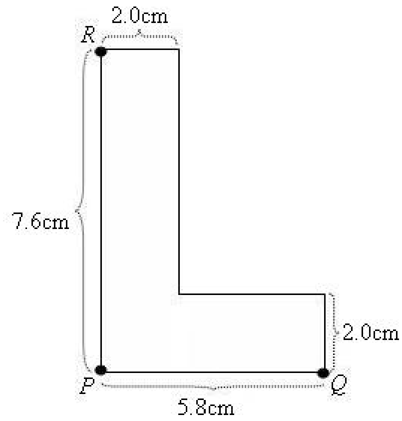

Figure 8.1: The base of a L-shaped object

Basically, $\check{\check{M}}$ for rotated and translated objects are examined. In order to demonstrate the effect on the coefficients of $\check{\check{M}}$ under rotation and translation, we consider $B_\alpha = L$ as a conducting and magnetic three-dimensional L-shaped object where, it is actually the steel gun in [60]. A real situation is actually considered as our main motivation for this investigation where a person might carry a gun with many possible orientations on any part of his body when passing a metal detector during security checking. Here, the base of the object if viewed in two dimensions, is shown in Figure 8.1 (dimension of the object is in centimeter (cm)). Three points P, Q and R are also chosen for references when translating or rotating the object.

We now assign the base to be above the xy-plane. For any point, $p \in L$ such that (x_p, y_p, z_p) is the coordinate of p in the three dimensional Cartesian coordinate system, $x_p, y_p, z_p \geq 0$. We also let the height of the object to be equal to 1.5 so that $0 \leq z_p \leq 1.5$. In this case, P, Q and R are firstly set to be (0,0,0), (5.8,0,0) and (0,7.6,0) respectively. Then, a linear mesh for L with 57456 tetrahedra is created in *Netgen* and after setting $\sigma_* = 4.5 \times 10^6$ S/m (Siemens per meter) and $\mu_* = 1.26 \times 10^{-4}$ NA^{-2} (Newton per ampere^2), each coefficient of $\check{\check{M}}$ for the object is approximated by the hp-FEM method with the degree of polynomial equal to three. The approximated $\check{\check{M}}$ for L is now denoted as $\check{\check{M}}_L$ and is written in the form $\check{\check{M}}_L = \mathcal{R} + \mathcal{J}\mathrm{i}$ where

$$\mathcal{R} = 10^{-3} \times \begin{bmatrix} 0.2274 & -0.0814 & 0.0001 \\ -0.0814 & 0.3484 & 0 \\ 0.0001 & -0 & 0.0671 \end{bmatrix} \tag{8.1}$$

Table 8.1: Rotation of the L-shaped object

Rotation, r	P	Q	R	$z_p^{(min)}$	$z_p^{(max)}$	$\mathtt{N}$	$\boldsymbol{R}$
$90°$ about z-axis	(0,0,0)	(0,-5.8,0)	(7.6,0,0)	0	1.5	41583	$R_z(90°)$
$90°$ about y-axis	(0,0,0)	(0,0,5.8)	(0,7.6,0)	0	5.8	58648	$R_y(90°)$
$90°$ about x-axis	(0,0,0)	(5.8,0,0)	(0,0,7.6)	0	7.6	42358	$R_x(90°)$

and

$$\mathcal{J} = 10^{-3} \times \begin{bmatrix} -0.0200 & 0.0168 & 0 \\ 0.0168 & -0.0400 & 0 \\ 0 & 0 & -0.0024 \end{bmatrix}. \tag{8.2}$$

As given by (8.1) and (8.2), $\check{\check{M}}_L$ for the object at the chosen position is complex symmetric as predicted by the theory in [29] for a conducting and magnetic object.

8.1.1 $\check{\check{M}}$ for a rotated object

The L-shaped object at the original position in the Cartesian plane is now rotated three times. Points P,Q and R after rotation as well as minimum and maximum value for z_p of point p lying in the object, are given in Table 8.1. $\check{\check{M}}$ for each object at the new position after rotation is denoted by $\check{\check{M}}_{L^r}$ and computed after that. Similarly, linear mesh for each rotated object is firstly generated in *Netgen*. The number of tetrahedral elements $\mathtt{N}$, for the mesh needed in order to approximate $\check{\check{M}}_{L^r}$ for all rotated objects by using the *hp*-FEM method with third order polynomial are also given in Table 8.1.

Next, $\check{\check{M}}_L$ for the object at the original position (given by (8.1) and (8.2)) is transformed three different times according to each rotation performed to the object by also using Theorem 2 (see Chapter 2) where rotation matrix $\boldsymbol{R}$ used are given in Definition 1 (see Chapter 2) and shown in Table 8.1. The resulting transformed $\check{\check{M}}_L$ is then denoted by $\tilde{\check{\check{M}}}_{L^r}$ for each rotation r. Each coefficient of $\tilde{\check{\check{M}}}_{L^r}$ is then compared to the coefficient of $\check{\check{M}}_{L^r}$ for every rotation r in Figure 8.2 until Figure 8.4 where the coefficients are denoted by mij for $i,j = 1,2,3$.

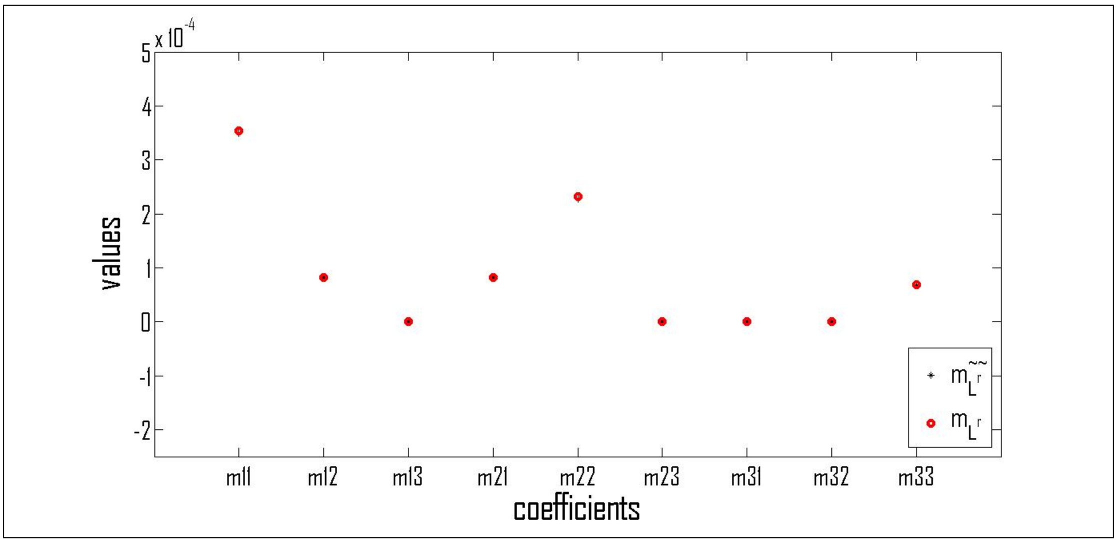

(a)

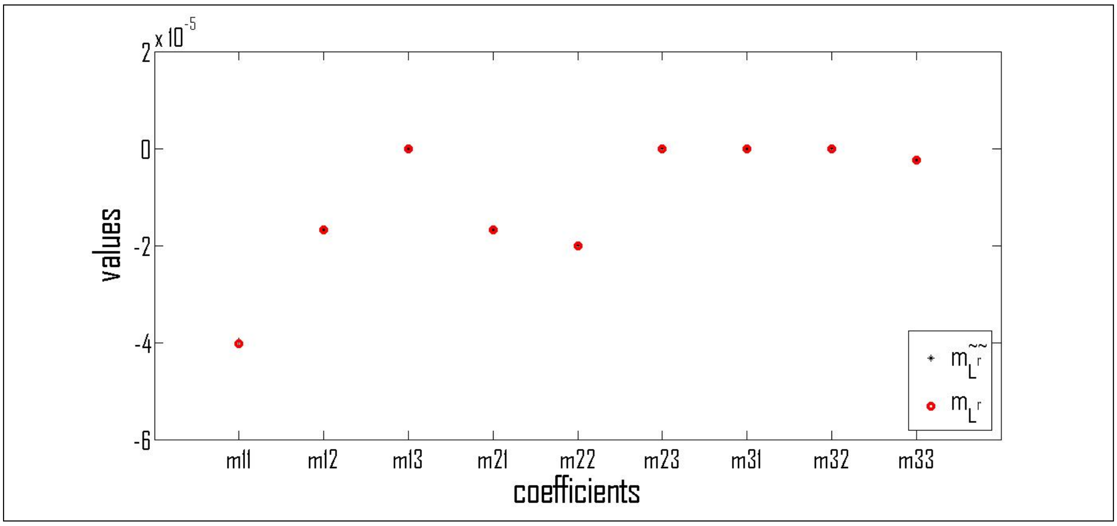

(b)

Figure 8.2: A comparison between the coefficients for $\check{\check{M}}_{L^r}$ (m_{L^r}) and $\tilde{\tilde{M}}_{L^r}$ ($\tilde{\tilde{m}}_{L^r}$) for r = rotation 90° around z-axis (a) real part (b) imaginary part

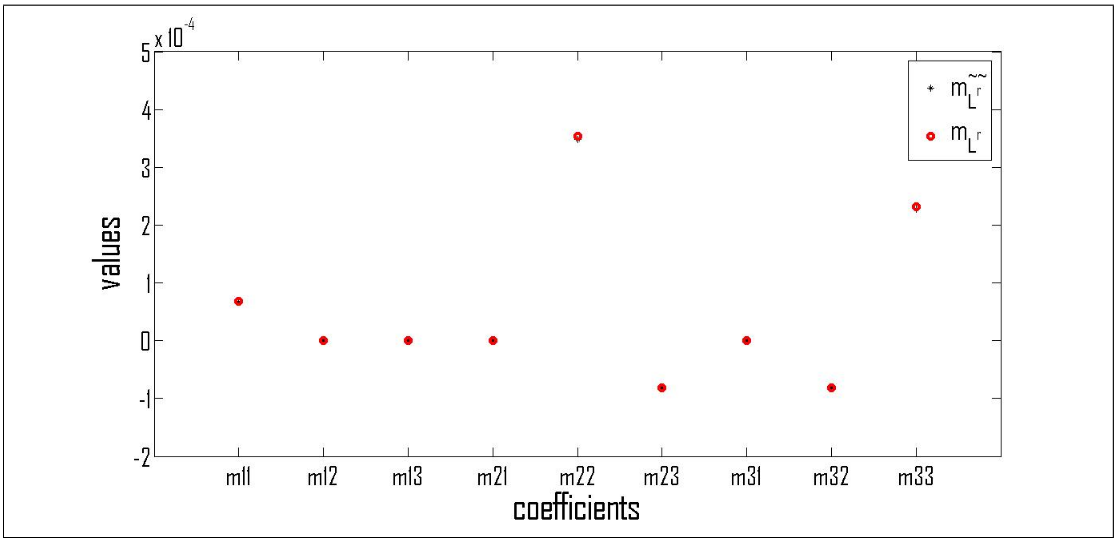

(a)

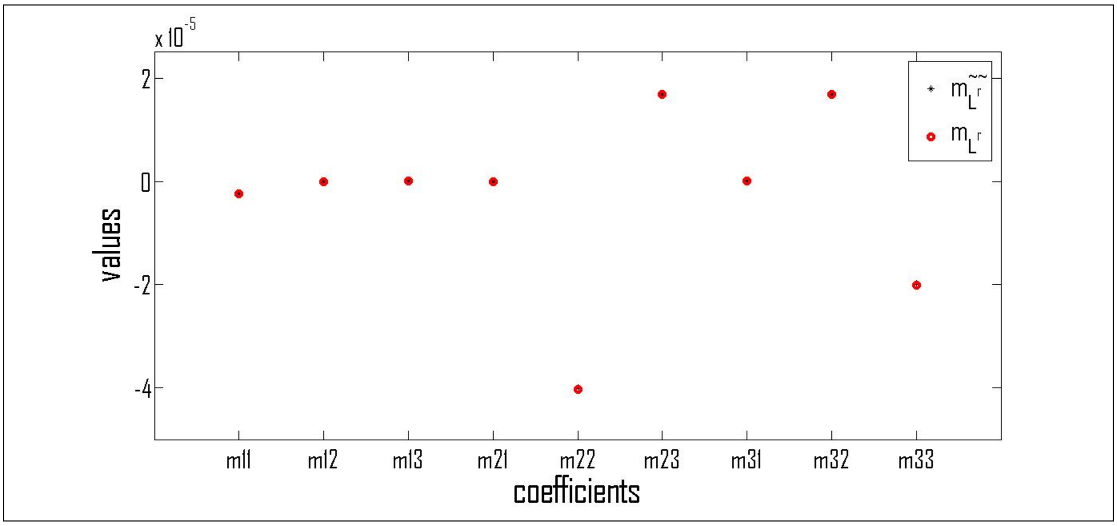

(b)

Figure 8.3: A comparison between the coefficients for $\check{\check{M}}_{L^r}$ (m_{L^r}) and $\tilde{\tilde{M}}_{L^r}$ ($\tilde{\tilde{m}}_{L^r}$) for r = rotation 90° around y-axis (a) real part (b) imaginary part

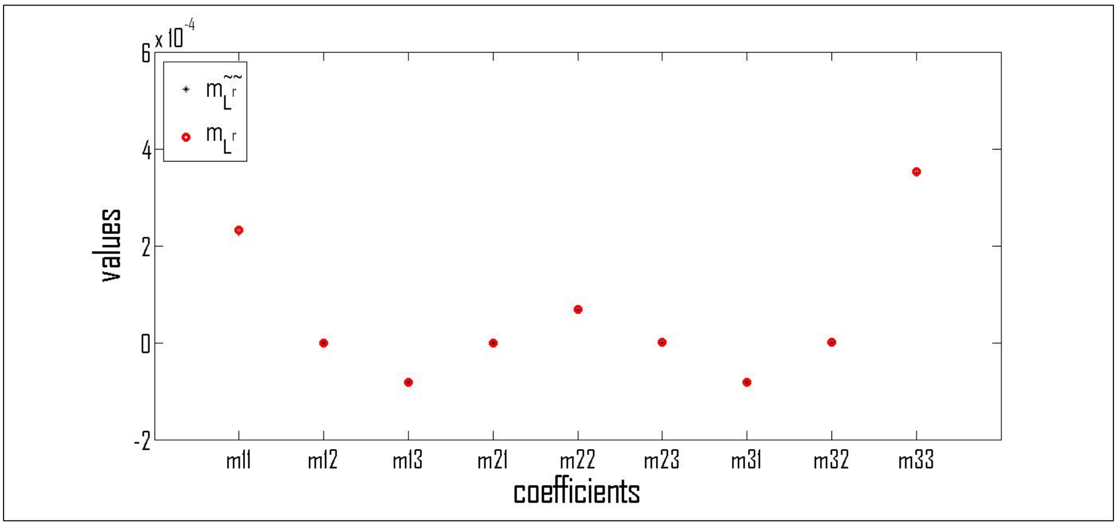

(a)

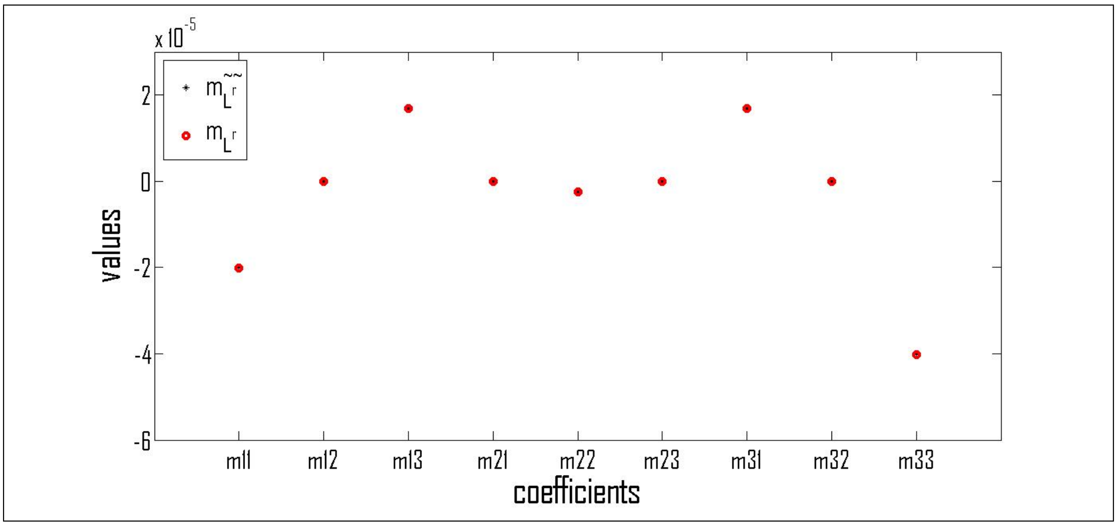

(b)

Figure 8.4: A comparison between the coefficients for $\check{\check{M}}_{L^r}$ (m_{L^r}) and $\tilde{\tilde{M}}_{L^r}$ ($\tilde{\tilde{m}}_{L^r}$) for r = rotation 90° around x-axis (a) real part (b) imaginary part

In these figures, each coefficient of $\check{\check{M}}_{L^r}$ and $\tilde{\check{\check{M}}}_{L^r}$ for every r is very similar and thus suggests that $\check{\check{M}}_{L^r}$ computed after the object L is rotated is the same as transforming $\check{\check{M}}_L$ to $\tilde{\check{\check{M}}}_{L^r}$ for every rotation r. These also give numerical evidences to suggest that $\check{\check{M}}$ for an object at the original position can be used directly to find $\check{\check{M}}$ for the same object after it is rotated, as given by Theorem 2 (see Chapter 2). Therefore, it is then possible to identify any object from experiments by estimating its $\check{\check{M}}$ and then comparing the $\check{\check{M}}$ to a transformed $\check{\check{M}}$ for a known object.

8.1.2 $\check{\check{M}}$ for a translated object

In order to investigate $\check{\check{M}}_L$ under a few translations, every point p that lies in the object is translated from its initial position by a translation coordinate $v = (v_x, v_y, v_z)$ such that every p for the translated object becomes $(x_p + v_x, y_p + v_y, z_p + v_z)$. A few v are considered, as listed in Table 8.2, where the new P, Q, R as well as the new minimum and maximum values of z_p are given. 9 translations have been performed to the object where the first eight of L' move the object in each octant of the three dimensional space without including the origin. The last L' translates the object from its initial position and lies within the intersection of every octant in three dimensional space, which will include the origin. Each translated object is then created in *Netgen* as well as approximated by a linear tetrahedral mesh. Using these approximations, $\check{\check{M}}$ for the object at every translation L' denoted by $\check{\check{M}}_{L'}$ is recomputed with the *hp*-FEM method. Here, every approximated $\check{\check{M}}_{L'}$ which is complex symmetric is obtained by using the third order polynomial on the mesh with `N` number of tetrahedra, where `N` is also included in Table 8.2.

After that, in making comparison between $\check{\check{M}}_L$ with $\check{\check{M}}_{L'}$, the coefficients m_{ij}, $i, j = 1, 2, 3$ in (8.1) for $\mathcal{R}$ of $\check{\check{M}}_L$ are firstly normalized by taking the ratio for each m_{ij} to the largest absolute value of m_{ij} for $\mathcal{R}$. Then, the ratio for each m_{ij} in (8.2) for $\mathcal{J}$ to the largest absolute value of m_{ij} of $\mathcal{J}$ is also determined. Similarly, the coefficients for both real and imaginary parts of each $\check{\check{M}}_{L'}$ are also normalized. Next, using the normalized coefficients, we compute $\left\|\mathcal{R}_{\check{\check{M}}_L} - \mathcal{R}_{\check{\check{M}}_{L'}}\right\|_2$ and $\left\|\mathcal{J}_{\check{\check{M}}_L} - \mathcal{J}_{\check{\check{M}}_{L'}}\right\|_2$ for all L' where $\|\cdot\|_2$ denotes the similar matrix entry-wise norm in Chapter 2 and Chapter 3. The values for $\left\|\mathcal{R}_{\check{\check{M}}_L} - \mathcal{R}_{\check{\check{M}}_{L'}}\right\|_2$ and $\left\|\mathcal{J}_{\check{\check{M}}_L} - \mathcal{J}_{\check{\check{M}}_{L'}}\right\|_2$ are then displayed in Table 8.3.

Table 8.2: Translation, L' for the object L

L'	v	P	Q	R	$z_p^{(min)}$	$z_p^{(max)}$	N
1	(2,2,2)	(2,2,2)	(7.8,2,2)	(2,9.6,2)	2	3.5	52993
2	(2,2,-2)	(2,2,-2)	(7.8,2,-2)	(2,9.6,-2)	-2	-0.5	55096
3	(-6,2,2)	(-6,2,2)	(-0.2,2,2)	(-6,9.6,2)	2	3.5	55871
4	(-6,2,-2)	(-6,2,-2)	(-0.2,2,-2)	(-6,9.6,-2)	-2	-0.5	54844
5	(2,-8,2)	(2,-8,2)	(7.8,-8,2)	(2,-0.4,2)	2	3.5	54242
6	(2,-8,-2)	(2,-8,-2)	(7.8,-8,-2)	(2,-0.4,-2)	-2	-0.5	51678
7	(-6,-8,2)	(-6,-8,2)	(-0.2,-8,2)	(-6,-0.4,2)	2	3.5	53723
8	(-6,-8,-2)	(-6,-8,-2)	(-0.2,-8,-2)	(-6,-0.4,-2)	-2	-0.5	51248
9	(-1,-1,-0.5)	(-1,-1,-0.5)	(4.8,-1,-0.5)	(-1,6.6,-0.5)	-0.5	1	54918

In this case, $\check{\check{M}}_L = \check{\check{M}}_{L'}$ if and only if $\left\| \mathcal{R}_{\check{\check{M}}_L} - \mathcal{R}_{\check{\check{M}}_{L'}} \right\|_2 = 0$ and $\left\| \mathcal{J}_{\check{\check{M}}_L} - \mathcal{J}_{\check{\check{M}}_{L'}} \right\|_2 = 0$ where $\check{\check{M}}_L = \mathcal{R}_{\check{\check{M}}_L} + \mathrm{i}\mathcal{J}_{\check{\check{M}}_L}$ and $\check{\check{M}}_{L'} = \mathcal{R}_{\check{\check{M}}_{L'}} + \mathrm{i}\mathcal{J}_{\check{\check{M}}_{L'}}$. Based on Table 8.3, we can see that all $\left\| \mathcal{R}_{\check{\check{M}}_L} - \mathcal{R}_{\check{\check{M}}_{L'}} \right\|_2$ and $\left\| \mathcal{J}_{\check{\check{M}}_L} - \mathcal{J}_{\check{\check{M}}_{L'}} \right\|_2$ have small values so, $\check{\check{M}}_{L'}$ for each L' is close to $\check{\check{M}}_L$ as expected. For convenient, the graphs in Appendix A.2 are included to show the agreement between the original real and complex coefficients of $\check{\check{M}}_L$ with the coefficients of $\check{\check{M}}_{L'}$ for all L'.

8.2 $\check{\check{M}}$ for Magnetic non-Conducting Objects

In their studies, [29] show that (7.7) reduces to the real symmetric $\check{\check{M}} = N$ when B_α has $\sigma_* = 0$ such that B_α is magnetic but non-conducting. Not only that, they also explain that $\check{\check{M}} = N$ does not depend on frequency, ω and actually reduces to the first order generalized polarization tensor (GPT), M of [8] and can now be determined by solving boundary integral equations (1.3)-(1.5) where the parameter k is the contrast μ_*/μ_0 (or the relative permeability of B_α). In this case, the analytical formula of M of the first order GPT for ellipsoids and spheres are also applicable.

Let B_α be the ellipsoid defined by $\dfrac{x^2}{a^2} + \dfrac{y^2}{b^2} + \dfrac{z^2}{c^2} = 1$ where $a = 3$, $b = 2$, $c = 1$ cm and suppose that B_α is non-conducting and its relative permeability is equal to 1.5. By using 11665 tetrahedral elements and polynomial of degree three in the *hp*-FEM method, an agreement of the coefficients of the approximated $\check{\check{M}}$ for B_α to the analytical solution (2.2) is obtained. Figure 8.5 compares every coefficient of M denoted by mij

Table 8.3: The difference between $\check{\check{M}}_L$ and $\check{\check{M}}_{L'}$

L'	$\left\Vert \mathcal{R}_{\check{\check{M}}_L} - \mathcal{R}_{\check{\check{M}}_{L'}} \right\Vert_2$	$\left\Vert \mathcal{J}_{\check{\check{M}}_L} - \mathcal{J}_{\check{\check{M}}_{L'}} \right\Vert_2$
1	0.0025	0.0034
2	0.0021	0.0030
3	0.0018	0.0036
4	0.0017	0.0034
5	0.0023	0.0046
6	0.0019	0.0037
7	0.0016	0.0032
8	0.0008	0.0024
9	0.0016	0.0031

where $i, j = 1, 2, 3$ for B_α based on analytical solution (2.2) with the same coefficients of the approximated $\check{\check{M}}$ computed by the *hp*-FEM method.

On the other hand, Figure 8.6 shows a comparison of the coefficients of M and $\check{\check{M}}$ for a non-conducting toroidal object with relative permeability 500 computed respectively based on boundary integral formula of the first order GPT (1.3)-(1.5) and also by *hp*-FEM method. The diameter and height of the object are 0.2 and 0.1 cm, respectively, and the object has a cylindrical hole with diameter and height both approximately equal to 0.1 cm. Here, the approximated $\check{\check{M}}$ in the *hp*-FEM method is obtained on the mesh with quadratic elements consisting 27919 tetrahedra and using polynomial of degree three. On the other hand, M is approximated by *BEM++* on the mesh with 16174 triangular elements.

In these two examples, $\check{\check{M}}$ for magnetic but non-conducting objects are verified with M of the first order GPT. In this case, the ellipsoid and the torus each is an example of simply and multiply connected objects. Moreover, we consider a low permeability contrast for ellipsoid and a high permeability contrast for torus. The ellipsoid is chosen because there is a specified analytical formula for its first order GPT (as given by (2.2)). On the other hand, the torus with the chosen permeability is a model of toroidal

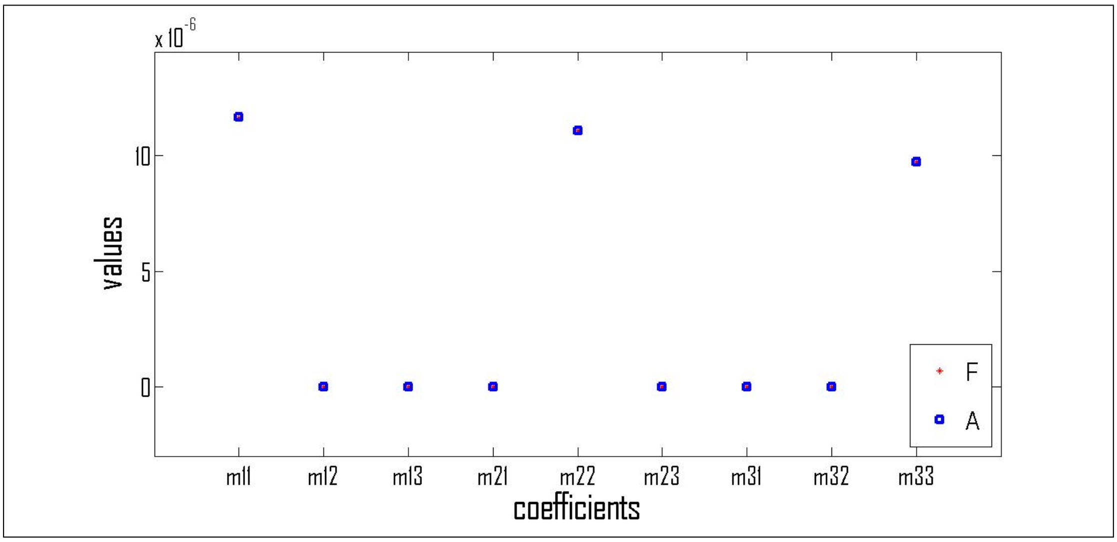

Figure 8.5: A comparison between the values of coefficients for $\check{\check{M}}$ and M for a magnetic non-conducting ellipsoid (at relative permeability equal to 1.5) as obtained by *hp*-FEM method (F) and the analytical solution (A)

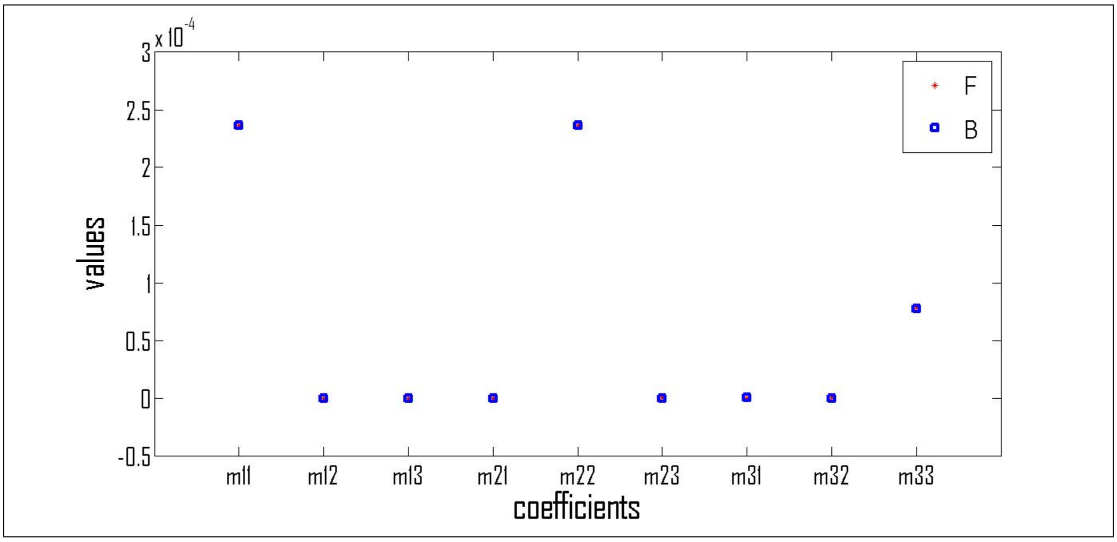

Figure 8.6: A comparison between the values of coefficients for $\check{\check{M}}$ and M for a magnetic non-conducting torus (at relative permeability equal to 500) as obtained by *hp*-FEM method (F) and the boundary integral formulation of the first order GPT in *BEM++* (B)

inductor, built by strong magnetic material, for example ferrite (nickel zinc). Figure 8.5 and Figure 8.6 show excellent agreement between the approximated $\check{\check{M}}$ computed by *hp*-FEM method and the approximated M of the first order GPT for both objects. It can be seen that $\check{\check{M}}$ and M for both ellipsoid and torus here are diagonal matrices. In addition, the first diagonal and the second diagonal entries of $\check{\check{M}}$ and M for the torus are equal.

8.3 $\check{\check{M}}$ for Conducting non-Magnetic Objects

An object B_α is conducting and non-magnetic if it has $\mu_* = \mu_0$. For this kind of object, $\check{\check{M}} = -C$ is complex symmetric as given by (7.7)-(7.9) and depends on σ_* of the object. On the other hand, if B_α is a magnetic and non-conducting object such that B_α has $\sigma_* = 0$, its $\check{\check{M}}$ (where $\check{\check{M}} = N$) depends on the relative permeability $\mu_r = (\mu_*/\mu_0)$. Moreover, $\check{\check{M}}$ (where $\check{\check{M}} = N$) can be recognized according to μ_r by adapting Theorem 3 (see Chapter 2). This is because N here reduces to the first order GPT as shown in [29]. In this case, $\check{\check{M}}$ (where $\check{\check{M}} = N$) is positive definite if $\mu_r > 1$ while it is negative definite if $0 < \mu_r < 1$. Consequently, we are motivated to investigate $\check{\check{M}}$ (where $\check{\check{M}} = -C$) at different σ_* to further describe $\check{\check{M}}$ for a conducting and non-magnetic object.

Previously, $\check{\check{M}}$ for a conducting and non-magnetic sphere with $\sigma_* = 5.96 \times 10^7$ S/m has been numerically investigated in [29]. In this section, in order to achieve our purpose, we repeatedly compute $\check{\check{M}}$ for the conducting non-magnetic sphere of radius 1 cm with a few different values of σ_* (Sm^{-1}) by using the analytical formula given in [29]. Since $\check{\check{M}}$ in this case is a diagonal matrix where the diagonals are all equal and also complex-valued, we only consider the values for the diagonal to investigate the relationship between σ_* and $\check{\check{M}}$ of the object.

Figure 8.7 (a) and Figure 8.7 (b) show the values for the real and imaginary parts of the diagonal of $\check{\check{M}}$ for the conducting non-magnetic sphere of radius 1 cm as σ_* increases from 0.5 to 1×10^{11}. Based on Figure 8.7 (a), the real part of the diagonal decreases from 0 (at six decimal places) to -6×10^{-6} as σ_* increases from 0.5 to 1×10^{11} where, it is only non-zero and strictly negative when $\sigma_* \geq 1 \times 10^8$. On the other hand, according to Figure 8.7 (b), the imaginary part of the diagonal is zero (at six decimal places) for $0.5 \leq \sigma_* \leq 1 \times 10^7$ but, when $1 \times 10^7 < \sigma_* \leq 1 \times 10^{11}$, the imaginary part of the diagonal is strictly negative and has a minimum value at σ_* around 1×10^9. Therefore, we can conclude that $\check{\check{M}}$ are zero matrices (at six decimal places) when $0.5 \leq \sigma_* \leq 1 \times 10^7$ since the diagonal for both real and imaginary parts of $\check{\check{M}}$ are zero. Moreover, by using Definition 2 (see Chapter 2), it can be shown that when $\sigma_* > 1 \times 10^7$, the real part of $\check{\check{M}}$ are either zero or negative definite matrices whereas the imaginary part of $\check{\check{M}}$ are strictly negative definite matrices. Thus, these results provide extra information which might increase the possibility of correctly identifying objects based on their $\check{\check{M}}$ in the future. For example, we may claim that an object is a conducting non-magnetic sphere if the real and complex parts of $\check{\check{M}}$ for the object each is a diagonal and also a negative definite matrix.

However, the results in Figure 8.7 might not be very helpful to describe objects that has σ_* between 0.5 and 1×10^7 since their $\check{\check{M}}$ are equal to zero matrices (at six decimal places). In fact, many popular conductors has σ_* between 1×10^6 and 1×10^8 so, we are going to further investigate $\check{\check{M}}$ for conducting non-magnetic sphere to extract more information about $\check{\check{M}}$ when σ_* is between 0.5 and 1×10^7. Note that unlike $\check{\check{M}}$ for magnetic non-conducting objects, $\check{\check{M}}$ for conducting non-magnetic objects also depend on the frequency, ω where the results in Figure 8.7 are actually generated when $\omega = 133.5$ rad/s (around 20 Hz). Now, by using the analytical formula given in [29] as well as fixing the frequency f equal to 500 Hz, 10 kHz, 43 kHz, 700 kHz, 3 MHz and 75 MHz such that $\omega = 2\pi f$, we again determine $\check{\check{M}}$ for the conducting non-magnetic sphere of radius 1 cm at σ_* also between 0.5 and 1×10^{11}. After that, we extend the graphs in Figure 8.7 by including the values for the diagonal of $\check{\check{M}}$ as σ_* increases from 0.5 to 1×10^{11} for the other six frequencies in Figure 8.8.

Based on Figure 8.8, except for $f = 20$ Hz, we can now see that $\check{\check{M}}$ are non-zero matrices at σ_* between 1×10^6 and 1×10^8 for all other frequencies, f. In this case, the real part of $\check{\check{M}}$ is either a zero matrix or a negative definite matrix but the imaginary part of $\check{\check{M}}$ is always a negative definite matrix. For each frequency, the imaginary part of $\check{\check{M}}$ also has a minimum value at a fixed σ_*.

Thus, by using the appropriate frequency and combining the unique real and imaginary parts of $\check{\check{M}}$, we might be able to estimate σ_* from $\check{\check{M}}$. For example, let us consider a standard metal detector where the frequency used is around 10 kHz. According to Figure 8.8, at that frequency, the imaginary part of the diagonal of $\check{\check{M}}$ has

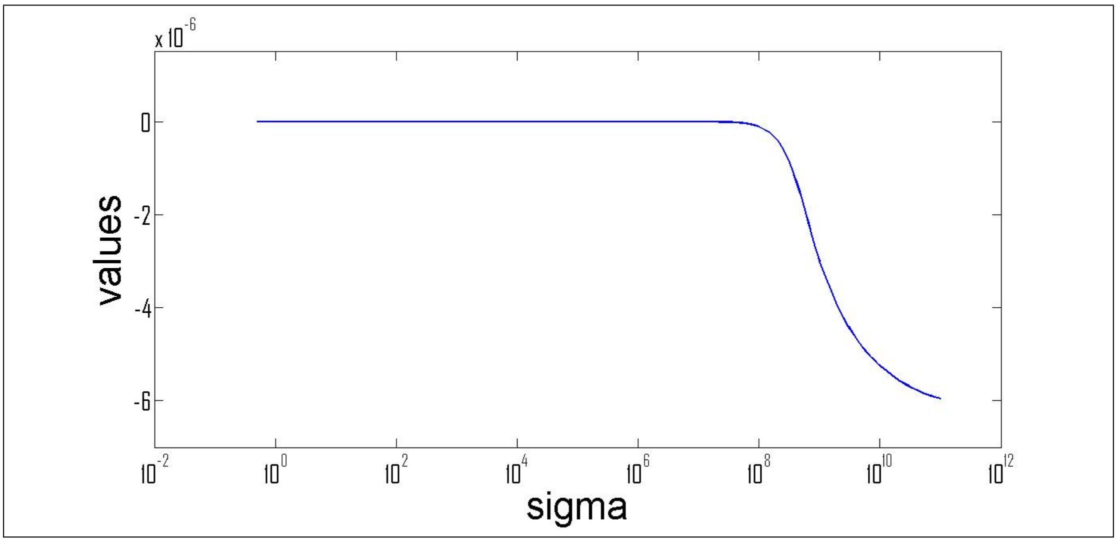

(a)

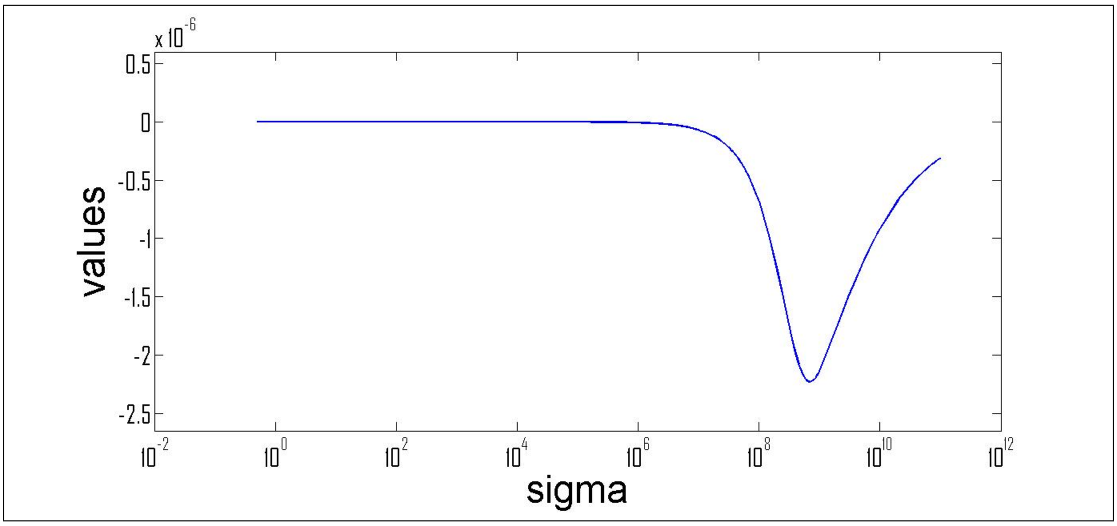

(b)

Figure 8.7: The values for the diagonal of $\check{\check{M}}$ for the conducting non-magnetic sphere of radius 1 cm when σ_* in Sm^{-1} (denoted as sigma in the figures) is between 0.5 and 1×10^{11} (a) real part (b) imaginary part

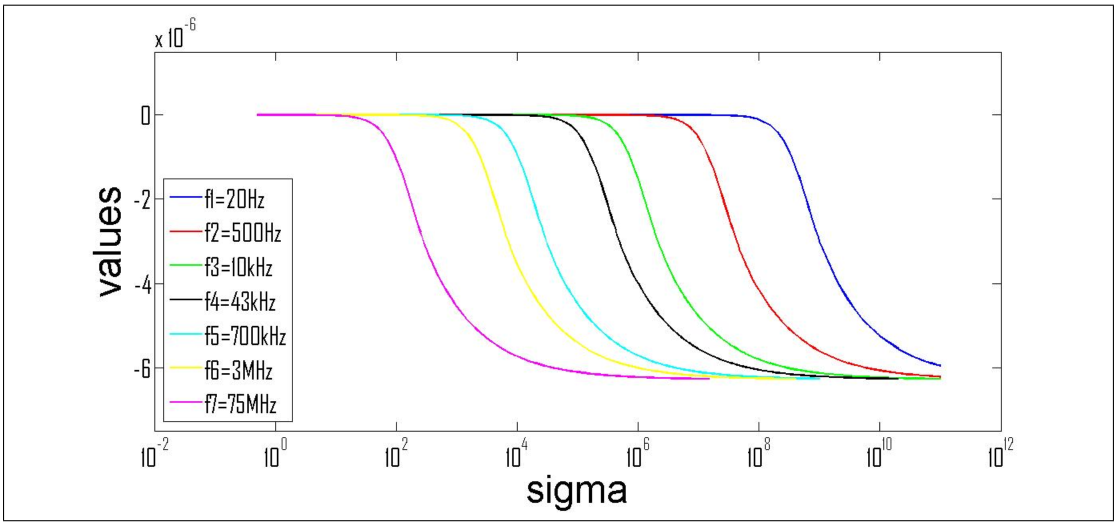

(a)

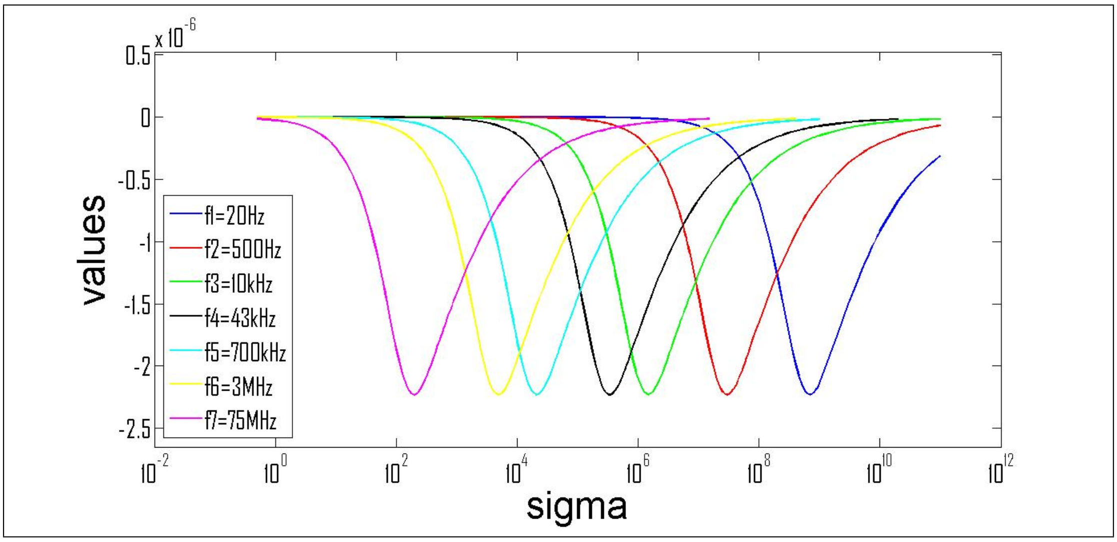

(b)

Figure 8.8: The values for the diagonal of $\check{\check{M}}$ for the conducting non-magnetic sphere of radius 1 cm when σ_* in Sm^{-1} (denoted as sigma in the figures) is between 0.5 and 1×10^{11} at seven different frequencies (a) real part (b) imaginary part

a minimum value at σ_* around 1×10^6 which is around -2×10^{-6} and the correspond real part is also around -2×10^{-6}. So, if $\check{\check{M}}$ for an object is produced as a diagonal matrix by the metal detector where the diagonals are all equal to $(-0.5 \times 10^{-6})\mathrm{i}$, it is possible that σ_* for the object is less than 1×10^6 while if the diagonals are all equal to $10^{-6} \times (-5.5 - 0.5\mathrm{i})$, it is possible that σ_* for the object is greater than 1×10^6. This helps us to classify the material of conducting non-magnetic object based on its $\check{\check{M}}$.

8.4 Conclusions

In this chapter, we have numerically explored some properties of the polarization tensor for the eddy current problem (like metal detection) as a rank 2 tensor. First of all, we investigate some invariants (translation and rotation) for the tensor. After that, we numerically show the agreemeent between the first order GPT and the rank 2 tensor for magnetic non-conducting objects. Lastly, we also investigate conductivity response of the rank 2 tensor for conducting non-magnetic sphere at a few fixed frequencies. While specific geometries and materials are used during the studies, we believe that the properties will hold for any other objects as well.

Chapter 9

Summary and Recommendation

This chapter concludes the study on some mathematical aspects and applications of the polarization tensor (PT) in electrics and electromagnetics. A few real applications are highlighted (electro-sensing fish, GPR and metal detector) in using the PT specifically to characterize objects presented in electric and/or electromagnetic fields without reconstructing the image of the objects. Moreover, this study also discusses the mathematical background for the related PT for each application. For the GPR, the PT arises from the time harmonic Maxwell's equations is the same as the first order PT when the conductivity of the first order PT is complex. On the other hand, in metal detection, when the magnetic fields are perturbed by magnetic but non-conducting object, the rank 2 PT for the object which is derived from the eddy current approximation to the Maxwell's equations reduces to the first order PT where, the conductivity of the first order PT is now the relative permeability of the object. We show the PT discussed in this study and a few relations between them in Figure 9.1. Now, all works done in the thesis are summarized here. After that, this chapter ends with several recommendations for future researches.

9.1 Summaries for each Chapter

This research begins with the revision about the first order PT or the first order generalized polarization tensor (GPT) for three dimensional (3D) domains in Chapter 2 as it is the basis for the whole study. This in fact probably is the main reason why the first order PT appears in every chapter of the thesis. During the review, the quadrature

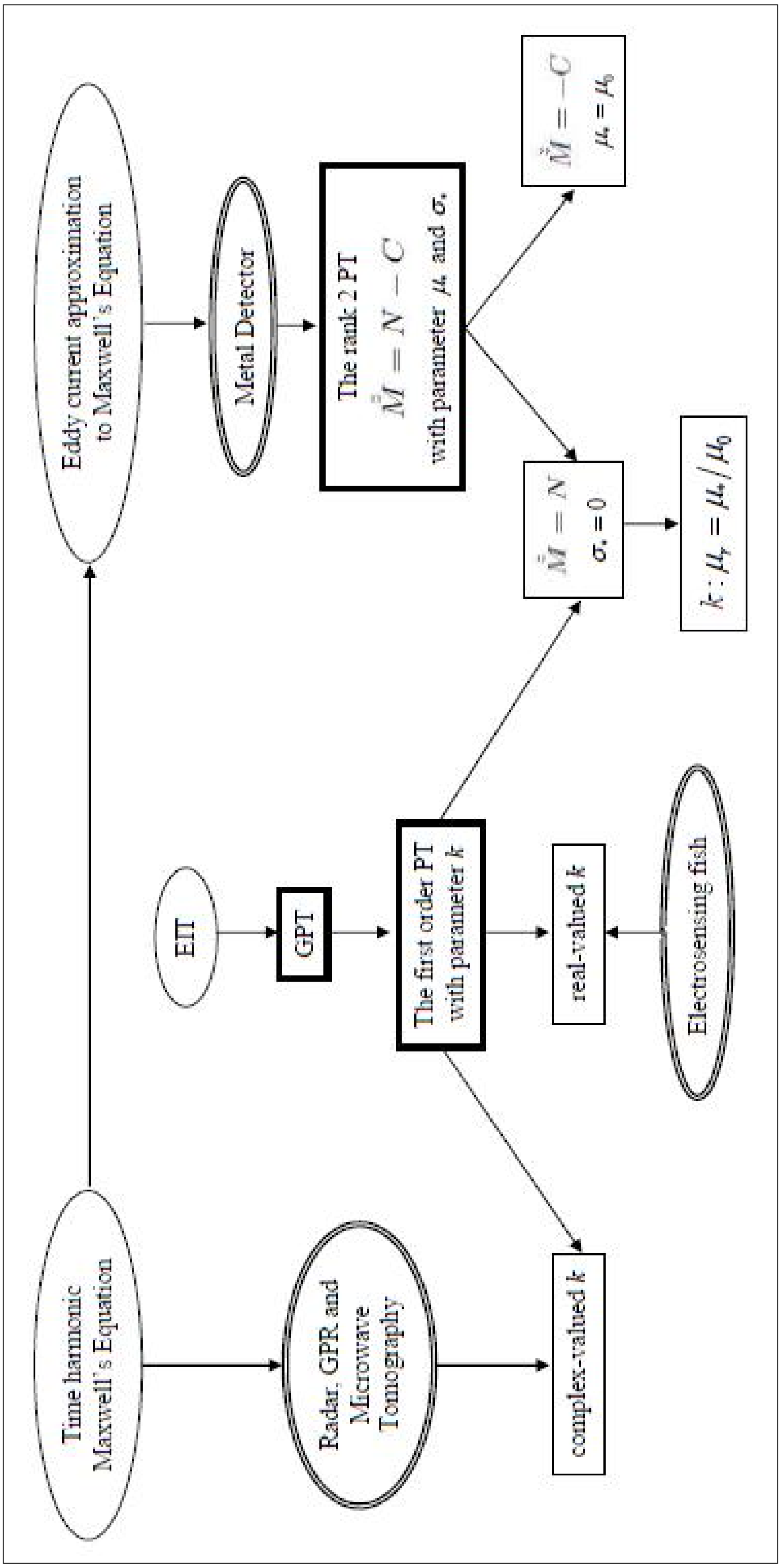

Figure 9.1: The relations between each PT in the study

method is firstly used to numerically compute the first order PT. A code in *Matlab* is then written for this purpose (see Appendix B.2). By using the code, the first order PT for a few objects are computed as well as desribed while transformation and positivity of the first order PT are also numerically investigated.

In order to improve the previous numerical method, a recent developed code called as *BEM++* is also used to compute the first order PT. In Chapter 3, the reasons and procedures to use *BEM++* are explained. Furthermore, when comparing the results computed with both codes in *Matlab* and *BEM++*, the chapter shows better approximations for the first order PT in *BEM++*.

Chapter 4 then describes a strategy to numerically determine an ellipsoid from the given first order PT for an object. The analytical and numerical results from the study show that it is possible for an object and an elliposid to have the same first order PT (accurately at some decimal places). Moreover, if the first order PT for the object and the ellipsoid are different, the eigenvalues for their first order PT can still be the same.

The parameter conductivity of the first order PT is then extended to be a complex number to investigate the PT for the time-harmonic Maxwell's equations in Chapter 5. By using *BEM++*, the first order PT for a few objects with complex conductivity are numerically computed and discussed. The study also investigates the frequency response for the first order PT of two objects with complex permittivities to further describe the objects.

After that, the role of the first order PT in electrosensing fish is mathematically investigated in Chapter 6. The results obtained in the chapter are consistent with the hypothesis that the fish use the first order PT to recognize object. However, the findings are inconclusive, thus, further investigations are also suggested in the chapter.

Following recent mathematical works which introduce the new PT for the eddy current approximation to the Maxwell's equations, Chapter 7 presents numerical agreements between the introduced rank 2 PT and the polarizibility tensor from engineering literatures. For this purpose, the explicit formula of the rank 2 PT is firstly given and computed for a few objects used in the experiments conducted by the engineers. The results suggest that the formula for the rank 2 PT can be an alternative to determine the PT (or the polarizibility tensor) for a few targets relevance in metal detection in the future.

Finally, a few properties of the rank 2 PT are numerically investigated in Chapter 8. Some of the properties discussed there are actually similar to the properties of the first order PT stated in Chapter 2. In this case, understanding the properties could be useful to further describe and characterize the objects represented by the rank 2 PT in the related applications.

9.2 Recommendations for Future Researches

During this research, two programmes to numerically compute the first order PT for 3D domains are developed in both *Matlab* and *BEM++*. It can be seen that from the results, both codes are capable to approximate the first order PT to an acceptable level of accuracy. However, we do not perform numerical analysis to the results in more details as we have other priorities in this study. Therefore, it is suggested to do numerical analysis to the results to further describe the effectiveness of both methods. Here, another suitable method to improve the approximation of the first order PT can also be investigated. Moreover, only positivity and rotation of the 3D first order PT are discussed here. Perhaps, other properties can also be explored to further describe and characterize objects represented by the first order PT in the future.

This study also investigates the role of the first order PT in electrosensing fish and highlights how electrical objects can be discriminated based on only their first order PT from the experiments conducted by [12] but the results presented are inconclusive. In order to further justify this, similar experiments to [12] can be conducted in the future to test whether the fish during electrosensing can discriminate a few objects with different shapes such that the first order PT for all objects are similar. However, it seems like only two objects can be used for this purpose at the moment where one of them is an ellipsoid. We can determine an ellipsoid from a given first order PT for an object since the first order PT for ellipsoid has an analytical solution as given by (2.2). Therefore, it might be useful to derive an analytical solution of the first order PT for the other object and used the formula to construct the object from a given first order PT. If the fish can discriminate two or more objects that have similar first order PT, we can then conclude that the fish use more than the first order PT to discriminate the objects. For example, they might use the higher order PT as well in the recognition mechanism.

Instead of real values for the conductivity, we also introduce the first order PT with complex conductivity and complex permittivity as it is useful for object characterization and description in many applications of the Maxwell's equations especially the GPR. Numerical examples are given in the study but the discussion about the properties of the PT for this case are still less and can be further explored. Moreover, we also hope to improve the related applications by performing real measurements from the appropriate system such as the GPR to determine the first order PT with complex conductivity and complex permittivity.

Meanwhile, the polarizibility tensor determined from measurements in metal detectors has been compared to the recently introduced rank 2 PT during this study. Here, numerical agreements between the polarizibility tensor and the rank 2 PT are discussed. Our results suggest that the polarizibility tensor can be computed from the explicit formula of the rank 2 PT. For later improvement, the code in *BEM++* can be used as an alternative to approximate the rank 2 PT especially since the rank 2 PT is defined as transmission boundary value problem. Besides, another suitable method such as statistical approaches or fuzzy algorithms to compare the polarizibility tensor and the rank 2 PT can also be explored and investigated in the future.

Moreover, only two invariant (rotation and translation) and two material properties of the rank 2 polarization tensor are discussed in this study. Unlike the established first order GPT, the rank 2 polarization tensor is a new terminology in electromagnetics and eddy current. There are still many of its properties that can be explored and investigated to further understand and properly use it in the related applications.

During this study, the explicit formula of the PT for each application (the first order GPT and the rank 2 $\check{\check{M}}$) is derived from the leading order term of the related asymptotic formulas. However, using the higher order term of the asymptotic formula could also be useful to further describe and classify electrical and electromagnetic objects in the presented applications. In electrosensing fish, the higher order term of the GPT might discriminate two objects that have the same first order PT. On the other hand, the higher order term will provide more information and increase the possibility of identifying the correct target in metal detection. Therefore, we also recommend to investigate the PT from the higher order term of the asymptotic formulas in the future.

Bibliography

[1] G. Pólya. *A minimum problem about the motion of a solid through a fluid*, Proc. Nat. Acad. Sci. U.S.A, **33**, 218–221, 1947.

[2] M. Schiffer and G. Szegő. *Virtual Mass and Polarization*, Trans. Amer. Math. Soc., **67**, 130–205, 1949.

[3] G. Pólya and G. Szegő. *Isoperimetric Inequalities in Mathematical Physics. Annals of Mathematical Studies Number 27.* Princeton University Press, Princeton, 1951.

[4] R. E. Kleinman and T. B. Senior. *Low frequency scattering by space objects*, IEEE Transactions Aerospace Electron. Syst., **AES-11**, 672–675, 1975.

[5] R. E. Kleinman and T. B. Senior. *Rayleigh Scattering*, in V. K. Varadan and V. V. Varadan. (eds) *Low and High Frequency Asymptotics*. ELSEVIER, Holland, 1986.

[6] G. Milton. *Theory of Composites*. Cambridge University Press, USA, 2002.

[7] R. E. Raab and O. L. De Lange. *Multipole Theory in Electromagnetism : Classical, Quantum and Symmetry Aspects, with Applications*. Cambridge University Press, USA, 2002.

[8] H. Ammari and H. Kang. *Polarization and Moment Tensors : with Applications to Inverse Problems and Effective Medium Theory*. Springer-Verlag, New York, 2007.

[9] A. Adler, R. Gaburro, and W. Lionheart. *Electrical Impedance Tomography*, in O. Scherzer. (ed) *Handbook of Mathematical Methods in Imaging*. Springer-Verlag, USA, 2011.

[10] D. S. Holder. (ed) *Electrical Impedance Tomography : Methods, History and Applications.* Institute of Physics Publishing, London, 2005.

[11] G. von der Emde. *Electroreception : Object Recognition in African Weakly Electric Fish*, in T. Hara and B. Zielinski. (eds) *Sensory Systems Neuroscience.* Academic Press ELSEVIER, USA, 2007.

[12] G. von der Emde and S. Fetz. *Distance, shape and more : Recognition of object features during active electrolocation in a weakly electric fish*, The Journal of Experimental Biology, **210**, 3082–3095, 2007.

[13] G. von der Emde, K. Behr, B. Bouton, J. Engelmann, S. Fetz and C. Folde. *Three-dimensional scene perception during active electrolocation in a weakly electric pulse fish*, Frontiers in Behavioral Neuroscience, **4**(26), 1–13, 2010.

[14] M. E. Nelson. *Electrosensory data acquisition and signal processing strategies in electric fish*, Plenary talk at 10th International Conference on Biomedical Applications of Electrical Impedance Tomography (EIT 2009), 16th–19th June 2009, Manchester.
http://livestream.manchester.ac.uk/livelecture/plenary_talk_20090618/index.htm2009

[15] M. E. Nelson. *Biological smart sensing strategies in weakly electric fish*, Smart Structures and Systems, **7**(6), 2011.

[16] N. J. Cowan and E. S. Fortune. *The critical role of locomotion mechanics in decoding sensory systems*, The Journal of Neuroscience, **27**(5), 1123–1128, 2007.

[17] H. Ammari, T. Boulier, and J. Garnier. *Modeling active electrolocation in weakly electric fish*, SIAM Journal on Imaging Sciences, **5**, 285–321, 2013.

[18] H. Ammari, T. Boulier, J. Garnier and H. Wang. *Shape recognition and classification in electrosensing*, Proceedings of the National Academy of Sciences of the United States of America, **11**, 11652–11657, 2014.

[19] J. Blitz. *Electrical and Magnetic Methods of Nondestructive Testing*, Adam Hilger, Norfolk, 1991.

[20] C. Nelson. *Metal detection and classification technologies*, Johns Hopkins APL Technical Digest, **25**(1), 2004.

[21] J. Schulz. *Field Reconstructions and Range Tests for Acoustics and Electromagnetics in Homogeneous and Layered Media*, Dissertation, University of Göttingen, 2007.

[22] B. Bjerrum and K. D. Kristiansen. *Concept Development for the Next Generation of Metal Detectors*, Master Thesis, Aalborg University, 2008.

[23] D. F. He and M. Yoshizawa. *Metal detector based on high-T_C RF SQUID*, Physica **C** (378–381), 1404–1407, 2002.

[24] L. A. Marsh, C. Ktistis, A. Järvi, D. W. Armitage and A. J. Peyton. *Three-dimensional object location and inversion of the magnetic polarizability tensor at a single frequency using a walk-through metal detector*, Measurement Science and Technology, **24**(4), 045102, 2013.

[25] L. A. Marsh, C. Ktistis, A. Järvi, D. W. Armitage and A. J. Peyton. *Determination of the magnetic polarizability tensor and three dimensional object location for multiple objects using a walk-through metal detector*, Measurement Science and Technology, **25**(5), 055107, 2014.

[26] B. Dekdouk, L. A. Marsh, D. W. Armitage and A. J. Peyton. *Estimating magnetic polarizability tensor of buried metallic targets for landmine clearance*, in *Springer Science and Business Media*. LLC, pg. 425–432, 2014. (alternatively in 10th Conference on Ultra-Wideband, Short-Pulse Electromagnetics, 5th–9th July 2010, UWBSP, Ottawa, ON, Canada.)

[27] H. Ammari, J. Chen, Z. Chen, J. Garnier and D. Volkov. *Target detection and characterization from electromagnetic induction data*, J. Math. Pures Appl., **101**, 54–75, 2014.

[28] H. Ammari, J. Chen, Z. Chen, D. Volkov and H. Wang. *Detection and classification from electromagnetic induction data*, Journal of Computational Physics, **301**, 201–217, 2015.

[29] P. D. Ledger and W. R. B. Lionheart. *Characterising the shape and material properties of hidden targets from magnetic induction data*, IMA J Applied Mathematics, open access, 2015.

[30] P. D. Ledger and W. R. B. Lionheart. *Understanding the magnetic polarizibility tensor*, submitted to IEEE Trans. Mag., 2015.

[31] C. King. (ed) *Jane's Mines and Mine Clearance.* Jane's Information Group, Coulsdon, 2011.

[32] B. Sai and L. P. Ligthart. *GPR phase-based techniques for profiling rough surfaces and detecting small, low-contrast landmines under flat ground*, IEEE Transactions on Geoscience and Remote Sensing, **42**(2), 318–326, 2004.

[33] H. Ammari, M. S. Vogelius and D. Volkov. *Asymptotic formula for perturbations in the electromagnetic fields due to the presence of inhomogeneities of small diameter II. The full Maxwell equations*, J. Math. Pures Appl, **8**, 769–814, 2001.

[34] Y. Capdeboscq, A. B. Karrman and J.-C. Nedelec. *Numerical computation of approximate generalized polarization tensors*, Applicable Analysis, **91**(6), 1189–1203, 2012.

[35] J. Schöberl. *NETGEN : An advancing front 2D/3D-mesh generator based on abstract rules*, Comput Visual Sci, **1**, 41–52, 1997.

[36] J. Schöberl. *NETGEN - 4.3.* May 7, 2003
`http://www.hpfem.jku.at/netgen/ng4.pdf`

[37] P. C. Hansen. *Discrete Inverse Problems : Insight and Algorithms.* SIAM, Philadelphia, 2010.

[38] S. Rjasanow and O. Steinbach. *The Fast Solution of Boundary Integral Equations.* Springer, Berlin Heidelberg, 2007.

[39] H. Anton and C. Rorres. *Elementary Linear Algebra : Applications Version.* John Wiley, New York, 2000.

[40] Mathematical Programming Glossary
`http://glossary.computing.society.informs.org`

[41] W. Śmigaj, S. Arridge, T. Betcke, J. Phillips and M. Schweiger. *Solving boundary integral problems with BEM++*, ACM Trans. Math. Software, **41**(2), Article 6, 2015.

[42] C. A. Brebbia and J. Dominguez. *Boundary Element : An Introductory Course*. WIT Press, Southampton, 1992.

[43] O. Steinbach. *Numerical Approximation Methods for Elliptic Boundary Value Problems*. Springer, New York, 2008.

[44] J. Tausch and J. White. *Capacitance extraction of 3D conductor systems in dieletric media with high-permittivity ratios*, IEEE Transactions on Microwave Theory and Techniques, **47**(1), 18–26, 1999.

[45] L. Greengard and J.Y. Lee. *Electrostatics and heat conduction in high contrast composite materials*, Journal of Computational Physics, **211**, 64–76, 2006.

[46] J. Tausch and J. Wang. *Improved integral formulations for fast 3D method-of-moments solvers*, IEEE Transactions on Computer-Aided Design of Integrated Circuits and Systems, **20**(12), 1398–1405, 2001.

[47] J. Osborn. *Demagnetizing factors of the general ellipsoid*, Physical Review, **67**, 351–357, 1945.

[48] P. J. Davis and P. Rabinowitz. *Numerical Integration*. Blaisdell Publishing Company, USA, 1967.

[49] A. S. N. Alfhaid. Numerical analysis Part 2, Lecture Note, Mathematics Department, King Abdulaziz University.
`http://aalfhaid.kau.edu.sa/CVEn.aspx?Site_ID=0001726&Lng=EN`

[50] D. Bhardwaj. Solution of nonlinear equations, Lecture Note, Department of Computer Science and Engineering, Indian Institute of Technology Delhi.
`http://www.cse.iitd.ernet.in/~dheerajb/CS210.htm`

[51] T. M. Heath. *Scientific Computing : An Introductory Survey*. McGraw-Hill, New York, 2002.

[52] W. H. Press, S. A. Teukolsky, W. T. Vetterling and B. P. Flannery. *Numerical Recipes in Fortran 77 Second Edition : The Art of Scientific Computing*. Cambridge University Press, USA, 1992.

[53] F. Watson and W. Lionheart. *Polarization tensors for ground penetrating radar : maximising distinguishability for landmine detection*, in BAMC Conference, Cambridge, 2015.

[54] VS-50 Landmine.
`http://www.nolandmines.com/minesVS50.htm`

[55] O. Rehim, J. L. Davidson, L. A. Marsh, M. D. O'Toole, D. W. Armitage and A. J. Peyton. *Measurement system for determining the magnetic polarizibility tensor of small metal targets*, in IEEE Sensors Applications Symposium, 2015.

[56] B. J. Roth. *The Electrical Conductivity of Tissues*, in J. D. Bronzino. (ed) *The Biomedical Engineering Handbook*. CRC Press LLC, Boca Raton, 2000.

[57] H. Ammari, A. Buffa and J.-C. Nedelec. *A justification of eddy currents model for the Maxwell's equations*, SIAM J. APPL. MATH., **60**(5), 1805–1823, 2000.

[58] A. A. Rodríguez and A. Valli. *Eddy Current Approximation of Maxwell Equations : Theory, Algorithm and Applications*. Springer-Verlag Italia, Italy, 2010.

[59] P. D. Ledger and S. Zaglmayr. *hp-Finite element simulation of three-dimensional eddy current problems on multiply connected domains*, Computer Methods in Applied Mechanics and Engineering, **199**, 49–52, 2010.

[60] Walk-Through Metal Detectors for Use in Concealed Weapon and Contraband Detection.
`https://www.ncjrs.gov/pdffiles1/nij/193510.pdf`

[61] J. F. Mangin, C. Poupon, C. Clark, D. Le Bihan and I. Bloch. *Eddy current distortion correction and robust tensor estimation for MR diffusion imaging*, in

W. Niessen and M. Viergever. (eds) *Medical Image Computing and Computer Assisted Intervention - MICCAI 2001*. Springer, Berlin, 2001.

[62] A. Orlowsky. *Theoretical study on peculiarities of small ellipsoidal defects detecting and evaluation in layered medias.*
http://www.gruppofrattura.it/ocs/index.php/ICF/ICF8/paper/viewFile/4032/4637

Appendix A

Additional Results

A.1 A unique Solution to the Depolarization Factors for Spheroids

For a fixed conductivity, k where $0 < k \neq 1 < +\infty$, let λ_i, $i = 1, 2$ and 3 be the eigenvalues of the M_E, the first order PT for ellipsoid E such that M_E is positive definite if $k > 1$ or M_E is negative definite if $0 < k < 1$. The corresponding depolarization factor, d_i of E for $i = 1, 2$ and 3 can be evaluated by using (4.4) if the volume of E is also given. In this section, we use the explicit formula of d_i (or $d_i(a, b, c)$) given in [6] and [47] to determine a unique solution a, b and c for $d_i(a, b, c)$ when E is either a prolate or oblate spheroid with a fixed volume such that a, b and c each is the semi principal axes of the spheroid.

A.1.1 Prolate spheroids

The first order PT for a prolate spheroid (with $a > b = c$ and volume $|B| = (4/3)\pi ab^2$) has two distinct eigenvalues $\lambda_1 > \lambda_2 = \lambda_3$. Therefore, by using (4.4), we can see that its depolarization factors are d_1 and $d_2 = d_3$. According to [6] and [47],

$$d_1 = \frac{1-\psi^2}{\psi^2}\left\{\frac{1}{2\psi}\ln\left(\frac{1+\psi}{1-\psi}\right) - 1\right\} \tag{A.1}$$

where $\psi = \sqrt{1-(b/a)^2}$ and $d_1 = 1 - (d_2/2)$. Next, it can be shown that $\lim\limits_{\psi\to 0} d_1 = \frac{1}{3}$ while $\lim\limits_{\psi\to 1} d_1 = 0$. We now plot the graph of d_1 defined by (A.1) in Figure A.1 for $\psi \in (0, 1)$ (ψ is denoted by psi in the figure). Moreover,

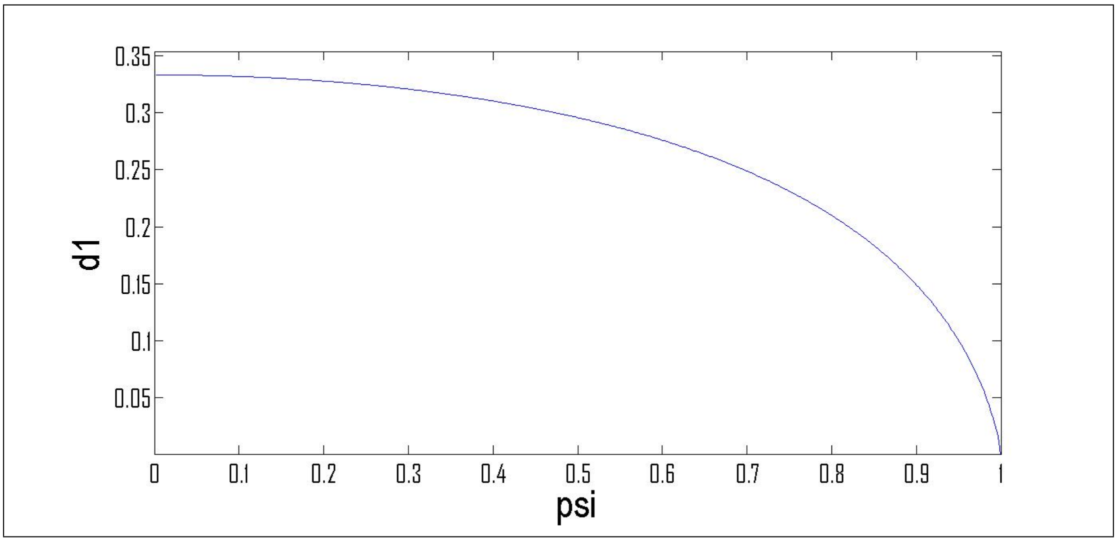

Figure A.1: The graph of d_1 in (A.1) for $\psi \in (0,1)$

$$\begin{aligned} \frac{d}{d\psi}(d_1) &= \frac{6\psi + (\psi^2 - 3)\ln\left(\frac{1+\psi}{1-\psi}\right)}{2\psi^4} \\ &\approx -\frac{4\psi}{15} - \frac{8\psi^3}{35} - \frac{4\psi^5}{21} - \frac{16\psi^7}{99} - \frac{20\psi^9}{143} \end{aligned} \tag{A.2}$$

and suggests that the derivate of d_1 with respect to ψ is negative for $\psi \in (0,1)$ so, d_1 is a monotonic decreasing function on $(0,1)$. Therefore, d_1 is invertible and there exist a unique solution ψ for d_1 when $\psi \in (0,1)$.

Next, by using the volume $|B|$ and the solution ψ, we have $\psi = \sqrt{1 - \frac{3|B|}{4\pi a^3}}$. By definition from [6] and [47], $0 < \psi < 1$ for $0 < b < a$. Let $f : a \to \psi$ be a function $\psi = f(a) = \sqrt{1 - \frac{3|B|}{4\pi a^3}}$ for $a > 0$ and $0 < f(a) < 1$ where, it can be shown that f is one to one and hence, invertible. Therefore, there is a unique solution a for $f(a) = \psi$. Finally, the unique $b > 0$ can be obtained from a by solving $|B| = (4/3)\pi ab^2$ for b.

A.1.2 Oblate spheroids

The first order PT for an oblate spheroid (with $a < b = c$ and volume $|B| = (4/3)\pi ab^2$) has two distinct eigenvalues $\lambda_1 < \lambda_2 = \lambda_3$. Moreover, its depolarization factors are also d_1 and $d_2 = d_3$. In this case, d_1 is given by [6] and [47] as

$$d_1 = \frac{1}{\varphi^2}\left\{1 - \frac{\sqrt{1-\varphi^2}}{\varphi}\sin^{-1}\varphi\right\} \tag{A.3}$$

where $\varphi = \sqrt{1 - (a/b)^2}$ and $d_1 = 1 - (d_2/2)$. It can also be shown that $\lim_{\varphi \to 0} d_1 = \frac{1}{3}$ while $\lim_{\varphi \to 1} d_1 = 1$. Next, we include Figure A.2 to show the graph of d_1 defined by (A.3)

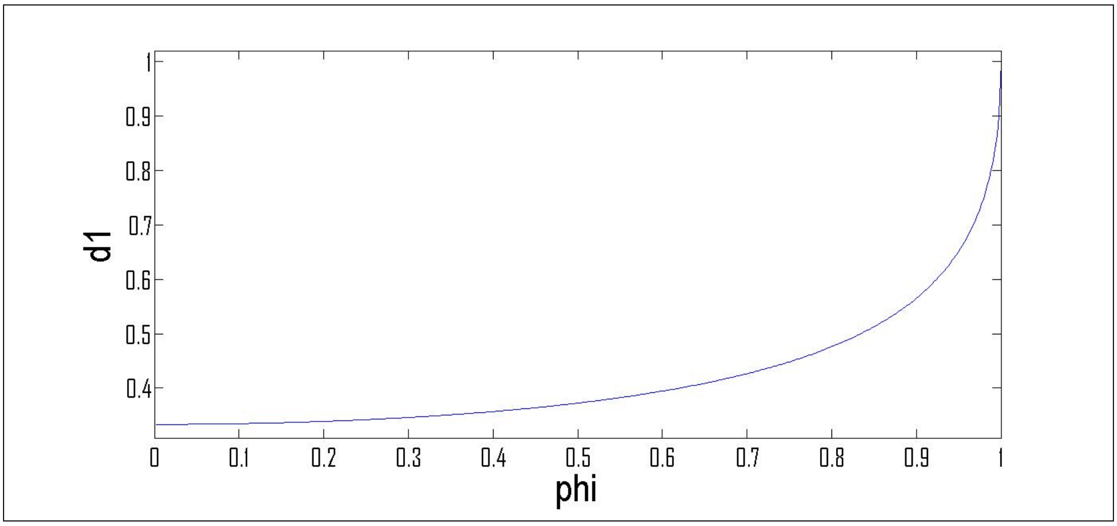

Figure A.2: The graph of d_1 in (A.3) for $\varphi \in (0,1)$

for $\varphi \in (0,1)$ (φ is denoted by phi in the figure). Furthermore,

$$\begin{aligned} \frac{d}{d\varphi}(d_1) &= \frac{3\sin^{-1}\varphi - 3\varphi\sqrt{1-\varphi^2} - 2\varphi^2\sin^{-1}\varphi}{3\varphi^4\sqrt{1-\varphi^2}} \\ &\approx \frac{4\varphi}{15} + \frac{32\varphi^3}{105} + \frac{32\varphi^5}{105} + \frac{1024\varphi^7}{3465} + \frac{2560\varphi^9}{9009} \end{aligned} \tag{A.4}$$

and suggests that the derivate of d_1 with respect to φ is positive for $\varphi \in (0,1)$ so, d_1 is a monotonic increasing function on $(0,1)$. Therefore, d_1 is invertible and there exist a unique solution φ for d_1 when $\varphi \in (0,1)$. Similarly, the unique solution a and b for d_1 such that $0 < a < b$ can be obtained by solving $|B| = (4/3)\pi ab^2$ and $\varphi = \sqrt{1-(a/b)^2}$.

A.2 Graphs of $\check{\check{M}}$ for Translated Objects

Following Section 8.1.2, in order to alternatively compare $\check{\check{M}}_L$ with $\check{\check{M}}_{L'}$, each coefficient of $\check{\check{M}}_L$ and $\check{\check{M}}_{L'}$ denoted by mij for $i,j = 1,2,3$ is plotted in the same graph for every L' in Figure A.3 until Figure A.11. It can be seen in all figures that all coefficients for both real and imaginary parts of $\check{\check{M}}_L$ and $\check{\check{M}}_{L'}$ are the same for all translation L' and suggest that $\check{\check{M}}_{L'}$ for each translated object is the same as $\check{\check{M}}_L$ for the object before translation. The results here consistent with our previous theory that $\check{\check{M}}$ does not depend on the position of the object.

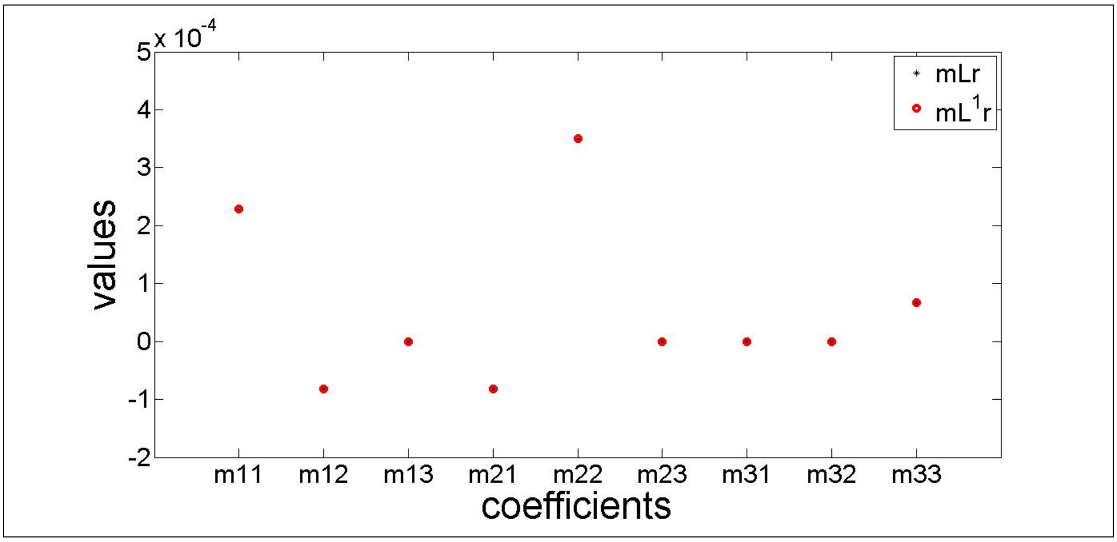

(a)

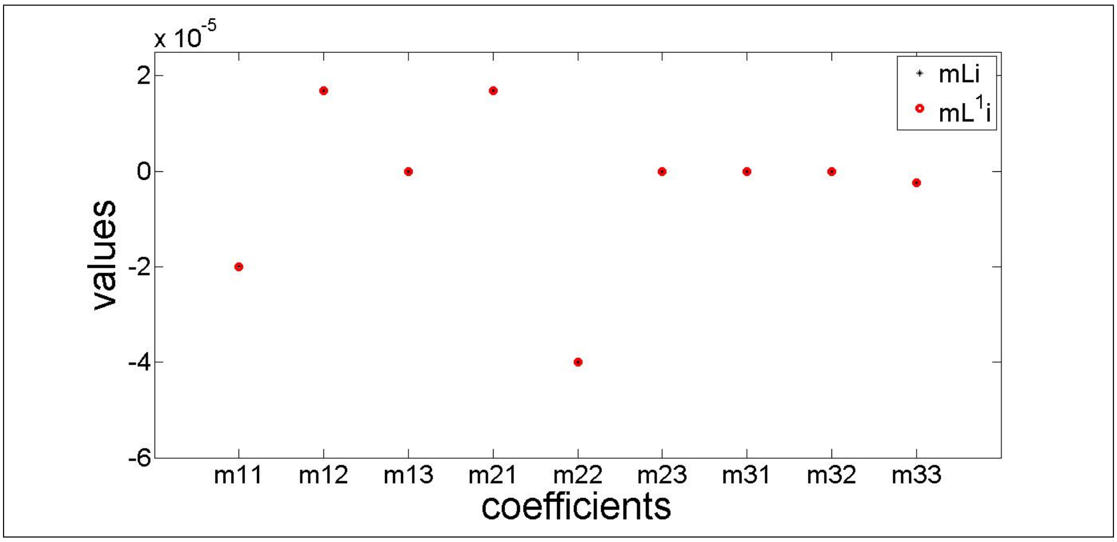

(b)

Figure A.3: A comparison between the coefficients for $\check{\check{M}}_L$ and $\check{\check{M}}_{L'}$ for $L' = 1$, both are computed by hp-FEM (a) real part (b) imaginary part

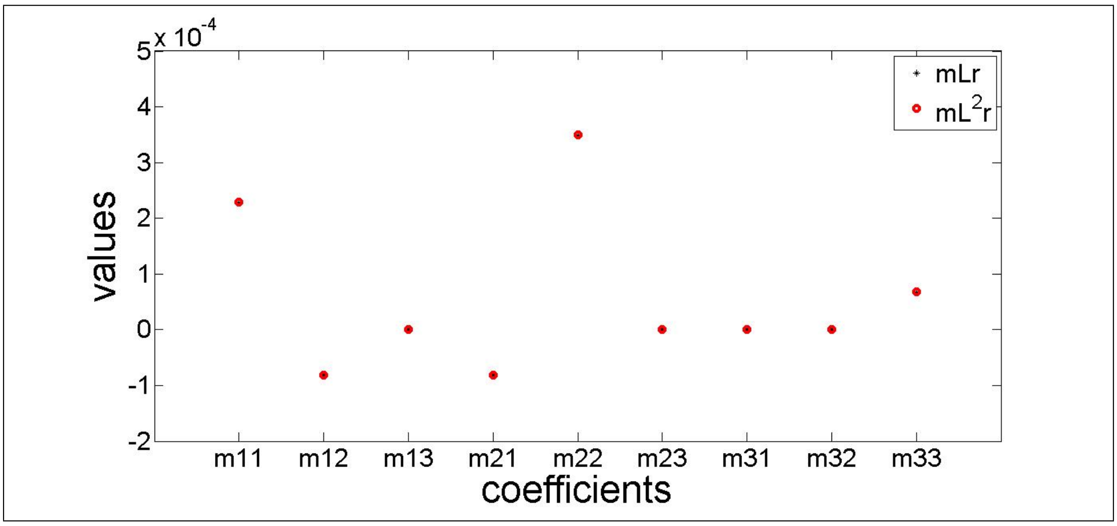

(a)

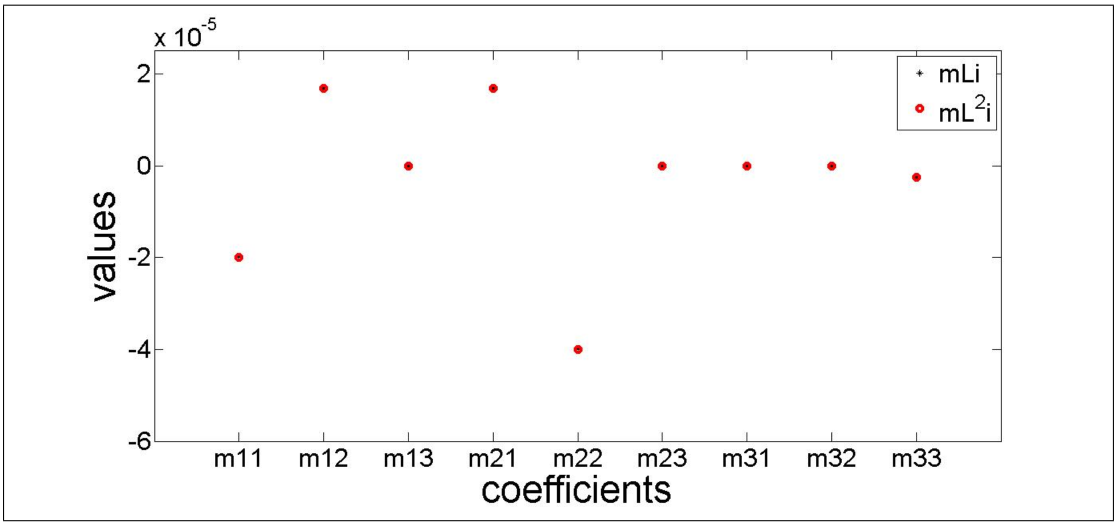

(b)

Figure A.4: A comparison between the coefficients for $\check{\check{M}}_L$ and $\check{\check{M}}_{L'}$ for $L' = 2$, both are computed by hp-FEM (a) real part (b) imaginary part

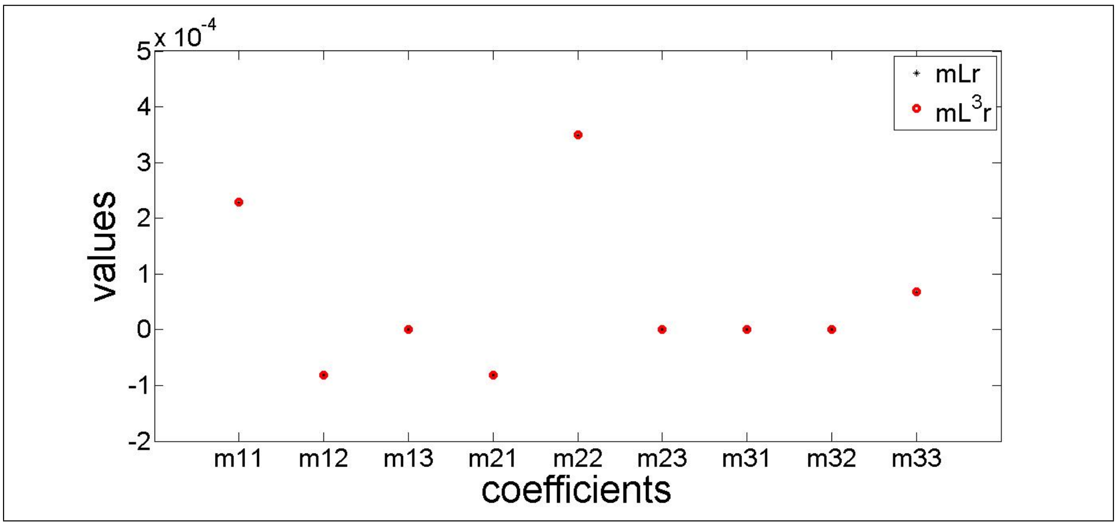

(a)

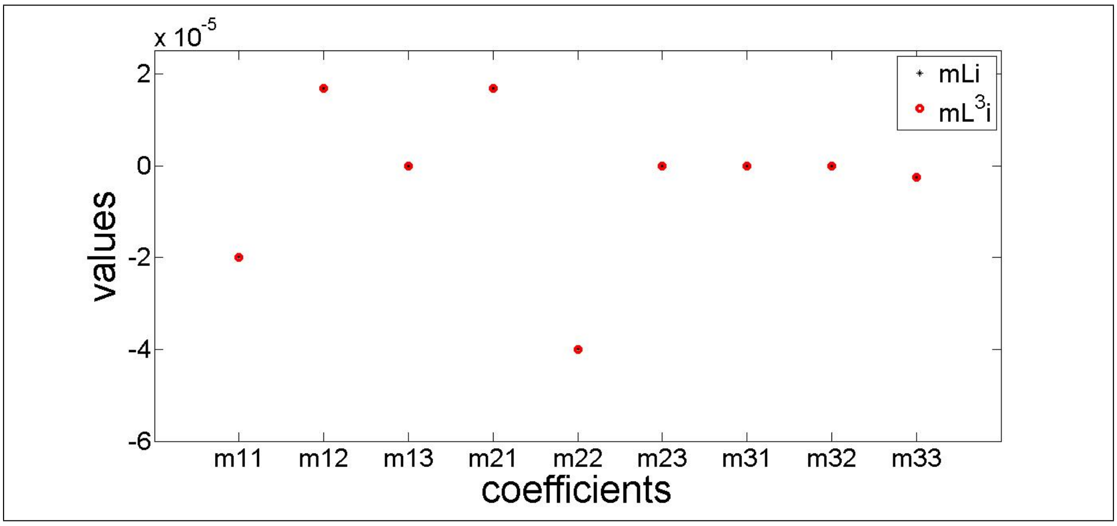

(b)

Figure A.5: A comparison between the coefficients for $\check{\check{M}}_L$ and $\check{\check{M}}_{L'}$ for $L' = 3$, both are computed by hp-FEM (a) real part (b) imaginary part

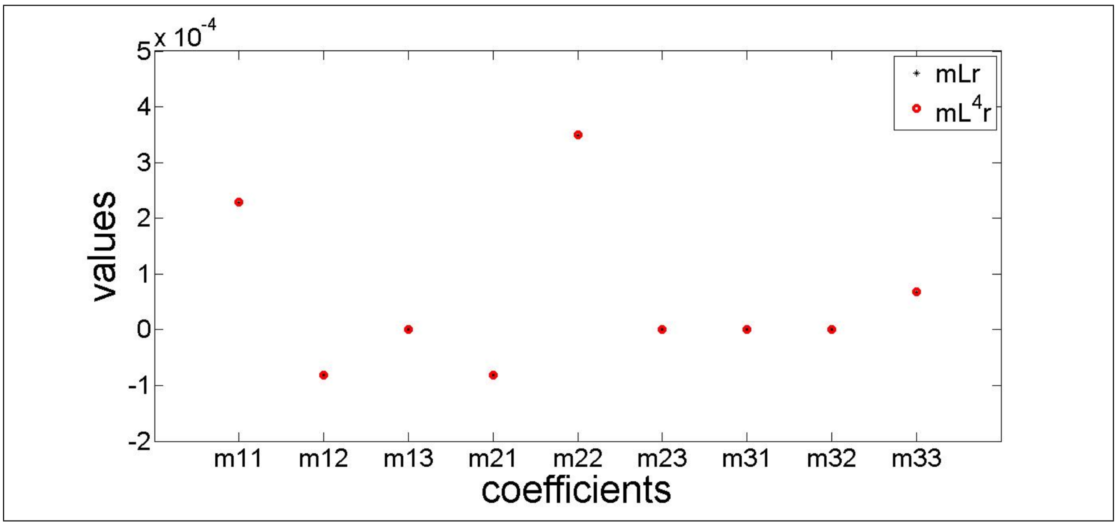

(a)

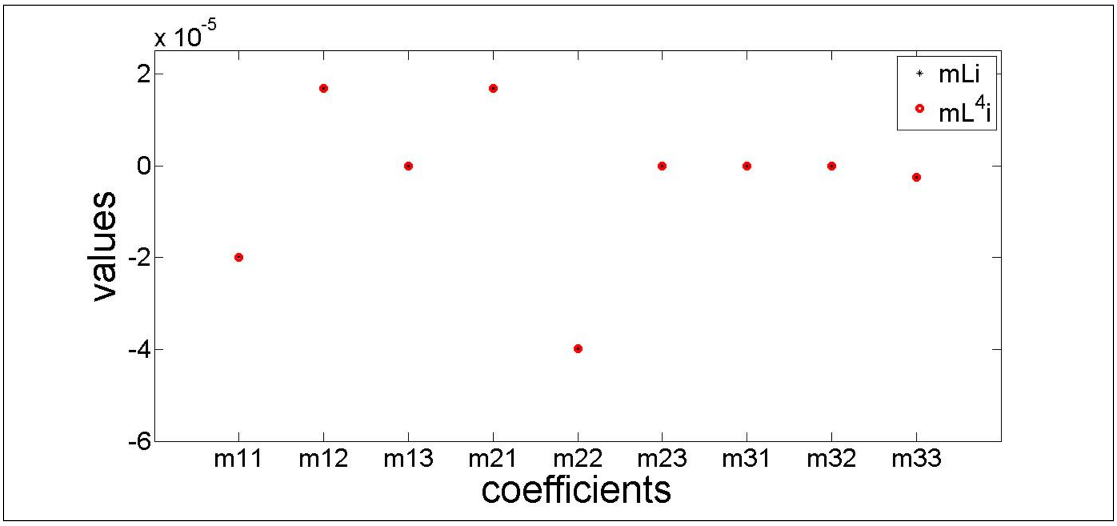

(b)

Figure A.6: A comparison between the coefficients for $\check{\check{M}}_L$ and $\check{\check{M}}_{L'}$ for $L' = 4$, both are computed by hp-FEM (a) real part (b) imaginary part

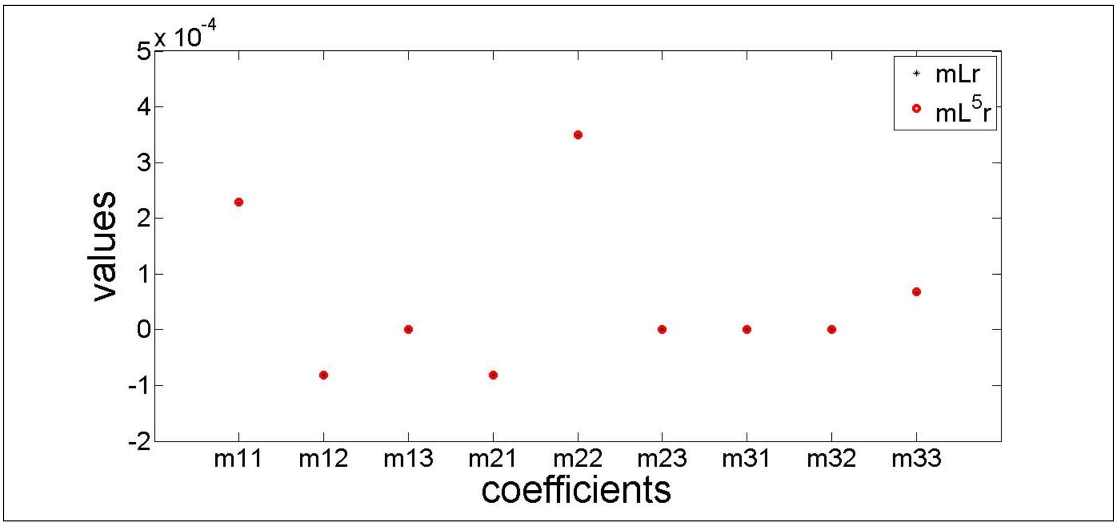

(a)

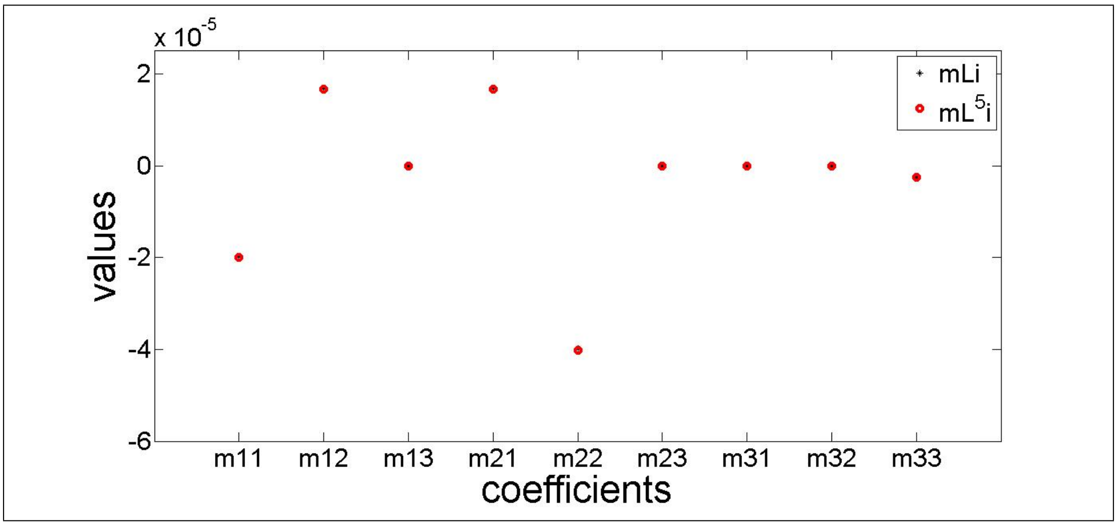

(b)

Figure A.7: A comparison between the coefficients for $\check{\check{M}}_L$ and $\check{\check{M}}_{L'}$ for $L' = 5$, both are computed by *hp*-FEM (a) real part (b) imaginary part

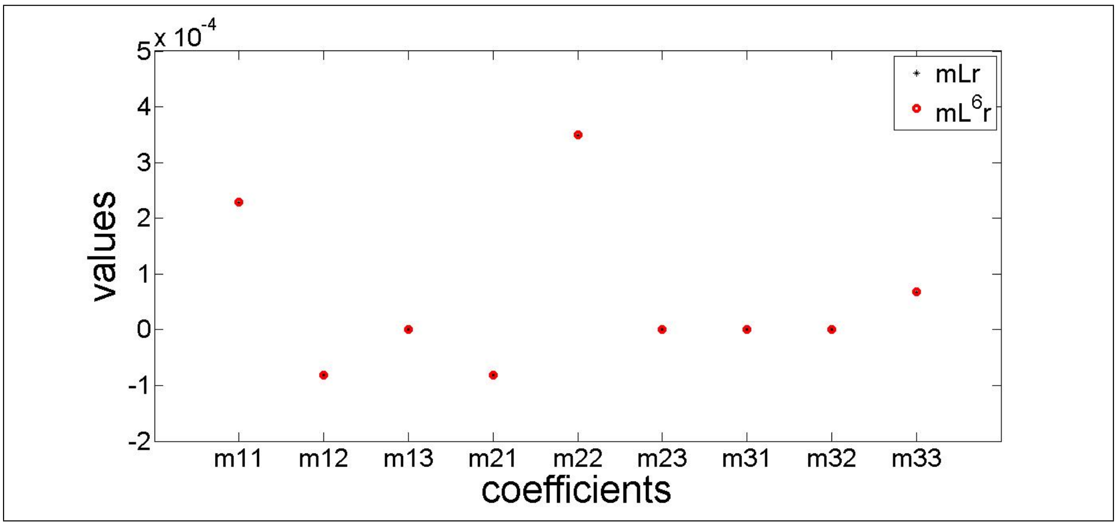

(a)

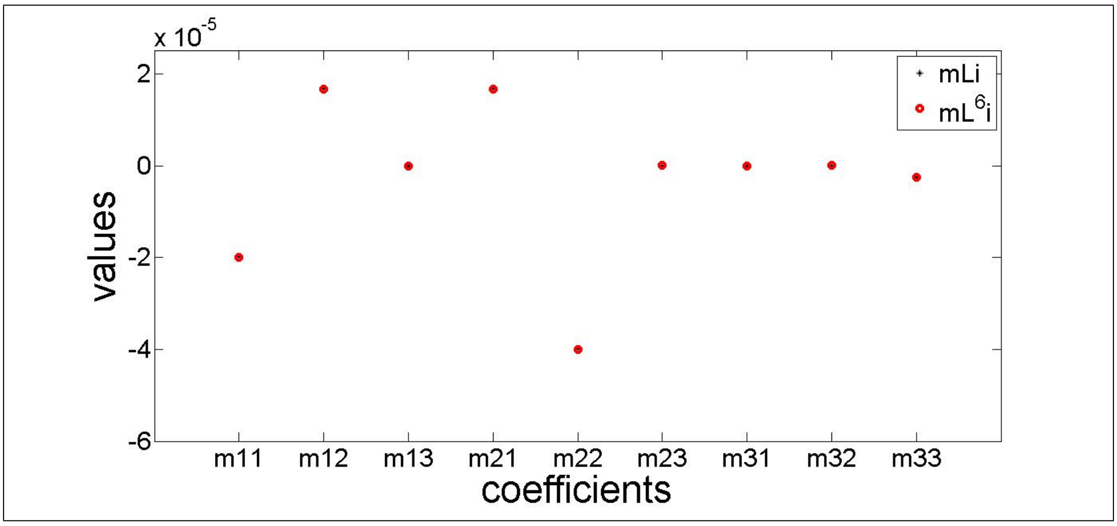

(b)

Figure A.8: A comparison between the coefficients for $\check{\check{M}}_L$ and $\check{\check{M}}_{L'}$ for $L' = 6$, both are computed by hp-FEM (a) real part (b) imaginary part

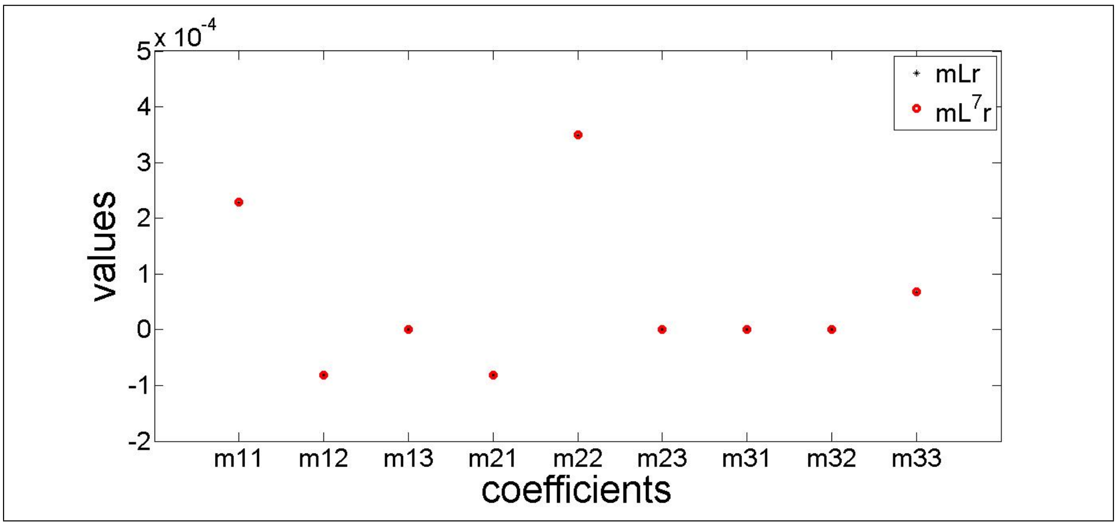

(a)

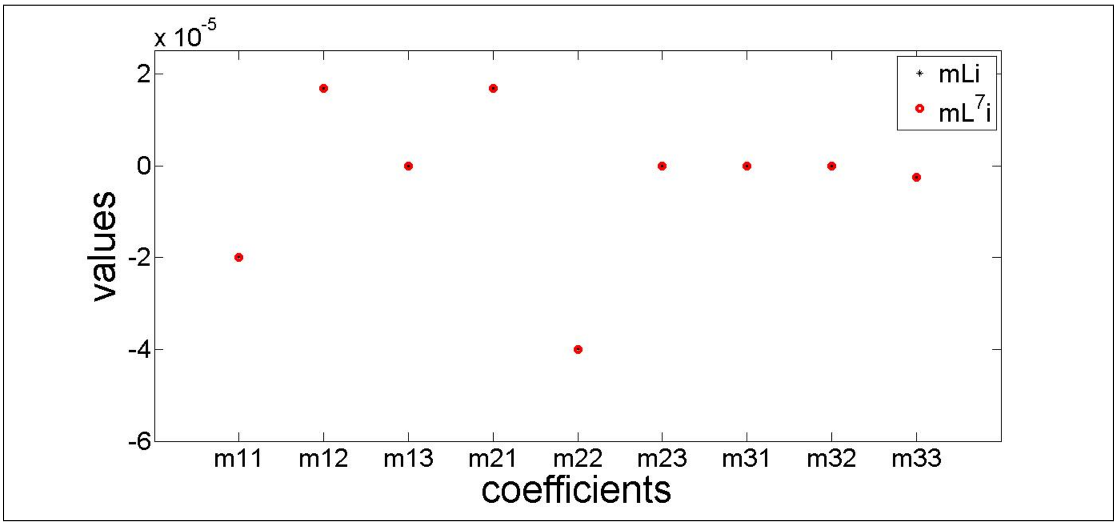

(b)

Figure A.9: A comparison between the coefficients for $\check{\check{M}}_L$ and $\check{\check{M}}_{L'}$ for $L' = 7$, both are computed by hp-FEM (a) real part (b) imaginary part

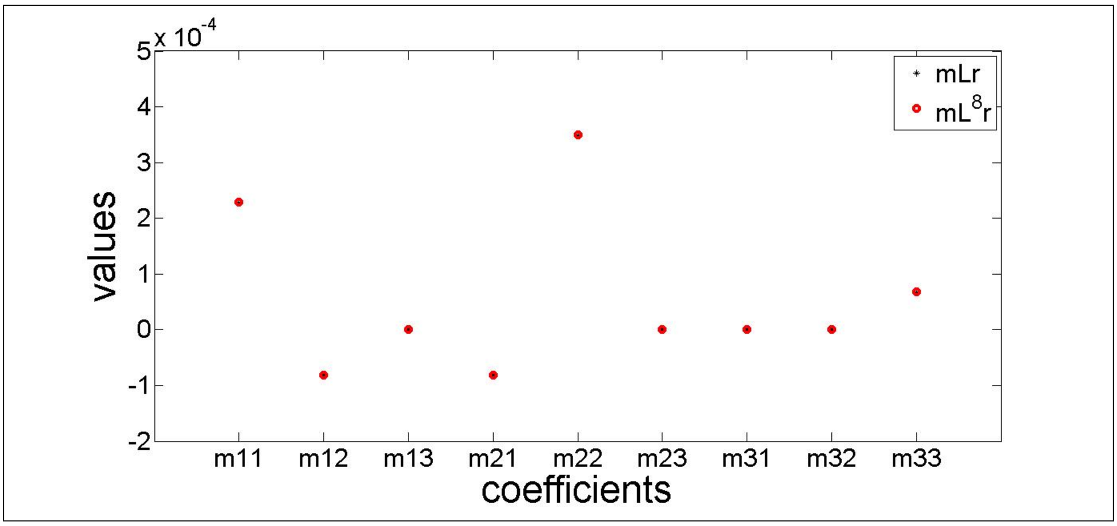

(a)

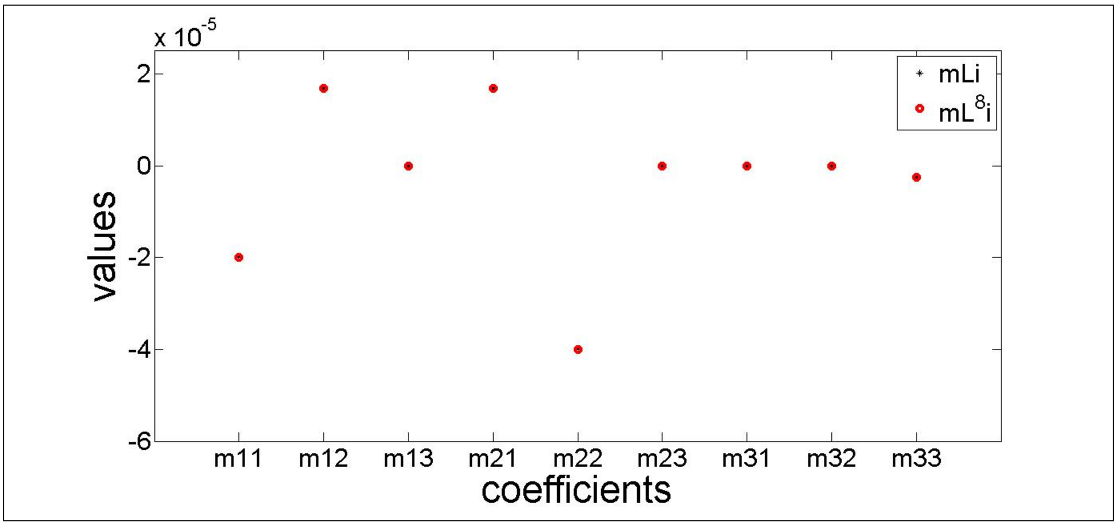

(b)

Figure A.10: A comparison between the coefficients for $\check{\check{M}}_L$ and $\check{\check{M}}_{L'}$ for $L' = 8$, both are computed by hp-FEM (a) real part (b) imaginary part

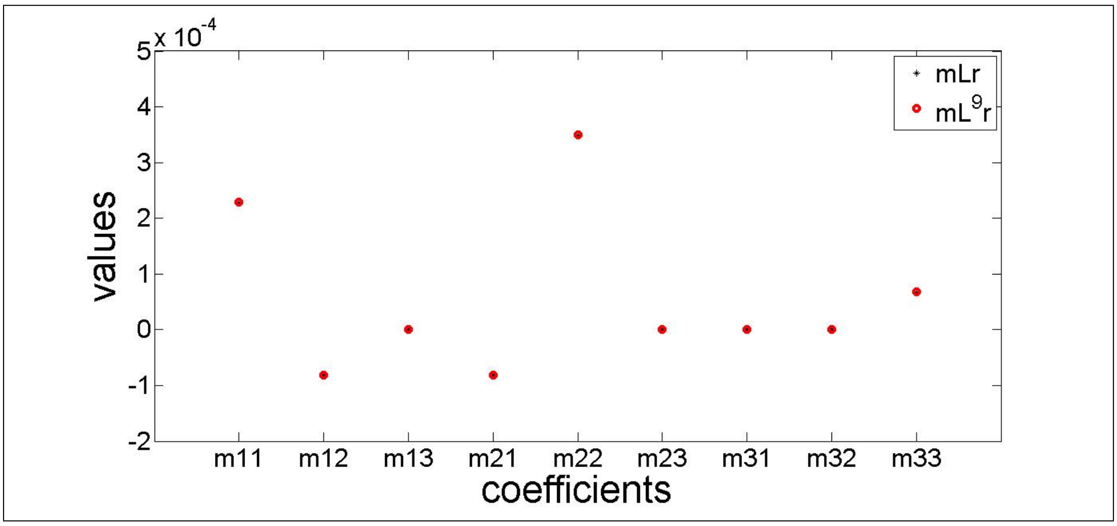

(a)

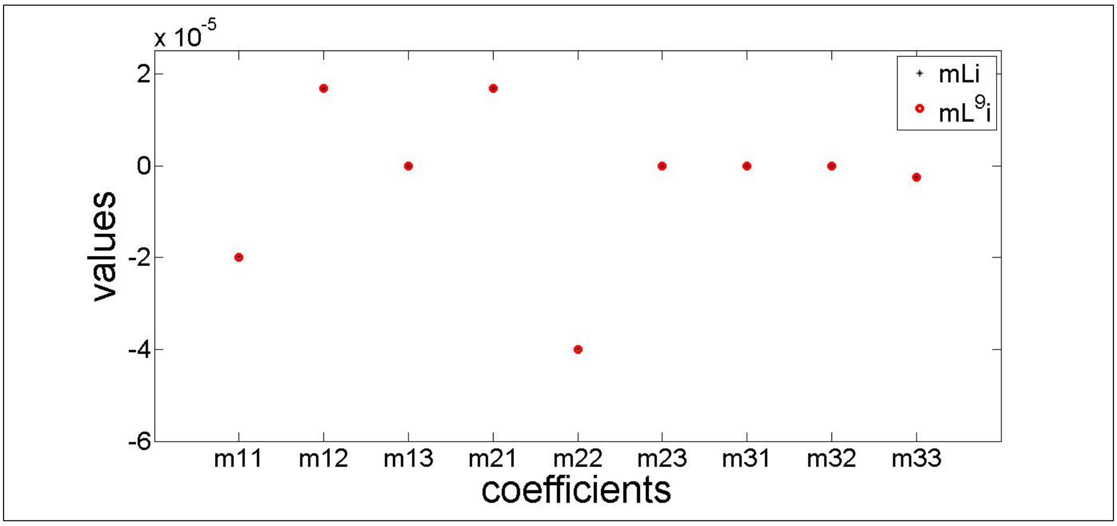

(b)

Figure A.11: A comparison between the coefficients for $\check{\check{M}}_L$ and $\check{\check{M}}_{L'}$ for $L' = 9$, both are computed by *hp*-FEM (a) real part (b) imaginary part

Appendix B

The Matlab Codes

B.1 A code to explicitly compute the first order PT for ellipsoid

The following is the code in *Matlab* to compute the first order PT for ellipsoid with semi principal axes $a = 3$ cm, $b = 2$ cm and $c = 1$ cm at conductivity $k = 1.5$ Sm^{-1} by using (2.2) and (2.3). In order to use it, the code can simply be copied to a `.m` file of *Matlab*. The code can also be modified to compute the first order PT for any ellipsoid at any conductivity by specifying `a,b,c` and `k` in the code.

Note : k can also be a complex number

```
%A code to compute the first order PT for ellipsoid with semi principal
axes a,b and c at conductivity k
%Specify the conductivity, k
k=1.5;
%Specify the semi principal axes
a=0.03; b=0.02; c=0.01;
%Approximate the integrals (2.3) of the thesis
valA = quadgk(@(x) b*c/a/a *(x.^2.*(x.^2-1+(b/a)^2).^0.5.*(x.^2-1+(c/a)
^2).^0.5).^(-1), 1, Inf);
valB = quadgk(@(x) b*c/a/a *((x.^2-1+(b/a)^2).^1.5.*(x.^2-1+(c/a)^2).
^0.5).^(-1), 1, Inf);
```

```
valC = quadgk(@(x) b*c/a/a *((x.^2-1+(b/a)^2).^0.5.*(x.^2-1+(c/a)^2).
^1.5).^(-1), 1, Inf);
%Computing the first order PT by using (2.2) of the thesis
M = zeros(3, 3);
for i=1:size(k,2)
M(1,1) = (k-1)*4/3*pi*a*b*c/((1-valA)+(k*valA));
M(2,2) = (k-1)*4/3*pi*a*b*c/((1-valB)+(k*valB));
M(3,3) = (k-1)*4/3*pi*a*b*c/((1-valC)+(k*valC));
end;
disp('The first order PT is')
disp(M)
```

B.2 A code to compute the first order PT by solving the boundary equations (1.3)-(1.5)

In this section, we provide a code in *Matlab* to compute the first order PT for a choosen object at conductivity $k = 1.5$ Sm^{-1} by solving the boundary equations (1.3)-(1.5) according to the method presented in Chapter 2. The code can also be modified to compute the first order PT at any real and complex conductivity by specifying `k` in the code. However, in order to use the code, the mesh of the boundary for the chosen object must firstly be given where, barycentre, outward normal vector and area for each element of the mesh must be determined. In this study, we use the mesh generated by *Netgen* and compute the barycentre, outward normal vector and area for all elements with our own other code. However, some codes such as *Gmsh*, *BEM++* and *Mesh Doctor* also provide barycentre, outward normal vector and area for each element of most popular mesh (such as sphere, ellipsoid, cube, etc). Therefore, one can access one of those codes to obtain the barycentre, outward normal vector and area for all elements and use the given values as inputs to our code to compute the first order PT for the object represented by the mesh. Here, barycentre, outward normal vector and area for each element are called by vectors `Midpoints`, `Normals` and `Areas`. In addition, we also assume the mesh has `N` total elements in the code.

```
%A code to compute the first order PT at conductivity 1.5 according
to the method presented in Chapter 2 of the thesis.
%Specify the conductivity, k.
k=1.5;
%Specify the number of elements for the mesh.
s=N;
%Discritize the integral operator (1.5) of the thesis based on
(2.5), (2.6) and (2.7).
KB = zeros(s);
for i=1:s
   for j=1:s
      if i==j
         KB(i,j)=0;
      else
         L=Midpoints(i,:)-Midpoints(j,:);
         KB(i,j)=(dot(L,Normals(i,:))*Areas(j))/(4*pi*(norm(L))^3);
      end
   end
end
%Solve the system of equations (1.4) of the thesis (see also (2.8)).
la=(k+1)/(2*(k-1));
A=la*eye(s)-KB;
Phi=A\Normals;
%Determine the first order PT from (2.10) of the thesis.
DA = eye(s);
for r=1:s
   DA(r,r)=Areas(r);
end
M=transpose(Phi)*DA*Midpoints;
disp('The first order PT is')
disp(M)
```

Appendix C

Published Papers

Below are some works published during the study.

C.1 Journal papers

1. T.K. Ahmad Khairuddin and W.R.B. Lionheart, *Some properties of the first order polarization tensor for 3D domains*, Matematika UTM, **29**(1), 1–18 (2013)
2. T.K.A. Khairuddin and W.R.B. Lionheart, *Fitting ellipsoids to objects by the first order polarization tensor*, Malaya Journal of Matematik, **4**(1), 44–53 (2013)
3. T.K. Ahmad Khairuddin and W.R.B. Lionheart, *Computing the first order polarization tensor : Welcome BEM++!*, Menemui Matematik, **35**(2), 15–20 (2013)
4. T.K.A. Khairuddin and W.R.B. Lionheart, *Does electro-sensing fish use the first order polarization tensor for object characterization? Object discrimination test*, Sains Malaysiana, **43**(11), 1775–1779 (2014)
5. T.K.A. Khairuddin and W.R.B. Lionheart, *Numerical comparisons for the approximated first order polarization tensor for ellipsoids*, App. Math. and Comp. Intel., **4**(1), 341–354 (2015)
6. T.K. Ahmad Khairuddin and W.R.B. Lionheart, *Polarization Tensor: Between Biology and Engineering*, Malaysian Journal of Mathematical Sciences, **10**(S), March : 179–191 (2016)

C.2 Conference papers

1. T.K.A. Khairuddin and W.R.B. Lionheart, *Do electro-sensing fish use the first order polarization tensor for object characterization?* in 100 years of Electrical Imaging, 149, Presses des Mines, Paris, (2012)

2. T.K. Ahmad Khairuddin and W.R.B. Lionheart, *Biological and Engineering Applications of the Polarization Tensor* in Proceedings of the 10th IMT-GT ICMSA 2014, October 14-16 2014, Kuala Terengganu, 228–234, Malaysia, (2014)

3. T.K.A. Khairuddin, P.D. Ledger and W.R.B. Lionheart, *Investigating the Polarization Tensor to Describe and Identify Metallic Objects* in Proceedings of the World Congress on Engineering 2015 Vol I, WCE 2015, July 1-3 2015, London, 122–127, UK, (2015)